Synthesis, Characterisation and Application of Nanoparticulate Additives for Vinyl Polymer Coatings

A THESIS

SUBMITTED TO THE

UNIVERSITY OF PUNE

FOR THE DEGREE OF

DOCTOR OF PHILOSOPHY

IN

CHEMISTRY

BY

NARENDRA R. SONAWANE

POLYMER SCIENCE AND ENGINEERING DIVISION

NATIONAL CHEMICAL LABORATORY,

PUNE-411008, INDIA

JUNE 2011

CERTIFICATE

This is to certify that the work incorporated in this thesis entitled **"Synthesis, Characterisation and Application of Nanoparticulate Additives for Vinyl Polymer Coatings"** submitted by Mr. Narendra R. Sonawane was carried out by him under my supervision at the National Chemical Laboratory, Pune. Such material as has been obtained from other sources has been duly acknowledged in this thesis.

Date:

National Chemical Laboratory — Dr. S. Radhakrishnan

Pune-411008 — Research Guide

DECLARATION

I hereby declare that the work incorporated in the thesis entitled **"Synthesis, Characterisation and Application of Nanoparticulate Additives for Vinyl Polymer Coatings"** submitted for the degree of Doctor of Philosophy to the University of Pune, has been carried out by me at the National Chemical Laboratory, Pune under the supervision of Dr. S. Radhakrishnan. The work is original and has not been submitted in part or full by me for any other degree of diploma to this or any other university.

Date:

National Chemical Laboratory Narendra Sonawane

Pune-411008 Research Student

Acknowledgements

First and foremost I would like to thank Dr. S. Radhakrishnan, my advisor for his constant support. Without his help, this work wouldn't have been possible. He provided a motivating, enthusiastic, and critical atmosphere during the many discussions we had. It was a great pleasure to me to conduct this thesis under his supervision. He provided valuable guidance, support, and the freedom to pursue my own ideas. I am sure I should have followed his advice more often than I did.

I would like to thank the Director of NCL for permitting me to submit this work in the form of Ph.D thesis, which I carried out in this research paradise.

I would like to acknowledge my colleagues in Lab No: 948 – Dr. Deshpande, Dr. Arindam, Dr. S. Subramanyam, Dr.Swarnendu, , Dr. Francis, Dr. Santosh, ,Dr. Ramanujam, Siju, Pradip, Rajshree, Kanchan, for keeping my spirits up during my tenure here.

My special thanks goes to Dr. Arun Salunke, Dr. Samadhan Patil, Shantibhushan Suryawanshi, Dr.Sandip Kothawade and for being with me, understanding and cooperating to great extend.

I wish to thank Mr.& Mrs. Ajay Kowley, Director, Vipraj Thermosets Pvt. Ltd., Pune and Mr. Ashok Sutrawe, Kansai Nerolac Paints Ltd., Lote. for their kind support during my thesis work.

I would also like to thank my dear friends Sunil Patil, Akshay Umale and many others whose good wishes have fuelled me along to this stage.

Finally, I would like to thank my parents, brothers, wife, son and relatives for their love, warmth, understanding and ethics.

There are many people whom I should thank but it is too difficult to put all names here. I extend my word of thank to all of them.

National Chemical Laboratory *(Narendra Sonawane)*

Pune 411008

Contents

Chapter II : Experimental

Chapter III : Effect of $CaCO_3$ Nanoparticles Addition on Optical and Corrosion Properties of PVAc and PVB nanocomposite Coatings

Chapter IV: Effect of Fe_2O_3 nanoparticle Addition on Optical and Corrosion Properties of PVAc and PVB nanocomposite Coatings.

Chapter V: Effect of $BaSO_4$ nanoparticle Addition on Optical and Corrosion Properties of PVB and Epoxy nanocomposite Coatings.

Chapter VI : Summary and Conclusion

Abstract

The world of composite is undergoing a tremendous revolution. Nanocomposites are a relatively new class of materials with ultra fine phase dimensions, typically of the order of a few nanometers. The control of nanometer scale structures and the preparation of nanometer scale composite materials are attracting the attention of the researcher in the fields of chemistry and physics. As new molecular structures for specific purposes can be designed by the fine chemistry, materials with unique characteristics can be realized by designing nanometer scale composites or materials. These materials exhibit dramatically different properties as compared to their macro analogues by virtue of their size, which ensures a greater interfacial interaction between the filler and the matrix.

Particulate fillers like calcium carbonate, barium sulphate, iron oxide, zinc oxide, etc. are commonly used in the coating industry to reduce the cost and add a few gross properties such as colour, reflectance, gloss, opacity, whiteness, etc. to the final product. Amongst all additives, Fe_2O_3, $BaSO_4$ and $CaCO_3$ are exceptional fillers due to their outstanding chemical, physical, mechanical, electrical and thermal properties. The reduction of fillers size to nanoscale level can significantly enhance the mechanical, barrier and fire retardant properties. In fact, nano clay research was pioneering due to the extensive application in coatings used by automotive industry such Toyota Research center.

Nanomaterials such as $CaCO_3$, TiO_2, Al_2O_3, Fe_2O_3, etc. have been synthesized and their characteristics have been investigated in the past. Among all above mentioned nanomaterials, $CaCO_3$, Fe_2O_3 and $BaSO_4$ are the most attractive nanomaterials in high corrosion resistant coatings, highly transparent composites, cosmetics, etc because of their excellent performance and properties. Amongst the various methods, polymer mediated growth has drawn considerable attention in recent years, since it offers a new and easy route to material synthesis. In this technique a polymer such as PEG, -PVAc, etc can be used to modify and control the morphology, crystalline phase, and orientation and growth habit of the final product. Hence, the nano particulate fillers

synthesized by this route have been studied in the present case especially for coating application.

The present thesis is delineated in six chapters. Chapter-I is the introduction chapter wherein a brief overview of polymer nanocomposites used for coating applications is given and the details of the various experimental techniques utilized in the present work are described in Chapter-II. Chapter-III outlines the results on synthesis and characterization of $CaCO_3$ nanaoparticles and their applications in polyvinyl acetate (PVAc) and polyvinyl butyral (PVB) matrices for optical and the enhancement of corrosion resistance properties. The results on synthesis and characterization of Fe_2O_3 nanaoparticles and their dispersion in PVAc and PVB matrices are investigated to study optical and corrosion resistance properties due to Fe_2O_3 are presented in Chapter-IV. The effect of addition of $BaSO_4$ nanoparticles on the performance of PVB and epoxy matrices especially optical and corrosion resistance properties are presented in Chapter-V. The summary and conclusions of the present work is outlined in Chapter-VI. A brief overview of each chapter is presented below.

List of Abbreviations

AC	Alternating Current
CNT	Carbon Nanotubes
CPVC	Critical Pigment Volume Concentration
Comm.	Commercial
DC	Direct Current
E_{corr}	Corrosion Potential
EIS	Electrochemical Impedance Spectroscopy
FWHM	Full Width at Half Maximum
FTIR	Fourier Transform Infra-red
I_{corr}	Corrosion Current
HEMA	2-Hydroxyethyl Methacrylate
HDPE	High Density Polyethylene
MA	Methyl Acrylate
MF	Melamine Formaldehyde
MMT	Montmorillonite
MMA	Methyl Methacrylate
MW	Molecular Weight
Nano	Nanoparticles
OCP	Open Circuit Potential
PAA	Polyacryl Amide
PANI	Polyaniline

PBO	Poly(benzoxazole)
PBS	Poly(butylenes succinate)
PBT	Poly(butylenes terephthalate)
PCL	poly(ε-caprolactone)
PEG	Polyethylene Glycol
PEO	Polyethylene Oxide
PET	Poly(ethylene terepthalate)
PIPN	Pseudo-interpenetrating Polymer Network
PLA	Polylactide
PMG	Polymer Mediated Growth
PMMA	Polymethyl Metheacrylate
POSS	Polyhedral Oligomeric Silsesquioxane
PP	Polypropylene
PS	Polystyrene
PU	Polyurathane
PVC	Polyvinyl Chloride
PVB	Polyvinyl Butyral
PVAc	Polyvinyl Acetate
PAA	Polyacryl Amide
PVA	Polyvinyl Alcohol
SAN	Poly(styrene-*co*-acrylonitrile)
SCE	Saturated Calomel Electrode
SEM	Scanning Electron Microscopy

TEM	Transmission Electron Microscopy
TGA	Thermal Gravimetric Analysis
TFEA	2,2,2-trifluoroethyl Acrylate
TMOS	Tetramethoxysilane
TiO_2	Titanium Dioxide
UF	Urea Formaldehyde
UV	Ultra Violet
WAXD	Wide Angle X-ray Diffraction

List of Symbols

D	Diffusion Constant
S	Solubility Parameter
E_{eq}	Equilibrium Potential
η	Overpotential
η_a	Anodic Overpotential
η_c	Cathodic Overpotential
E	Applied Potential
α	Charge Transfer Barrier
n	Number of Participating Electrons
R	Gas Constant
T	Absolute Temperature
P	Diffusion and Solubility Co-efficient
F	Faraday Constant
i_0	Exchange Current Density
b	Tafel Slope
E_{corr}	Corrosion Potential
I_{corr}	Corrosion Current Density
C_R	Corrosion Rate
Rp	Polarization Resistance
A	Corroded Area
d	Density of the Materials
Cc	Coating Capacitance
ε	Dielectric Constant
ε_0	Permittivity of free space
d	Thickness
C_t	Capacitance after time t
C_0	Initial Capacitance

φ	Volume fraction of water
Ω	Ohm
V	Voltage
A	Ampere
lZl	Vector of length
|Z|0	Low frequency impedance at time t=0
|Z|m	Impedance of bare metal
|Z|fail	Specific failure modulus
$\theta_{.}$	Decay constant
C	Capacitance
R	Resistance
R_{ct}	Charge transfer resistance
R_{Ω}	Solution resistance
C_{dl}	Double layer capacitance
Z_{war}	Warburg impedance
R_a	Aggregate resistance
R_p	Bulk resistance
ω	Angular frequency
Z	Impedance
θ’	Phase angle
t’	Crystallite size
λ_i	Wavelength
l	Thickness of sample
θ	Diffraction angle
$\Delta\theta$	Breadth of the peak in radian
T_g	Glass transition temperature

List of Tables

List of Figures

CHAPTER – 1

INTRODUCTION

1.1 Introduction :

Nanotechnology is the creation of new materials, devices, and systems through the control of matter on the nanometer-length scale, at the level of atoms and molecules. The essence of nanotechnology is the ability to work at these levels to generate nanostructures with fundamentally new molecular organization. Nanotechnology and engineering stand to produce significant scientific and technological advances in diverse fields from commodity to speciality applications, including paints and coatings. In a broad sense, they can be defined as the science and engineering involved in the design, synthesis, characterization, and application of materials and devices whose smallest functional organization in at least one dimension is on the nanometer scale, ranging from a few to several hundred nanometers. A nanometer is one billionth of a meter or three orders of magnitude smaller then a micron, roughly the size scale of a molecule itself. Nanomaterials are materials with one or more external dimensions / internal structure on the nanoscale. Nanomaterials /nanoparticles possess novel properties and characteristics that differ from the same large scale materials [1].

Nanotechnology is mainly defined by size and comprises the visualization, characterization, production and manipulation of structures, which are smaller than 100 nanometers (nm) [2]. Nanoparticles are particles with one or more dimensions at the nanoscale [3]. According to the ISO /TR 27628 nanoparticles are particles with a nominal diameter smaller than 100 nm [4]. These particles originate from primary sources (natural sources, e.g. sea-air, volcanic ashes / pumicite) and /or secondary sources (artificial sources, such as. technical products and by-products, cigarette smoke, diesel engine exhaust, cutting and welding fumes, open fire) [1, 5]. Engineered nanoparticles are intentionally engineered and produced with specific properties [4]. Nanoparticles / nanomaterials include, for example, metals or metal oxides, carbon black, carbon nanotubes, fullerenes, silicate, organic nanoparticles or nanocomposites [1, 6]. The term “nanoparticles” means only solitaire nanoparticles. Aggregates and agglomerates are not covered by this term. However in practice, aggregates and agglomerates are mostly also part of an investigated “nano-

substance". Currently many authors use the term "nanoparticles" including also agglomerates and aggregates. Finely dispersed nanostructures or nanoparticles are used in numerous technological applications e.g. as ceramics, polymer composites, filler materials, pigments, electronics, catalysts, and many others [7-11].

When particle size is decreased to the nanoscale range, physical and chemical properties often change with consequent new product opportunities. Thus a considerable future expansion of the nano-market is expected. [12-15]. The potential impact of nanotechnology stems directly from the spatial and temporal scales being considered materials and devices engineered at the nanometer scale imply controlled manipulation of individual constituent molecules and atoms in how they are arranged to form the bulk macroscopic substrate. This, in turn, means that nano engineered substrates can be designed to exhibit very specific and controlled bulk chemical and physical properties as a result of the control over their molecular synthesis and assembly.

The definition of a nanocomposites material has broadened significantly to encompass a large variety of systems such as one-dimensional, two-dimensional, three-dimensional and amorphous materials, made of distinctly dissimilar components and mixed at the nanometer scale. The general class of nanocomposites organic/inorganic materials is a fast growing area of research. Significant effort is focused on the ability to obtain control of the nanoscale structures via innovative synthetic approaches. The properties of nanocomposites materials depend not only on the properties of their individual parents but also on their morphology and interfacial characteristics.

This rapidly expanding field is generating many exciting new materials with novel properties. The latter can be derived by combining properties from the parent constituents into a single material. There is also the possibility of new properties, which are unknown in the parent constituent materials. Nanostructure can significantly change the properties of materials, such as optical properties, hardness, shape and morphology. However when nanometer sized $CaCO_3$ particles are used the polymer-particle interface area increases drastically and steric hindrances are reduced. This can cause significant changes in the properties of the composite [16-21].

Polymer nanocomposite normally exhibit superior properties over unfilled polymers, including higher modulus, reduced gas permeability, improved solvent resistance, and enhanced conductivity [22-25].In addition to mechanical performance, ablation performance, thermal stability, and flame retardancy may also be improved [26-28].

The enhanced properties are the result of the much greater surface-to-volume ratio of nanofillers that are often characterized by very high aspect ratios. Nanofillers most often used are calcium carbonate barium sulphate iron oxides, clay, silica, alumina, nanotubes, graphite, gold, silver/zinc oxide, indium/tin oxide, copper oxide, and antimony/tin oxide [29-31].

Due to the unique nanometer-size dispersion in the polymer matrix of fibrous or layered fillers resulting in high aspect ratio, high surface area and high stress transfer efficiency nanocomposites generally exhibit improvements in the properties of polymeric materials even at very low volume fraction loadings (1–10 %); this is in contrast to the higher volume fraction loadings (10–50 %) of macrosize fillers in the traditional advanced composites. The low loadings of inorganic nanoparticles maintain, in general, high clarity and low cost, and also allow for conventional polymer processing.

1.2 Advantages of nanocomposites over conventional composites :

Several advantages of these nanocomposites have been identified. They include efficient reinforcement with minimal loss of ductility and impact strength, heat stability, flame retardance, improved abrasion resistance, reduced shrinkage and residual stress and altered electronic and optical properties. The decrease in size of the domain to less than 100 nm enables good optical transparency. e.g., ultra fine TiO_2 produces pearlescent effects [32]. High surface area in comparison with small pore size can be used as catalysts for a wide variety of chemical reactions. For example, porous silica by pyrolysis of polymer hybrid. In addition to this Lithium, Calcium and Zinc salts can also be used to form homogeneous metal containing polymer hybrids for interesting ion conductive properties [33, 34]. Thirdly, molecular aggregates and boundary structure differs for nanosized particles as compared to

conventional ones. The number of grain boundaries, pore density and the boundary energies are high for nanocrystals and hence exhibit novel electrical, magnetic and improved mechanical behavior. e.g.; ferric oxide and cadmium sulphide [35].

1.3 Techniques for preparing nanoparticle polymer composite :

There are three major techniques for preparing nanoparticles in a polymer matrix. These are:

1. In situ generation
2. Polymerization reaction induced
3. External mixing

1.3.1 In-situ generation of the nanoparticles :

The matrix mediated control of growth and morphology has drawn considerable attention among various group of research since it offers a new route to material synthesis. Amongst the various methods, which have been established for the synthesis of nanosize particle, the sol-gel technique has been studied extensively [36-39].

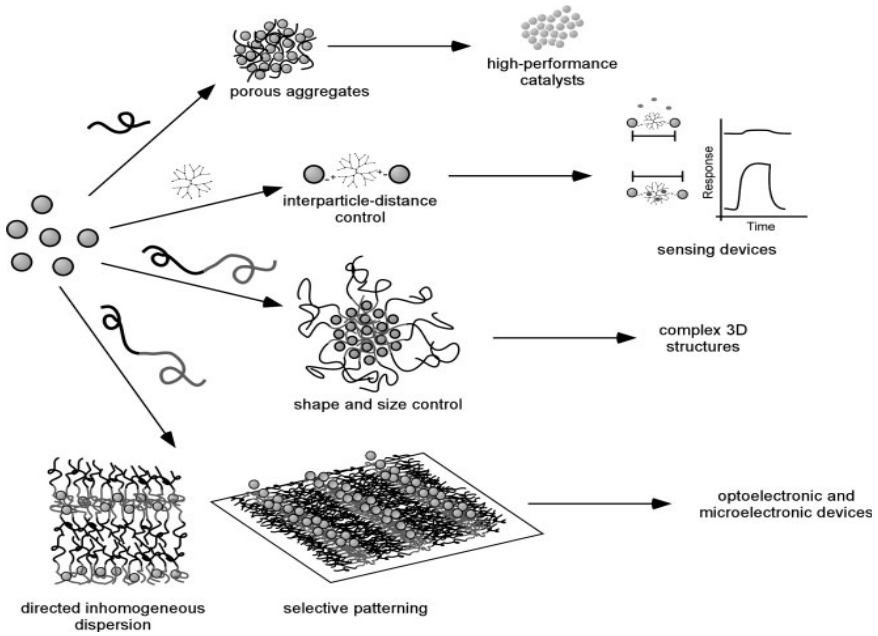

Figure 1.1 : Polymer-mediated assemble approaches to the fabrication of ordered nanocomposites, and their possible utilization

Different types of materials such as $CaCO_3$ $CuCl_2$, K_2CO_3, CdS, $CaSO_4$, Fe_2O_3, $BaSO_4$ etc. have been prepared in situ within a polymer matrix such as polyethylene glycol (PEG), Polyethylene oxide (PEO) which modified or controlled morphology, crystalline phase, orientation and growth habit of these compounds [40-43]. This method involves two steps. First, incorporation of a metal ion in the polymer by immersion of the polymer matrix, or polymer membrane, in an aqueous solution containing the metal ions. The ion(s) is absorbed or adsorbed to the polymer matrix. The second step is the formation of particles in the polymer matrix, by reacting the product of the first step with the proper reactants; e.g., reducing compounds. An example of such synthesis is formation of Copper Sulphide particles in PVA-PAA matrix [44].

The polymer mixture was immersed into copper sulphate aqueous solution, where the acidic groups of PAA serve as complexation sites for cuprous ions. Subsequently, the ions in the polymer were reduced using sodium sulphide to form ~10nm CuS particles.

Synthesis of nanoparticles by polymer mediated growth is one of the great technique in which the diffusion, sorption and permeation has been focus of great attention because these basic phenomena play a vital role in several important areas of engineering and industry. Recently, a combination of improved processes for nanoparticulate synthesis and better technology has resulted in the commercial use of nanoparticulate additives. PMG technique has been successfully used for the past several years for synthesizing and controlling the shape and size of various materials especially nanoparticulate fillers [40-43]. In this route, one of the reactant is form complexes with polymer. While the second reactant is allowed react with first reactant and formed nanoparticles to enter from external solution. Polymer-mediated nanoparticles assembly provides a versatile method for the creation of structured nano-composite material where control over composite morphology is paramount. In addition to their role in assembling nanoparticles, functionalized polymers can be used to control interparticle distances, assemble shape, size and porosity, and to induce an anisotropic ordering of nanoparticles [45-46].

Although the synthesis of nanoparticles by this method especially using partially miscible polymer blends has been successfully demonstrated, the underlying phenomena are very clear. For example, the diffusion and transport of ions through the polymer medium depend upon the nature of ions i.e. their size, charge etc., the free volume in the polymer which also depends on its glass transition temperature, degree of interaction with the polymer medium, molecular weight of polymer medium, solvent concentration used for polymer dissolution, etc. If the carbonate ions are used for the synthesis of nanoparticles of calcium carbonate, would the particle size change is as yet not known. A decrease in diffusivity with an increase in the size of the penetrant molecule may change the rate of reaction but it is not clear whether it will affect the subsequent particle formation, its size, etc [44-45]. This process is also present in the synthesis of nanoparticulate materials by sol-gel technique. Hence, the presented studies in this chapter are aimed at investigating the role of ionic diffusion in polymer-mediated synthesis of nanoparticulate fillers using Polyethylene Glycol (PEG) polymer, polymer with different molecular weights, and variety of ions so as to form variety of materials to bring out the common factor determining the ultimate particle size.

1.3.2 Preparation of nanoparticles by polymerization :

The second method of synthesizing nanoparticles is via polymerization of colloidal solutions containing metal ions and monomers. The particle size can be controlled by the reaction temperature and properties of the colloidal solution, thermal coagulation and Ostwald ripening. One example of such synthesis of PbS nanoparticles in polymer matrices is the polymerization of Pb $(MA)_2$ (lead methyl acrylic acid) with styrene [47].

1.3.3 Mechanical mixing of nanoparticles with polymers :

This method involves the direct mechanical mixing of a polymer solution with a pre-synthesized, highly dispersive nanoparticle solution. Several authors reported the synthesis of these types of composites.. Harmer et al. [48] prepared Cobalt oxide/PMMA nanocomposite. Room temperature synthesis of Mn-Ferrites in a polymer matrix has been the work of Shen and Egerton [49]. A non-aqueous solution route to prepare PAm-silver nanocomposite at room temperature has been reported by

Giannelis et al. [34]. This has been done by the gamma-irradiation to the substrates and the products obtained were transparent.

1.4 Polymer nanocomposites :

In polymer nanocomposites research, the primary goal is to enhance the strength and toughness of polymeric components using molecular or nanoscale fillers. Most notable are increased modulus, increased gas barrier, increased heat distortion temperature, resistance to small molecule permeation, improved ablative resistance, increase in atomic oxygen resistance and retention of impact strength etc. Interestingly, these performance improvements are achieved without increasing the density of the base polymer, without degrading its optical qualities and without making it any less recyclable. It is a remarkable fact that in addition to the profound changes in physical properties, which materials display when they are nanometer in scale, the chemical behavior is profoundly altered as well. When an inorganic solid is composed of only a few thousands of atoms, it has a great deal of surface area. By binding an appropriate organic molecule to this inorganic surface, it is possible to make nanocrystals behave chemically just like an organic macromolecule. Typically an inorganic nanocrystal will be coated with a monolayer of surfactant, rendering the nanocrystals hydrophobic. In this configuration the nanocrystals are soluble in non-polar solvents. If the solvent is removed the nanocrystals aggregate but not fuse, since a layer of surfactant separates them. These nanocrystals can be redissolved. Further the surfactant can be exchanged of with another organic molecule, enabling the nanocrystals to be placed in almost any chemical environment.

1.5 Classification of nanocomposites :

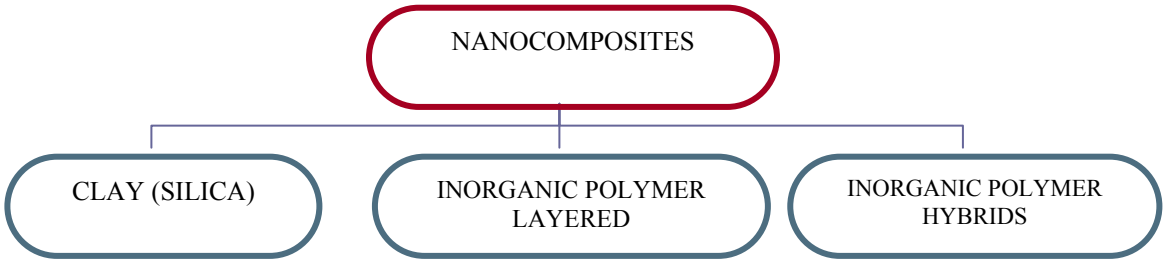

Nanocomposites can be classified based on the filler into three, viz., clay (silica) based, inorganic-polymer layered and inorganic-polymer hybrids. In the clay variety considerable work was done in the recent years[50-51]. The filler particles are the individual layers of a lamellar compound, most typically clay. Since a single clay layer is only 10 A^o thick, it has a very large aspect ratio, usually in the range of 200-2000. This makes it possible to use very small amounts (i.e., a few weight percent) of clay to interrupt the structure of a polymer matrix on a nanometer length scale. The resulting nanocomposites can exhibit dramatically altered physical properties relative to the pristine polymer. The key to forming such novel materials is understanding and manipulating the guest-host intercalation chemistry occurring between the polymer and the layered compounds. Pioneering advances at Toyota research during the early 1990's has stimulated the development of various polymer/organoclay nanocomposites with attractive property profiles. There are two end members that define the realm of structures possible in such nanocomposites. At one end are well-ordered, stacked multi layers that result from intercalated chains within host silicate clay layers. At the other end are the delaminated materials, in which the host layers have lost their registry and are randomly dispersed in a continuous polymer matrix. The organoclay as precursors to nanocomposites formation has been extended into various systems including epoxies, polyurethanes, polyimides, nitrile rubber, polyester, polystyrenes, and siloxanes. For true nanocomposites, the clay nanolayers must be uniformly dispersed (exfoliated) in the polymer matrix, as opposed to being aggregated as tactoids or simply intercalated.

The second type of nanocomposites focuses on layered compounds such as transitional metal dichalcogenides, hybrid metal oxides and layered metal polymer chalcogenides. Layered silicates dispersed as a reinforcing phase in an engineering polymer matrix are one of the important forms of such "hybrid organic-inorganic nanocomposites." Although the high aspect ratio of silicate nanolayers is ideal for reinforcement, the nanolayers are not easily dispersed in most polymers due to their preferred face-to-face stacking in agglomerated tactoids.

In the third category the focus is on the nanocomposites formed from inorganic fillers in polymer matrix. These are materials in which nanoscopic inorganic particles, typically 10-100 angstrom in at least one dimension, are dispersed in an organic polymer matrix in order to improve dramatically the performance properties of the polymer. In this process first we have to prepare the nanosize particles of inorganic moiety and then to incorporate it in the matrix. One of the primary objectives of the various synthesis techniques is to control the particle size either by spatial conditions, such as size of pores and entities in the media, or by reaction kinetics. Stabilizing nanosize metal or semiconductor particles are critical. Several advantages have been reported for the usage of polymer as the matrix.

1.6 Methods for preparation of nanocomposites :

There are a lot of methods to synthesize nanoparticles in general, but the discussion here would be restricted to preparation of nanoparticles using polymer matrices, [52-53] which would eventually result in nanocomposites. These strategies could be classified in to five major categories. They are :

1) Sol-gel processing
2) Incorporation of metals and metal complexes in polymers by coordination interactions
3) Intercalation in 2D layered structures
4) Intercalation in 3D frameworks
5) Incorporation of inorganic particles and clusters

. 1.6.1 Sol-gel Processing :

The formation of a nanocomposites or an organic/ inorganic hybrid material is carried out either by a sequential two-step process, wherein a secondary network is formed in a primary one, or by the simultaneous formation of the two networks. The resulting materials are microscopically phase separated, but macroscopically uniform. A major drawback in this approach is the difference in the relative thermal stabilities of the two components placing a severe restriction on the preparative conditions due to the lower thermal stability of the organic polymer. This problem could be easily circumvented by the sol-gel process in which complex metal oxide frameworks are accessed by simple hydrolysis and condensation reactions at ambient temperatures

starting with the respective molecular precursors. The morphologies and properties of the resulting materials can be controlled by the reaction conditions and the precursors used, e.g. type of solvent/ catalyst used, catalyst to alkoxy ratios, etc.

Organic polymers with functional groups that have specific interactions with compounds created in the sol–gel process, e.g. hydrogen bonding to residual silanol groups on the formed silica can be chosen to have a high degree of homogeneity and optical transparency to avoid macrophase separation in the nanocomposites. Towards this end, organic polymers with hydrogen bonding ability such as poly (2MOx), PVP, poly (DMAA), PVA, PMMA, PVAc, polyamides, polyethersulfones,[54] polymeric perfluoroalkylsulfonates (Nafion) [55-58] and hydroxyl end-capped polysiloxanes were incorporated into sol–gel reaction mixtures [59-63]. The sol–gel process can be employed using a variety of different inorganic precursors and is not limited to SiO_2 alone

The high porosity of a silica network formed by the sol–gel process can be used for an impregnation of the material with polymers as well as with monomers, which can be polymerized in situ. Thus, PMMA/ silica hybrids were prepared, and it was found that the mechanical properties of the pure silica species could be improved significantly depending on the amount of PMMA included and by the addition of a coupling agent such as methacryloxytrimethoxysilane [64].

A slight variant of this process is the polymer mediated growth (PMG) or matrix mediated growth technique. Radhakrishnan et al. have utilized this technique to synthesize a number of compounds like $CaCO_3$, $CuCl_2$, CdS, $CaSO_4$, Fe_2O_3 etc. wherein the morphology, crystalline phase, orientation and growth habit of these compounds could be easily tailored [65-66].

1.6.2 Incorporation of Metals and Metal Complexes in Polymers by Co-ordination Interactions :

Polymerization and copolymerization of metal coordinating monomers, coordination of metals to preformed polymers and direct incorporation of the metal into the polymer chain are some of the methods for inclusion of metals in organic polymers. Metal ions such as Zn [67], Ni [68], Ru [69], Pd [70], and lanthanides [71] were incorporated as salts in to matrices of poly (vinyl pyridines) [67], poly (vinyl

amines) [72] or poly (L-histidine) [73], as homo or copolymers exploiting the Lewis basicity of the respective matrices. Palladium salts incorporated into a polyolefin containing unsaturated side groups such as polybutadiene or polyisoprene can cause cross linking between the polymer chains by palladium catalyzed Heck-type reactions. This methodology used to obtain crosslinked polymeric systems is called "reactive blending" [70, 74, and 75].

Metals could also be incorporated in to the polymers by the use of metal co-ordinating monomers and subsequent polymerization or copolymerization [76-79]. Metals coordinated with ligands that include functional groups that are able to initiate a polymerization reaction, or that can be transformed to have such a functionality [80-83] are used to form metal core macromolecules. Fe(II) and Ru(II) complexes, with one to three (4,4'-halomethyl)-2,2'-bipyridine (bpy) ligands, have been used to initiate living cationic oxazoline polymerizations [80,82,83] to obtain polymers with very low polydispersities.

1.6.3 Intercalation in 2D layered materials :

The 2D materials, which are of interest in these types of nanocomposites, are the layered silicates. The layered silicates belong to the family of 2:1 layered silicates popularly known as Phyllosilicates. Their crystal structure consists of layers made up of two tetrahedrally coordinated silicon atoms fused to an edge-shared octahedral sheet of either aluminum or magnesium hydroxide as shown in the figure 1.2. Sheets of atoms, of the general composition $(Si, Al)_4O_{10}(OH)_{2,}$ are stacked one above another in various ways and with different kinds of atoms lying between the layers and holding them together. The layer thickness is around 1 nm, and the lateral dimensions of these layers may vary from 30 nm to several microns or larger, depending on the particular layered silicate [84,85].

Stacking of the layers leads to a regular Van der Waals gap known as the inter layer gallery. Isomorphic substitution of the Al and Mg ions creates negative charges that are counter balanced by the alkali or alkaline metal cations residing in the gallery.

The silicates are generally hydrophobized by ion exchange reactions to improve the wettability of the silicate by the polymer. 2D materials intercalated in a

polymeric matrix, in principle fall in to three major categories based on the level and type of dispersion in the polymeric matrix. They are intercalated dispersed layer silicates and exfoliated/delaminated indivual silicate layers and completely exfoliated or delaminated structure.

(a) Intercalated nanocomposites in which the layered silicate is dispersed in the polymeric matrix in a crystallographically regular fashion with an interlayer spacing of a few nanometers (< 6 nm) irrespective of the polymer to silicate ratio. The polymer chain is intercalated between the silicate layers resulting in a well ordered multilayer morphology consisting of alternate silicate and polymer layers. Polymer matrix comprises a well dispersion of crtylographically layred silicates. In such system/nanocomposites the dispersion is in more ordered form/fashion with an interlayer spacing (6nm) and is not governed by polymer to silicate ratio.

(b) Delaminated/ Exfoliated nanocomposites in which the individual silicate layers are separated in the polymer matrix by average distances greater than 8 nm [86]. The silicate platelets are uniformly dispersed in the polymeric matrix and no peaks are seen in the XRD scans of these materials indicating the collapse of an ordered structure.

(c) Flocculated nanocomposites in which the intercalated and stacked silicate layers are flocculated to some extent due to the hydroxylated edge–edge interactions of the silicate layers. Exfoliated systems display greater property enhancements as compared to intercalated structures due to their superior dispersion but are more difficult to achieve. These nanocomposites can be prepared by three main strategies. They are as follows :

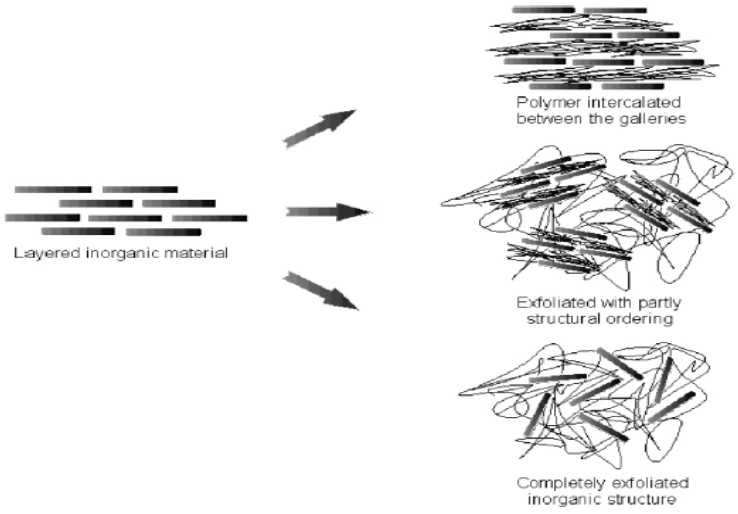

Figure 1.2 : Schematic showing different types of nanocomposites

1.6.3a Intercalation of Polymer / Prepolymer from Solution :

A negative variation in the Gibb's free energy is expected to be the prerequisite for the exchange of the polymer with the previously intercalated solvent in the interlayer gallery. The driving force for the polymer intercalation in to the layered silicate is the entropy gained by desorption of solvent molecules, which makes up for the loss in entropy of the confined intercalated chains. Intercalation from solution has been reported from both aqueous and non-aqueous media. PEO, [86] PVP, [87] PVA [88] and PEVA [89] have been intercalated from aqueous solutions whereas PCL, [90] PLA, [91], HDPE [92] and some liquid crystalline polymers [93] have been intercalated in organic solvents.

1.6.3b In situ Intercalative Polymerization :

This is a method in which the monomer is first intercalated in to the layered silicate and subsequently polymerized there itself resulting in an increase in the basal spacing. Polymerization can be initiated either by heat, radiation, by the diffusion of a suitable initiator or a catalyst. This was the actual method adopted by the Toyota researchers, which heralded a new dawn in the field of polymer nanocomposites.[93]

Nylon-6,[94] PCL,[95-97] PU,[98-99] PMMA,[100-101] PS,[102-105] PBO,[106] PE,[107-109] PP,[110-111] PET,[112-114] and epoxy[115-119] based MMT nanocomposites have been synthesized by this method.

1.6.3c Melt Intercalation :

In this method, the polymer and the silicate is annealed statically under shear by heat or radiation above the polymer's melting point. The method is environmentally benign due to the absence of solvents and is compatible with the current industrial processing techniques like extrusion and injection molding making it economically viable. A range of structures from intercalated to exfoliated can be obtained by this method depending on the degree of penetration of the polymer chains in to the silicate layer. PS,[120-121] PS/ PE,[122] PEO,[123] N6,[124-127] PP,[128-129] PE,[130] PET,[131] PBT,[132] SAN,[133] PC[134], PLA[135,136] and PBS95[137-138] based layered silicate nanocomposites have been realized by this method.

1.6.4 Intercalation in 3D Frameworks :

Zeolites are crystalline aluminosilicates with well defined pores smaller than 2 nm. There is a variety of naturally occurring as well as synthetic zeolites. Zeolites have attracted much interest as catalysts and adsorbents due to their thermal stability and intraporous acidity. Molecular sieves are also crystalline framework materials, but of a non-aluminosilicate nature. M41S-materials belong to the class of mesoporous three-dimensional (3D) solids with ordered porosity in the pore size range 2–10 nm. Due to their special properties, such as the controllable pore size, there is a plethora of possible applications of these materials [139-140]. All these porous inorganic solids are excellent hosts for intercalation reactions because they contain well defined empty pores and channels. A unique feature of these materials is their ability to discriminate between shapes and sizes of molecules. Therefore, the design of new materials requires a match of the features of the guest with those of the host. Contrary to the layered materials, which are able to delaminate completely if the forces produced by the intercalated polymers overcome the attracting energy of the single layers, this is not possible in the case of the stable 3D framework structures. The obtained composites can be viewed as host–guest hybrid materials. There are two

possible routes towards this kind of hybrid material: (i) direct threading of preformed polymer through the host channels (soluble and melting polymers) which is usually limited by the size, conformation, and diffusion behavior of the polymers, and (ii) the in situ polymerization in the pores and channels of the hosts as shown in the Figure 1.3.

Nanocomposites of zeolite 13X, and crosslinked or linear PS and poly(EA) were prepared to form either a pseudo-interpenetrating polymer network (PIPN) or a full

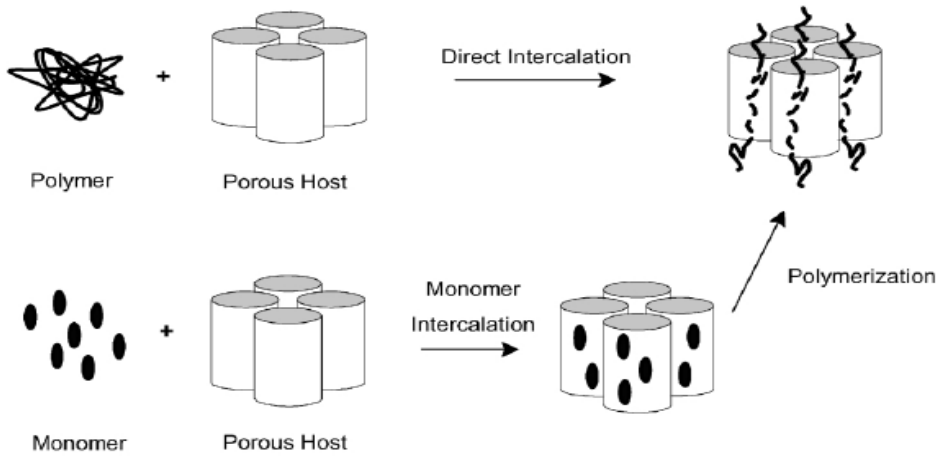

Figure 1.3 : Intercalation in 3D frameworks

Interpenetrating polymer network (IPN). A surface-mediated cationic polymerization technique was applied for the formation of poly(PVE)–HY–zeolite hybrid materials containing polyenylium sequences[141]. The active protons of HY zeolites were used for cationic polymerizations of several vinyl monomers inside the pores. In porous materials where no such protons are present, such as MCM-41, arylmethylium was incorporated. Utilizing this method, the synthesis of well-defined poly(vinyl ethers) or poly(vinylcarbazole) under conditions of constricted geometry can be achieved [142].

1.7 Physio-chemical behavior of nanocomposites :

When particle size is decreased to the nanoscale range, physical and chemical properties often change with consequent new product opportunities. Thus a

considerable future expansion of the nano-market is expected. The potential impact of nanotechnology stems directly from the spatial and temporal scales being considered: materials and devices engineered at the nanometer scale imply controlled manipulation of individual constituent molecules and atoms in how they are arranged to form the bulk macroscopic substrate. This, in turn, means that nano engineered substrates can be designed to exhibit very specific and controlled bulk chemical and physical properties as a result of the control over their molecular synthesis and assembly.

Nanocomposites based on nanosized inorganic particles and clusters are an emerging field of research activity due to the interesting properties of the particles, such as their behavior as quantum dots or their possible super-para and super-ferromagnetism, in combination with the other properties of the materials including, for example, their optical transparency. Another advantage of such hybrid composites/ particles in an organic polymer matrix is the possible protection of systems that are sensitive towards environmental conditions (oxygen, humidity, etc.) by coverage with a protecting polymeric skin or inclusion in a polymeric matrix.

The behavior of a typical composite material is controlled by the properties of the matrix, the distribution and properties of the filler as well as the nature of their interface. The interface may play a key role in controlling a number of composite properties such as its thermal conductivity, load carrying capacity, toughness and transport properties. For a characteristic filler particle size on the micrometer and large scale, the interface can be viewed as a two dimensional boundary between the components. By contrast, when the matrix is filled with nanosized particles, a significant fraction of the material is either at the interface or within its immediate vicinity. This interfacial region is believed to be responsible for the unique properties of nanocomposites materials. Polymer nanocomposites are particularly interesting due to their structural complexity. These significant changes in both chemistry and morphology in a large volume fraction of the polymer matrix are the basis for potentially tremendous changes in nanocomposites properties.

An emulsion polymerization process can carry out encapsulation of small inorganic particles by a polymer layer, the so-called core–shell particles.

Polymerization occurs primarily at the surface of unmodified particles due to the adsorption of the monomer on the surface, followed by polymerization in the adsorbed layer [142-145]. 3-(trimethoxysilyl) propyl coated silica particles were prepared by the Stober method followed by a surface-modification [146]. These particles were self assembled in a film and UV copolymerized with different monomers such as MA, MMA, HEMA, and TFEA. The systems were able to selectively filter light with a bandwidth less than 20 nm [147].

Polymer nanocomposites are constructed by dispersing a filler material into nanoparticles that form flat platelets. These platelets are then distributed into a polymer matrix creating multiple parallel layers, which force gases to flow through the polymer in a "torturous path", forming complex barriers to gases and water vapor. As more tortuosity is present in a polymer structure, higher barrier properties will result. The permeability coefficient of polymer films is determined using two factors:

Diffusion and solubility coefficients: $P = D \, x \, S.$ (1)

Effectively, more diffusion of nanoparticles throughout a polymer significantly reduces its permeability. According the Natick Soldier Center of the United States Army, "the degree of dispersion of the nanoparticles within the polymer relates to improvement in mechanical and barrier properties in the resulting nanocomposite films over those of pure polymer films". Nanoparticles allow for much lower loading levels than traditional fillers to achieve optimum performance. Usually addition levels of nanofillers are less than 5%, which significantly impact weight reduction of nanocomposite films. This dispersion process results in high aspect ratio and surface area causing higher performance plastics than with conventional fillers.

The thermal decomposition of volatile metal compounds in a polymer matrix leads to the formation of zero valent metal particles, or particles of their oxides dispersed in the polymer matrix. Cobalt and iron carbonyls in the presence of polymers such as polybutadiene, polystyrene, polypropylene, different block copolymers, etc. were accessed by this method [146-149].

The chemistry of organic-inorganic hybrid composite systems is based on the design of well-defined inorganic oligomers with only a single polymerization or initiation site per cluster. Each of these clusters has an inorganic silica-like core and is surrounded by eight organic groups, seven of which are inert towards polymerization and only one is active. Polymerization at this single site results in a linear polymer with pendent inorganic clusters of approximately 1.5 nm diameter. The unique property of such materials is that there is no crosslinking and the linear polymeric structure allows for an easier processing and characterization of these systems by conventional analytical methods [149]. Different polymer backbones have been synthesized using a variety of different substitution patterns at the silica cage.

Matrix mediated control of growth and morphology has received considerable attention in the recent years since it offers a novel route to material synthesis. This method presents various advantages over the conventional methods since sol-gel processing is a simple precipitation technique, which can be carried out at room temperature; in situ intercalative polymerization is easy to handle and process the powders; and in situ polymerization leads to control of the overall morphology, uniformity of size and dispersion, etc. Amongst the various methods that have been established for the synthesis of nanosized particles, the sol-gel technique has been studied extensively. However, this method is cumbersome to use and difficult to apply to all types of materials that can range from oxides, ceramics, etc to organic compounds which are desired in nanoparticulate form. Different types of materials such as $Al(OH)_3$, $CaCO_3$, $CuCl_2$, K_2CO_3, CdS, $CaSO_4$, etc. have been prepared in situ within a polymer matrix such as polyethylene oxide (PEO) or polyethylene glycol (PEG) which modified or controlled the morphology, crystalline phase, orientation and growth habit of these compounds.

Different types of fillers are utilized; the most common is nanoclay material called montmorillonite—layered smectite clay. Clays, in a natural state, are hydrophilic while polymers are hydrophobic. To make the two compatible, the clay's polarity must be modified to be more "organic" to interact successfully with polymers. One way to modify clay is by exchanging organic ammonium cations for inorganic cations from the clay's surface. Additional nanofillers include carbon

nanotubes, graphite platelets, carbon nanofibers, inorganic filler like calcium carbonate barium sulphate, titanium dioxide as well as other fillers being investigated such as synthetic clays, natural fibers (hemp or flax), and POSS. CNTs, a more expensive material than nanoclays or nanoparticulate mineral fillers, which are more readily available, offer superb electrical and thermal conductivity properties. There are three common methods used to enhance polymers with nanofillers to produce nanocomposites: melt compounding, in-situ polymerization and the solvent method. Melt compounding or processing of the nanofillers into a polymer is done simultaneously when the polymer is being processed through an extruder, injection molder, or other processing machine. The polymer pellets and filler (clay) are pressed together using shear forces to help with exfoliation and dispersion. With in-situ polymerization, the filler is added directly to the liquid monomer during the polymerization stage. Using the solution method, fillers are added to a polymer solution using solvents such as toluene, chloroform and acetonitrile to integrate the polymer and filler molecules. Since the use of solvents is not environmentally friendly, melt processing and in-situ polymerization are the most widely used methods of nanocomposite production.

1.8 Recent trends in nanocomposites :

Nanocomposites, defined as polymers bonded with nanoparticles to produce materials with enhanced properties, have been in existence for years but are recently gaining momentum in mainstream commercial packaging use [150-151].The United States is leading in nanotechnology research with over 400 research centers and companies involved with over $3.4 billion in funding. Europe has over 175 companies and organizations involved in nanoscience research with $1.7 billion in funding. Japan is also very involved in research with over 100 companies working with nanotechnologies. Globally, the market for nanocomposites is expected to grow to $250 million by 2008, with annual growth rates projected to be 18-25 % per year [152-153].

Flexible packaging consumption's rapid growth represents a $38 billion market in the global community [151]. As the demand in the industry continues to rise at an average of 3.5% each year, flexible materials need to meet and exceed the

high expectations of consumers and the stressors of the supply chain. Increased competition between suppliers along with government regulations translates into innovations in films that enhance product and package performance as well as address worldwide concerns with packaging waste. One such innovation is polymer nanocomposite technology, which holds the key to future advances in flexible packaging. According to Aaron Brody in a December, 2003 Food Technology article, "…nanocomposites appear capable of approaching the elusive goal of converting plastic into a super barrier the equivalent of glass or metal without upsetting regulators". This section will discuss how nanocomposites are made and the growth of nanocomposite materials as a function of their numerous advantages in the packaging industry today and in the future.

1.9 Effects of nanocomposites onto different properties :

1.9.1 Particle Loadings :

It is important to recognize that nanoparticulate/fibrous loading confers significant property improvements with very low loading levels, traditional microparticle additives requiring much higher loading levels to achieve similar performance. Composite with nano materials exhibits very good weight to strength ratio. This in turn can result in significant weight reductions (of obvious importance for various military and aerospace applications) for similar performance, greater strength for similar structural dimensions and, for barrier applications, increased barrier performance for similar material thickness.

1.9.2 Effect of nanoparticles on mechanical properties :

Nanocomposites offer numerous advantages over respective virgin materials or conventional composites, including high strength to weight ratios, resistance to electrochemical corrosion, ease and speed of application [154-156].

The inherent mechanical properties of the matrix material are modified by the introduction of the reinforcing nanoparticulates. The mechanical properties of composite material depend on the material properties of the two consistent components of their interface, as well as the amount of reinforcing materials of its geometrical arrangement within the matrix. The amount of reinforcements and their arrangement are determined by the composite fabrication process [157].

The mechanical properties with a high aspect ratio and a high Young's modulus and tensile strength, in combination with electrical and thermal conductivity make them interesting materials for the use of nano fillers in polymers and open up new perspectives for multi functional materials, e.g. conductive polymers with improved mechanical performance [158].

Modification of nano SiO_2 in epoxy resin based composite was more effective than that of standard SiO_2 for tensile properties and impact properties due to large specific surface area and active groups on surfaces of nano-SiO_2 particles. Similar behaviour has been shown for the toughness of epoxy resin based composites with nano-SiO_2 and standard SiO_2 in SEM images [159-160].

Data provided by Hartmut Fischer of TNO in the Netherlands relating to polyamide-montmorillonite nanocomposites indicates tensile strength improvements of approximately 40 and 20% at temperatures of 23ºC and 120ºC respectively and modulus improvements of 70% and a very impressive 220% at the same temperatures. In addition Heat Distortion Temperature was shown to increase from 65ºC for the unmodified polyamide to 152ºC for the nanoclay-modified material, all the above being achieved with just a 5% loading of montmorillonite clay. Similar mechanical property improvements were presented for polymethyl methacrylate – clay hybrids. Further data provided by Akkepeddi of Honeywell [157] relating to polyamide-6 polymers confirms these property trends. In addition, the further benefits of short/long glass fibre incorporation, together with nanoclay incorporation, are clearly revealed.

1.9.3 Flammability Reduction :

The ability of nanoclay incorporation to reduce the flammability of polymeric materials was a major theme of the paper presented by Gilman of the National Institute of Standards and Technology in the US [150]. Gilman demonstrated the extent to which flammability behavior could be restricted in polymers such as polypropylene with as little as 2% nanoclay loading. In particular heat release rates, as obtained from cone calorimetry experiments, were found to diminish substantially by nanoclay incorporation. Although conventional microparticle filler incorporation, together with the use of flame retardant and intumescent agents would also minimize

flammability behavior, this is usually accompanied by reductions in various other important properties. With the nanoclay approach, this is usually achieved whilst maintaining or enhancing other properties and characteristics.

1.9.4 Barriers Properties :

The gaseous barrier property improvement that can result from incorporation of relatively small quantities of nanoparticles materials is shown to be substantial. Data provided from various sources indicates oxygen transmission rates for Nanocomposites which are usually less than half that of the unmodified polymer [161-164].

Further data reveals the extent to which both the amount of nanoparticles incorporated in the polymer, and the aspect ratio of the filler contributes to overall barrier performance. In particular, aspect ratio is shown to have a major effect, with high ratios (and hence tendencies towards filler incorporation at the nano-level) quite dramatically enhancing barrier properties. Such excellent barrier characteristics have resulted in considerable interest in $CaCO_3$,Fe_2O_3 $BaSO_4$ nanocomposites in high performance coating, which is give excellent resistant of coating to penetrate the corrosive species. In food packaging applications, both flexible and rigid. Specific examples include packaging for processed meats, cheese, confectionery, cereals and boil-in-the-bag foods, also extrusion-coating applications in association with paperboard for fruit juice and dairy products, together with co-extrusion processes for the manufacture of beer and carbonated drinks bottles. The use of nanocomposite formulations would be expected to enhance considerably the shelf life of many types of food.

Honeywell have also been active in developing a combined active/passive oxygen barrier system for polyamide-6 materials [150]. Passive barrier characteristics are provided by nanoclay particles incorporated via melt processing techniques whilst the active contribution comes from an oxygen-scavenging ingredient (undisclosed). Oxygen transmission results reveal substantial benefits provided by nanoclay incorporation in comparison to the base polymer (rates approximately 15-20% of the bulk polymer value, with further benefits provided by the combined active/passive system). Akkapeddi suggests that the increased tortuosity provided by the nanoclay

particles essentially slows transmission of oxygen through the composite and drives molecules to the active scavenging species resulting in near zero oxygen transmission for a considerable period of time.

1.9.5 Optical Properties :

Optical properties are a function of the properties at the interfaces. The magnitude of the difference in refractive index across an interface determines, in part, the light-scattering efficiency. Other factors include the size of the scattering species relative to the light wavelength. Air voids included in the film act as additional scattering centers, improving the "dry hiding" in paint films. In a given system, the light scattering coefficient was found to be linearly proportional to coating porosity [165]. Gloss is the ratio of specularly reflected light to incident light. For optically smooth surfaces, gloss varies with refractive index and angle of incidence according to Fresnel's law. Gloss is a function of roughness, an increasing roughness degrades gloss [166] showed for a $Ti0_2$ paints with different lattices (particle size ranging from 200 nm to 1200 nm) the development for gloss for different incidence angles. A minimum in gloss was found at the critical pigment volume concentration. However the CPVC values were found to be different for different incident angles, depending on surface roughness. An incident angle of 85" was found to correlate best with the CPVC.

Size distributions of particles influence the bulk structure. A narrow distribution results in a bulky structure where a polydisperse pigment packs with a higher density. Brightness and opacity are a function of the coatings' light scattering ability. The light scattering coefficient was found to be linear proportional to coating porosity. The absorption or emission wavelength can be controlled by size selection, interaction with ligands and external perturbations. For example, transparency can be achieved if the nanoparticle size is below the critical wavelength of light. This makes nanoparticles (e.g. metals, silicates or metal oxide ceramics) very suitable for barrier films and coating applications, combining transparency with other properties (UV, IR-absorption, conductivity, mechanical strength, etc.). In addition, interesting optical (light absorbing/filtering) properties can be used for cosmetic applications.

1.10 Applications :

In the forgoing discussion, it has been observed that nanocomposites have set the current trend in the novel materials drawing considerable interest due to the unusual properties displayed by them. Several authors have adopted various techniques to prepare nanocomposites . However, the techniques they utilized are very cumbersome which require careful control of various parameters such as pH, moisture, temperature etc.

In recent years significant progress has been achieved in the synthesis of various types polymer-nanocomposites and in the understanding of the basic principles, which determine their optical, chemical, barrier, electronic and magnetic properties. As a result nanocomposite-based devices, such as light emitting diodes, photodiodes, photovoltaic solar cells and gas sensors, have been developed, often using chemically oriented synthetic methods such as soft lithography, lamination, spin-coating or solution casting. Milestones on the way in the development of based-based devices were the discovery of the possibility of filling conductive polymer matrices, such as polyaniline, substituted poly (paraphenylenevinylenes) or poly (thiophenes), with semi conducting nanoparticles like CdS, CdSe, CuS, ZnS, Fe_3O_4 or Fullerenes, and the opportunity to fill the polymer matrix with nanoparticles of both n- and p- conductivity types, thus providing access to peculiar morphologies, such as interpenetrating networks, p-n nanojunctions or fractal p-n interfaces, not achievable by traditional microelectronics technology [167-169].

The peculiarities in the conduction mechanism through a network of semiconductor nanoparticle chains provide the basis for the manufacture of highly sensitive gas and vapor sensors. These sensors combine the properties of the polymer matrix with those of the nanoparticles. It allows the fabrication of sensor devices selective to some definite components in mixtures of gases or vapors. Magnetic phenomena, such as superparamagnetism, observed in polymer-nanocomposites containing Fe_3O_4 nanoparticles in some range of concentrations, particle sizes, shapes and temperatures, provide a way to determine the limits to magnetic media storage density [170].

Over the last decades, the polymer nanocomposites application have gained their commercial footing, due in large part to the efforts of resin manufacturers, compounding and master batch producers who now offer user friendly products. Nanocomposites differ from traditional plastic composites in that they provide these properties with minimal impact on articles weight and they do so without providing penalties. Lastly in packaging nanocomposites deliver with good clarity, a combination not possible using traditional composites approaches.

Such mechanical property improvements have resulted in major interest in nanocomposite materials in numerous automotive and general/industrial applications. These include potential for utilization as mirror housings on various vehicle types, door handles, engine covers and intake manifolds and timing belt covers. More general applications currently being considered include usage as impellers and blades for vacuum cleaners, power tool housings, mower hoods and covers for portable electronic equipment such as mobile phones, pagers etc.

1.10.1 Food Packaging :

Triton systems and the US Army are conducting further work on barrier performance in a joint investigation. The requirement here is for a non-refrigerated packaging system capable of maintaining food freshness for three years. Nanoclay polymer composites are currently showing considerable promise for this application. It is likely that excellent gaseous barrier properties exhibited by nanocomposite polymer systems will result in their substantial use as packaging materials in future years. A somewhat more esoteric possibility arising from enhanced barrier performance recently suggested has been blown–films for artificial intestines [150-151].

1.10.2 Fuel Tanks :

The ability of nanoclay incorporation to reduce solvent transmission through polymers such as polyamides has been demonstrated. Data provided by De Bievre and Nakamura of UBE Industries reveals significant reductions in fuel transmission through polyamide 6/66 polymers by incorporation of nanoclay filler. As a result, considerable interest is now being shown in these materials as both fuel tank and fuel line components for cars. Of further interest for this type of application, the reduced

fuel transmission characteristics are accompanied by significant material cost reductions [123-124].

1.10.3 Films :

The presence of filler incorporation at nano-levels has also been shown to have significant effects on the transparency and haze characteristics of films. In comparison to conventionally filled polymers, nanoclay incorporation has been shown to significantly enhance transparency and reduce haze. With polyamide based composites, this effect has been shown to be due to modifications in the crystallization behavior brought about by the nanoclay particles; spherulitic domain dimensions being considerably smaller. Similarly, nano-modified polymers have been shown, when employed to coat polymeric transparency materials, to enhance both toughness and hardness of these materials without interfering with light transmission characteristics. An ability to resist high velocity impact combined with substantially improved abrasion resistance was demonstrated by Haghighat of Triton Systems [152-153].

1.10.4 Environmental Protection :

Water laden atmospheres have long been regarded as one of the most damaging environments, which polymeric materials can encounter. Thus an ability to minimize the extent to which water is absorbed can be a major advantage. Data provided by Beall from Missouri Baptist College indicates the significant extent to which nanoclay incorporation can reduce the extent of water absorption in a polymer [171]. Similar effects have been observed by van Es of DSM with polyamide based nanocomposites [172]. In addition, van Es noted a significant effect of nanoclay aspect ratio on water diffusion characteristics in a polyimide nanocomposite. Specifically, increasing aspect ratio was found to diminish substantially the amount of water absorbed, thus indicating the beneficial effects likely from nanoparticle incorporation in comparison to conventional microparticle loading. Hydrophobic enhancement would clearly promote both improved nanocomposite properties and diminish the extent to which water would be transmitted through to an underlying substrate. Thus applications in which contact with water or moist environments is likely could clearly benefit from materials incorporating nanoclay particles.

1.10.5 Pigments and coatings :

Nano products can be used for the creation of superior pigments and coatings. These can provide high U. V. attenuation, provide transparency to visible light when desired and can be dispersed in a wide range of materials easily. Nano coatings can offer more vivid colors that will resist the deterioration and fading over a time. These powders can also be used to make thixotropic materials that are used in paints to help them flow better [173-176].

The objective of this research was to develop nanoparticles of Fe_2O_3 to replace phosphate pigments in anticorrosive paints. The anticorrosive properties of nanocomposites coating were studied using electrochemical techniques, employing a dispersion of the inhibitor in the adequate supporting electrolyte and formulating anticorrosive coatings. Coatings performance was evaluated by accelerated (humidity chamber and salt spray test) and electrochemical (corrosion potential, ionic resistance, and polarization resistance) tests [177].E.g.: Al_2O_3, ZnO, $CaCO_3$, Fe_2O_3, TiO_2 is used for making corrosion resistant coatings, UV protecting clear coats and powder coatings, radar absorbing coating, transparent clear coating respectively.

1.10.6 Catalysis :

Noble metals such as palladium and platinum are used for catalysis in important chemical synthesis, including hydrogenation, oxidation etc. To achieve a high performance-to-cost ratio, catalysts are required to have, amongst other important attribute, a large surface area of the catalytically active metal. As such nanoparticles are, by virtue, highly suitable to surve as catalyst [178].

1.10.7 Magnetics :

Nano sized particles can provide new and unique magnetic properties for use in existing and future technologies. E.g.: Fe_2O_3 is used as Ferro fluids and magneto rheological fluids [177].

1.10.8 Corrosion :

Coating may be described by their appearance (eg: clear, pigmented, metallic, or glossy) and by their function (eg: corrosion protection, abrasive resistance, skid resistance, decorative or photo sensitive). Coating is used to describe the material

(usually, liquid and powder form) that is applied to substrate, the resulting to form uniform layer after drying or baking the process. Coatings were used for decorative and identification purpose thousands of years before they were used for the protective coating purpose. One of the most effective systems consisted of a red lead linseed oil primer plus a linseed oil-graphite top coat. This was the first real protective coating. The protective coating is a material composed essentially of synthetic resins or inorganic resin polymers which, when applied to a suitable substrate, will provide a continuous coating that will resist industrial or marine environment and prevent serious breakdown of basic structure [179-181].

In order to provide corrosion protection, the protective coating must also:

(1) Resist the penetration of ions from salts through the coating

(2) Resist the action of moisture osmosis

(3) Maintain a good appearance, under weather conditions.

(4) High degree of adhesion to the substrate

(5) Minimum discontinuity in coating (porosity)

(6) Sufficient thickness (the greater the thickness, the more the resistance)

(7) Low diffusion rate for ions such as Cl^- and for H_20

1.11 Nanoparticles for coatings :

To improve corrosion resistance of the whole system, we must consider the metal surface preparation, primer, intermediate and add organic and inorganic corrosion protective additives in synthetics resins [182-183].

Coatings can be classified in the following categories according to corrosion resistance:

(1) Conversion coatings

(2) Anodic coatings

(3) Cathodic coatings

(4) Barrier coatings

1.11.1 Conversion coatings :

Phosphate and chromate coatings are examples of conversion coatings. Conversion coatings are so-called because the surface metal is converted into a compound having the desired porosity to act as a good base for paint. The mechanical

and electrical properties of the nanotubes contribute to the critical corrosion control properties of these coatings. The electrical properties of the tubes enables the coatings to overcome a basic problem associated with organic coatings, they are non-conductive. In this coating system the nanotube provide a highly conductive electron path through the binder. In the event of a coating break a cathodic potential is established. Electrons are transferred from an optimized amount of sacrificial metal particles such as zinc or aluminum through the resin system to the steel substrate [184].

1.11.2 Anodic coatings :

By anodic coating, it is meant that a coating which is anodic to the substrate, such as zinc aluminum or cadmium coatings. On steel such coatings are generally called sacrificial coatings. If oxygen concentration near the anode is high enough, ferrous ions are oxidized to ferric ions soon after they are formed at the anodic surface. Since ferric hydroxide is less soluble in water than ferrous hydroxide, a barrier of hydrated ferric oxide forms over the anodic areas. Suppression of corrosion by retarding the anodic reaction is called *passivation.* The iron said to be passivated. It protects the substrate at the expense of the metallic coating applied. The zinc coatings protect the substrate by acting as a sacrificial anode for the steel. The electrons are consumed by the iron substrate, which acts as a cathode. The potential is made more negative by electrons and a cathodic reaction is forced to occur on it. A fine film of H_2 is formed on the surface. The steel being cathodic does not corrode. Thus, by acting as a sacrificial material, zinc corrodes while the steel substrate is protected [185].

1.11.3 Cathodic coatings :

If steel is connected to the positive pole of a battery or a direct current a source while the negative pole is connected to a carbon electrode, and both electrodes are immersed in salt water, the steel does not corrode. The impressed electrical potential makes the entire steel surface cathodic relative to the carbon anode. The result is electrolysis of water than corrosion of steel. This is an example of cathodic protection. In this type of coating, the metals, which are deposited, are electropositive to the substrate. For instance, for copper coated steel, copper ($E° = +0.337$ V) is

positive to steel (E^0=-0.440V). Cathodic protection is offered by sacrificial coatings, such as zinc rich epoxies, which prevent discharge of current from steel to electrolyte by electrical attachment of less passive anode. In this case, the metal surface becomes entirely cathodic and the corrosion is retarded .The cathodic protection with zinc is widely employed in coatings used as primers for naval industry but the only drawback of this technique is that large amounts of zinc is required to prolong the lifetimes of the metal which provide sometimes a loss of adherence, high porosity film and high solid content to the paint [186].

1.11.4 Barrier coatings :

Barrier coating with polymer filled system prevents oxygen and water ralter the chemicals to react with the base steel [187]. Because of the present of filler Nanoparticles particles, the chemical has to go through path and hence it is prevented to react based metal quickly. Increase in aspect ration of the filler will enhance the barrier properties. When the particle size of the filler is reduced, the increase in surface area . result in prevention of chemical to flow easily through the coated layer[188]. So nanoparticles filled insulating polymer act as anti corrosive coating. Good chemical resistant coatings are less sensitive for attack from water and chemicals and therefore formation of conductive pathway will be more difficult [189] must be in direct molecular contact with the surface of the steel. Barriers that can prevent oxygen and water from reaching the surface prevent corrosion. Barrier coatings are of four types anodic oxides, inorganic coatings, inhibitive coatings and organic coatings.

(1) Anodic Oxides :

A layer of AI_2O_3 is produced on aluminum surface by electrolysis. As the oxides are porous, they are sealed by a solution of potassium dichromate. The object of sealing is to minimize porosity. However, chromates have health hazards and are not allowed in some countries.

(2) Inorganic Coatings :

These include coatings like ceramics and glass. Glass coatings are virtually impervious to water. Cement coatings are impervious as long as they are not mechanically damaged.

(3) Inhibitive Coatings :

In several instances, inhibitors are added to form surface layers which serve as barriers to the environment. Inhibitors, like cinnamic acid, are added to paint coatings to prevent the corrosion of steel in neutral or alkaline media.

(4) Organic Coatings :

Epoxy, polyurethane, polyester, silicone chlorinated rubber and vinyl coatings are extensively used in industry. They serve as a barrier to water, oxygen, and prevent the occurrence of a cathodic reaction beneath the coating. The barrier properties are further increased by addition of an inhibitor, like chromate in the primer.

Organic paints as a barrier coating, has numerous advantageous. It presents a low cost, ease of manufacturing and application and a wide range of products available. However, the exact mechanism by which barrier coatings protect the metal surface from corrosion is still in debate. Some authors say that the barrier coating can block the passage of oxygen and water reaching the metal surface and others think that the protection offered by organic coating is owing to their high electrical resistance above the interface thus preventing external flow between anodic and cathodic areas [190-191].

Organic coatings are commonly used to protect metals against corrosion. The efficacy of these coatings, which provide thin, tough, and durable barriers to the substrate, depends on many factors like the suitability of organic materials by themselves, how they are applied on the metallic surface, the conditions of the corrosive environment, etc. Organic coating can be classified by thermoset and thermoplastics coating. Phenolic (phenyl formaldehyde), MF resin, UF resin, chlorinated rubbers, vinyl, silicone, alkyds, acrylics, epoxies, polyurethane resins are the few important examples for protective organic coatings. Epoxy resins are the most important example of thermoset coating and acrylic, alkyds, PVB etc are the example of thermoplastic resin. *Epoxy resins* are used for a wide variety of protective coatings because of their excellent adhesion, good mechanical properties and their notable chemical resistance under different aggressive environments, such as wet and high-humidity conditions [177].

The epoxy coating works well, but over time the barrier coating can fail due to prolonged exposure to the environment. The organic coating can develop what is called, "under coating corrosion" which initiates from weak spots and develops into blisters and film form threads leading to corrosion .The organic protective coating (barrier coating) fails by separation process known as delamination, caused by the separation at the coating/metal interface. The under film corrosion occurs as a direct consequence of the electrochemical mechanism of corrosion. At its simplest, a corroding system is driven by two spontaneous coupled reactions, which take place at the interface between the metal and an aqueous environment. One is a reaction in which chemical species from the aqueous environment remove electrons from the metal; the other is a reaction in which metal surface atoms participate to replenish the electron deficiency. The exchange of electrons between the two reactions constitutes an electronic current at the metal surface and an important effect is to impose an electric potential on the metal surface of such a value that the supply and demand for electrons in the two coupled reactions are balanced. In the sites where delamination has occurred, the anodic (electron generation) and the cathodic (electron consuming) reactions take place. The kinetics barriers are at a minimum due to the high electrical conductivity of the metal, which provides an easy pathway for electrons between the anodic and cathodic areas, i.e., promoting the metal to corrosion.

1.12 Vinyl Coatings :

Most vinyl coatings consist of a resin made up of a polymer of polyvinyl chloride (PVC), polyvinyl acetate (PVA), polyvinyl Butyral (PVB) and their copolymers in different the ratio of PVA. Vinyl coatings have excellent flexibility and resist abrasion, water, acids, and alkalis.(ref) Vinyl coatings are, however, susceptible to strong solvents. With nanocomposites such properties can be enhanced [192].

1.12.1 Polyvinyl Butyral :

PVB is used as a film-forming component in corrosion-inhibiting primers for metals called wash primers or metal conditioners. These wash primers are used as a pretreatment to provide good adhesion to a variety of surfaces including stainless steel, carbon steel, zinc, tin, aluminum, and galvanized steel among others. These

wash primers are effective at inhibiting underfilm corrosion in applications where exposure to salt water or salt spray is more or likely to be exposed. To achieve highest performance, incorporation of nanoparticulates of different particles size and particles can be used. Wash primers with a nano particulates coating is extremely effective in seawater and freshwater immersion exposures [192-193].

1.12.2 Polyvinyl Acetate :

Poly(vinyl acetate)s acquire a unique combination of the following properties adhesion to a wide variety of surfaces, chemical and solvent resistance (especially when crosslinked), good electrical properties, heat stability, film clarity, and physical toughness. These properties, alone or in combination, make these polymers useful in certain coating and adhesive formulations as the principal or as a minor constituent. Their compatibility with other resins, due largely to their unique chemical compositions, permits blending with other resins, resulting in properties not achievable with either component alone [194-195].

1.12.3 Polyvinyl Chloride-Polyvinyl Acetate Copolymers :

Polyvinyl chloride-polyvinyl acetate (PVC-PVA) copolymer solution coatings are known for excellent mechanical properties, high toughness, and water resistance. These coatings dry rapidly by solvent evaporation to form extremely durable coatings suitable for use in marine or corrosive environments. By incorporating nanoparticles its mechanical and chemical resistance gets enhanced further depending upon particulate loading and its size. PVC-PVAc coatings are generally low in solids; as a result each sprayed coat may yield better coat compare to coating without nanoparticulates. These coatings have the added advantage of drying rapidly enough that several coatings can be applied in a 24-hour period. The Navy has used these coatings for antifouling applications as well.

1.12.4 Epoxy :

Cured epoxy resins exhibit excellent adhesion to a variety of substrates; outstanding chemical and corrosion resistance; excellent electrical insulation; high tensile, flexural, and compressive strengths; thermal stability; a wide range of curing temperatures; and low shrinkage upon cure. Epoxy powder coatings are known to be

superior in many respects to regular paints due their scratch hardness, adhesion,and chemical resistant etc. [196-197].

1.13 Stability and corrosion protection by organic coatings :

The effectiveness of the coating is proven by its protection of the underlying metal surface. The performance of the coating depends among other factors, mainly on the barrier to diffusion of ions and prevention of corrosion by additives in the coating. The corrosion properties are studied by electrochemical impedance measurements. These are detailed in the following.

When two complementary processes: such as those illustrated in figure and given below occur over a single metallic surface:

Anodic reaction: $M \rightarrow M^{n+} + ne^{-}$

Cathodic reaction:

$2H^{+}+2e^{-} \longrightarrow H_2$ (in acidic medium)

$4H^{+}+O_2+4e^{-} \longrightarrow 2H_2O$ (in acidic medium containing dissolved oxygen)

$4H^{+}+O_2+2H_2O \longrightarrow 4OH^{-}$ (in neutral or basic medium)

1.13.1 Polarization measurements (Tafel Plot) :

The potential of materials will no longer be at an equilibrium value. This deviation from equilibrium potential is called polarization. Electrodes can also be polarized by the application of an external voltage. The magnitude of polarization is usually measured in terms of overpotential η, which is a measure of polarization with respect to the equilibrium potential E_{eq} of an electrode. This polarization is said to be either anodic, when the anodic processes on the electrode are accelerated by changing the specimen potential in positive direction, or cathodic, when the cathodic processes are accelerated by moving the potential in negative direction. Overpotentials corresponding to the anodic and cathodic polarization are called anodic (η_a) and cathodic (η_c) overpotential, respectively. Overpotential can be expressed as follows: $\eta = E - E_{eq}$ (*E* is applied potential).

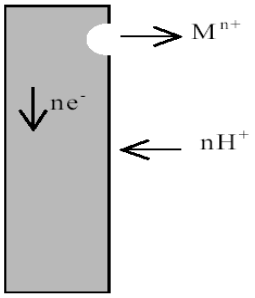

Figure 1.4 : Simple model describing the electrochemical nature of corrosion processes

During polarization, reduction and oxidation reactions occurring on the surface of metal produce a net electric current on the surface of metal. The sum of current density of these reactions is related to overpotential by Butler-Volmer equation:

$$i = i_0\left\{\exp\left(\alpha\frac{nF}{RT}\eta\right) - \exp\left[-(1-\alpha)\frac{nF}{RT}\eta\right]\right\} \quad (2)$$

Where: i_0 = exchange current density (anodic or cathodic current density at the equilibrium potential E_{eq})

α = charge transfer barrier or symmetry coefficient for the anodic or cathodic reaction, close to 0.5

η = overpotential and equal with $E_{applied} - E_{eq}$

n = number of participating electrons

R = gas constant

T = absolute temperature

F = Faraday constant

Under anodic and cathodic polarization individually, the Butler-Volmer reduces

$$i_a = i_0\left[\exp\frac{\alpha nF}{RT}\eta_a\right] \quad (\text{for } i_a >> i_c\ ,\ \eta_a >> \eta_c) \quad (3)$$

$$|i_c| = i_0\left[-\exp\frac{-(1-\alpha)nF}{RT}\eta_c\right] \quad (\text{for } |i_c| >> i_a\ ,\ |\eta_c| >> \eta_a) \quad (4)$$

Solving these two equations for the overpotential yields:

$$\eta_a = -(RT/\alpha nF)\ln i_0 + (RT/\alpha nF)\ln i_a \quad (5)$$

Both of these equations can be written in a short form called Tafel equation:

$$\eta = a \pm b \log i \qquad (6)$$

where: *b* is known as Tafel slope of the anodic or cathodic reaction (anodic) overpotential $b_a = (RT/\alpha nF)$, cathodic overpotential $b_c = RT/(1-\alpha)nF$, the ± sign uses for anodic and cathodic overpotential, respectively. A plot of applied potential (or overpotential) versus logarithm of current density is called Tafel plot in which the values of Tafel slopes, corrosion potential E_{corr}, and corrosion current density i_{corr} can be determined using extrapolation (Figure 12). Since, polarization resistance and corrosion rate will be obtained by using Stern-Geary equation: [50,52,53]

$$R_p = \frac{b_a \cdot b_c}{2.303(b_a + b_c)} \cdot \frac{1}{i_{corr} \cdot A} \qquad (7)$$

And corrosion rate can be calculated using equation: [54,55]

$$C_R = \frac{0.129 \cdot i_{corr} \cdot (EW)}{A \cdot d} \qquad (8)$$

Where: C_R = corrosion rate, icorr = current density of corrosion, ba, b_c = Tafel slope of anodic and cathodic reactions, Rp = polarization resistance, A = corroded area, d = density of the materials

Polarization measurements were carried out under ambient condition in a three electrode single electrochemical cell containing 3.5 % NaCl solution. All measurements were performed on computerized electrochemical analyzer (supplied by CH instruments, USA). SS 316 Steel electrode(after coating) as WE, Saturated Calomel Electrode (SCE) as Reference electrode and platinum electrode as counter electrode, using electrochemical analyzer (USA) unit of model CH1604B. Measurements were carried out at a potential range from -0.7 to +0.7 and scan rate of 5mV/s.

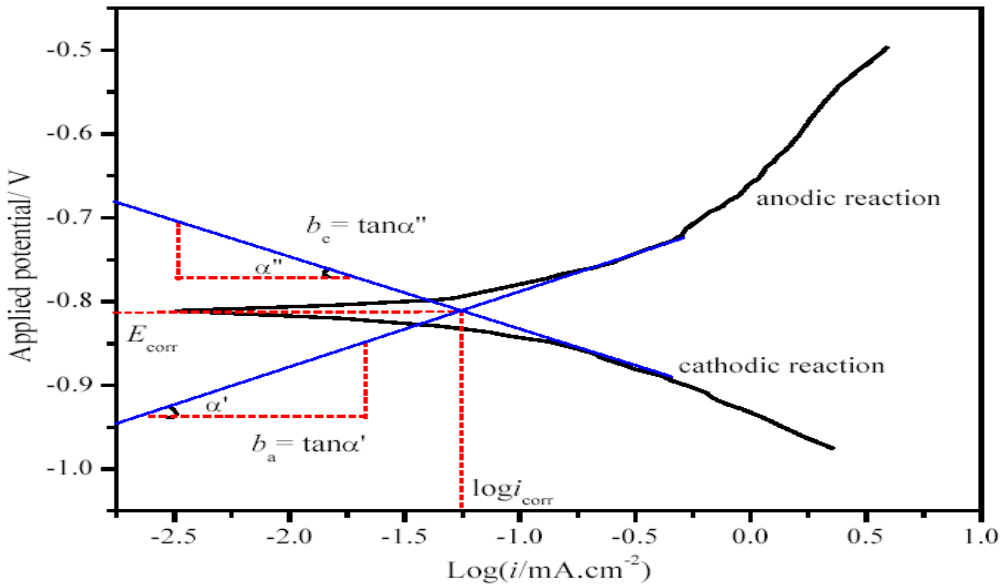

Figure 1.5 : Schematic polarization curve showing Tafel extrapolation

1.13.2 Electrochemical Impedance Spectroscopy (EIS) :

Electrochemical impedance is usually measured by applying an ac potential to an electrochemical cell and measuring the current through the cell. Suppose that we apply a sinusoidal potential excitation. The response to this potential is an ac current signal, containing the excitation frequency and its harmonics. This current signal can be analyzed as a sum of sinusoidal functions (a fourier series). EIS data is commonly analyzed by fitting it to an equivalent electrical circuit model. Most of the circuit elements in the model are common electrical elements such as resistors, capacitors, and inductors. To be useful, the elements in the model should have a basis in the physical electrochemistry of the system. Table 2.3 lists the common circuit elements, the equation for their current versus voltage relationship, and their impedance.

Table 1.1 : Component Current Vs. Voltage Impedance

Component	Current Vs. Voltage	Imedance
Resistor	**E = IR**	**Z = R**
Inductor	**E = L di/dt**	**Z = jwL**
Capacitor	**I = C dE/dt**	**Z = 1/jwC**

By analyzing the capacitance in organic coatings, it is possible to evaluate the water uptake phenomena occurring in organic coatings in wet environment, because water diffusion can modify the dielectric constant of the polymer even if present in very small amounts [198]. Capacitance is quite sensitive to water uptake since the dielectric constant of water is about 20 times larger than that of the coating. The coating capacitance can be expressed by the following equation :

$$C_c = \varepsilon \varepsilon_o A/d \qquad (9)$$

Where C_c is the capacitance, ε is the dielectric constant of the medium and ε_0 is the permittivity of free space and d is the thickness of the coating By applying a simple empirical mixing rule it is possible to correlate the dielectric constant at time t (ε_t) the dielectric constant of the polymeric matrix (ε_m), the dielectric constant of water (ε_w), the volume fraction of water at time t (φ_t) and the volume fraction of water at saturation (φ_s).

$$\varepsilon_t = \varepsilon_m^{1-\theta s} \varepsilon_w^{\theta t} \qquad (10)$$

Taking ln on both sides and rearranging the terms, we get

$$\theta_t = [\ln(\varepsilon_t) - \ln\{\varepsilon_m^{1-\theta s}\}]/\ln\varepsilon_w \qquad (11)$$

Replacing the values in equation 3, we get

$$\theta_t = \log(C_t / C_0) / \log\varepsilon_w \qquad (12)$$

Where C_t is the capacitance after time t, C_0 is the initial capacitance and . Equation 6 is the Brasher Kingsbury equation and it is widely used for calculation of the water amount from capacitance measurements in organic coatings. Electrochemical Impedance is normally measured using a small excitation signal. If the real part is plotted on the Z axis and the imaginary part on the Y axis of a chart, we get a "nyquist plot". Notice that the y axis is negative and that each point on the nyquist plot is the impedance at one frequency. This is true for EIS data where impedance usually falls as frequency rises. On the nyquist plot the impedance can be

represented as a vector of length |Z|. The nyquist plot in Figure 2.5 results from the electrical circuit of Figure 1.6.

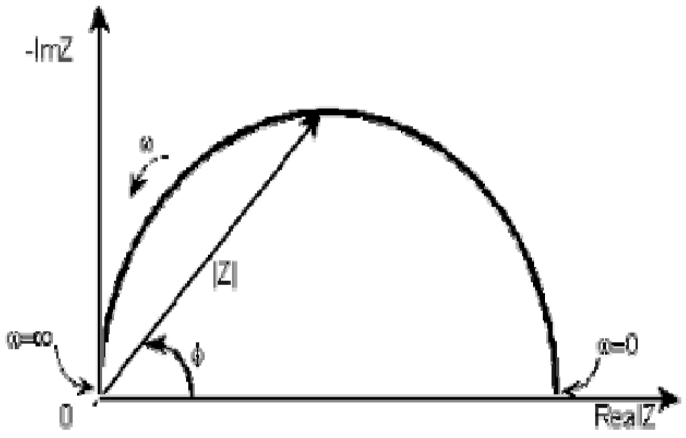

Figure 1.6 : Typical Nyquist plot with impedance vector

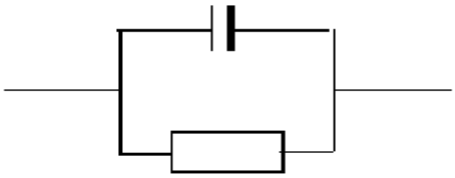

Figure 1.7 : Simple equivalent circuit with one time constant

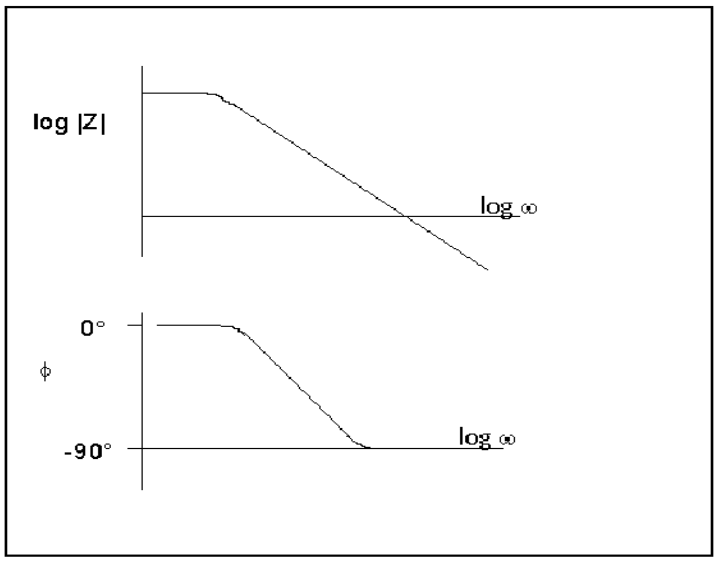

Figure 1.8 : Typical Bode plot with one time constant

The semicircle is characteristic of a single "time constant". Electrochemical Impedance plots often contain several time constants. Often only a portion of one or more of their semicircles is seen. Another popular presentation method is the "bode plot". The impedance is plotted with log frequency on the x-axis and both the absolute value of the impedance ($|Z| = Z_0$) and phase-shift on the y-axis. The bode plot for the electric circuit of Figure 1.6 is shown in Figure 1.7. Unlike the nyquist plot, the bode plot explicitly shows frequency information.

1.13.3 Lifetime Prediction Using EIS :

Accelerated life testing of polymeric coatings is used in many areas of science and technology to determine the effective lifetime of the coatings. In such a test, one seeks a physical or chemical acceleration of the coating by placing it under stress larger than it would receive in its normal lifetime and monitor its performance to failure from that stress[199]. Ideally stress only causes the system to fail faster than it normally would, but the mechanism of failure remains the same as in the non-accelerated conditions. Low frequency impedance ($|Z|_0$) data can be used to predict the corrosion protection lifetimes of organic coatings on metals. The time taken for a coating to decay to a specific failure modulus value, $|Z|_{fail}$ can be given by the following equation :

$$T_{fail} = \theta \left[\ln \left(\frac{|Z|_0 - |Z|_m}{|Z|_{fail} - |Z|_m} \right) \right] \qquad (13)$$

Where $|Z|_0$ = Low frequency impedance at time t=0
$|Z|_m$= Limiting bare metal value
$|Z|_{fail}$= Specific failure modulus
θ = Decay constant (inverse of slope of ln ($|Z|t - |Z|m$) vs. Exposure time.

Thus the electrochemical studies can lead to estimate of the parameters related to coating behaviour under corrosive environment and also these studies give an insight into the corrosion protection mechanism of the coatings.

1.14 Aim and Scope of work :

The above review of the historical development in the field of composite and nanocomposites indicate that there is a good scope for improvement in properties of organic coating in particular vinyl coating. By incorporating nanoparticulates of different sizes into the matrix so as to get tailor made properties.

The main aim of the present investigations is to explore various possibilities of synthesis of nanoparticles of various size for vinyl coating application amongst various vinyl coatings matrix we have selected nanocomposites of PVB, PVAc, Epoxy for coating application for corrosion resistance as they are widely used and most preferred, due to their excellent mechanical properties and resistance to acids and alkalis.

Amongst the various methods for nanoparticulates synthesis PMG method is most suitable for coating application because of the polymer system used for synthesis of nanoparticulates which is compatible with coating application or formulation.

The nanosize particles obtained from such synthesis will be incorporated in a polymer matrix, which can be subsequently mixed with PVB, PVAc, Epoxy, nanoparticulate filled composites. Nanocomposites prepared were studied for optical properties and barrier properties with emphasis on impedance spectroscopy. The nanocomposites were studied on application of nanoparticulate additive for coatings for effects of nano size on enhanced corrosion resistance properties. This includes not only the barrier to diffusion of ions through the bulk but also electrical potential barrier to charge transfer.

In addition to the corrosion resistance, the optical properties which are important for appearance of the coating like gloss, opacity and clarity are also likely to improve. Normally the commercial additive /fillers have to be incorporated at high level so as to obtain the barrier properties but similar performance is obtained at very less level of nano size filler. Thus, these studies will be useful in developing specialty coating for industrial and other application.

References :

[1] Feynman Richard, *Caltech Engineering and Science*, February **1960**, Volume 23:5, pp 22-36.

[2] BSI PAS 71: *vocabulary. Nanoparticles*, **2005**, accessed on 13 2008. www.bsigroup.com/nano.

[3] Hannah, W., Thompson, P.B., Nanotechnology, risk and the environment : a review, *Journal of environmental Monitoring*, **2008**, 10, 291-300.

[4] ISO/TR 27628: Workplace atmospheres, Ultrafine, nanoparticles and nano-Structured aerosols. *Inhalation exposure characterization and assessment*, **2007**, accesed on 13 Nov 2008. www.iso.org

[5] Herve-Bazin, B., Les nanoparticules-un enjeu majeur pour la sante au travail?, Les Ulis, EDP *Sciences*, **2007**

[6] Lauterwasser, C., Small sizes that matter;oppourtunities and risks of nanotechnologies, report in co-operation with the OECD *International Futures Programme*,2008, accessed on 13 November **2008**. http://www.oecd.org /dataoecd /37/19/37770473.pdf

[7] Tari G. and Ferreira J.M.F. , *Ceramics International*, **1998**, 24, pp. 527–532.

[8] Luis F. Hakim, David M. King, Yun Zhou, Christopher J. Gump, Steven M. George,and Alan W. Weimer *Adv. Funct. Mater*. **2007**, 17, 3175–3181.

[9] Ramanathan T, Stankovich S, Dikin DA, Liu H, Shen H, Nguyen ST, *J Polymer Sci B Polymer Phys* **2007**, 45, 2097–112.

[10] Dotzauer, D.M.; Dai, J.; Sun, L. & Bruening, M.L. **2006**, *Nano Letters*, 6, 10, 2268-2272.

[11] Gadhe, J.B. & Gupta, R.B. **2007**. *International Journal of Hydrogen Energy*, 32,13, 2374-2381.

[12] Royal Society and Royal Academy of Engineering **2004**, *Nanoscience and Nanotechnologies: Opportunities and Uncertainties*, London, www.nanotec.org.uk/ finalReport.htm>.

[13] Cientifica Ltd **2009**, *Nanotechnology takes a deep breath… and prepares to save the world,* 20/05, <http://cientifica.eu>.

[14] Cientifica Ltd **2008**, *Nanotechnology Opportunity Report-3rd* edition, Executive

Summary, www.cientifica.eu

[15] Berger M **2007**, *Nanowerk*, <www. nanowerk.com/spotlight/ spotid=1792.php>.

[16] Norio Tobori and Takeshi Amari *Colloids and Surfaces A: Physicochemical and Engineering Aspects,* Volume 215, 28 March **2003**, Issues 1-3, , Pages 163-171.

[17] Avella M, Errico ME, Martuscelli E. *Nano Lett* **2001**; 1: 213–7.

[18] Fayna Mammeri, Eric Le Bourhis, Laurence Rozes and Clement Sanchez *J. Mater. Chem*., **2005**, 15, 3787-3811.

[19] Ziolo R.F, Giannelis E.P.,.Weinstein B.A, O'Horo M.P., Ganguly B.N., Mehrotra V., Russel M.W., Huffman D.R. *Science,* **1992**;(257) 219.

[20] Guy A.R., *TAPPI Polymers, Laminations, and Coatings Conference Proceedings* **2004**", Indianapolis, IN.

[21] Bartzcak Z, Argon, A.S., Cohen, R.E., and Weinberg, M., *Polyme*r, **1999**, 40, 2347.

[22] Gopakumar T.G., Patel N.S., Xanthos M., *Polymer Composites*,August **2006**, Volume 27, Issue 4, pages 368–380.

[23] Abacha1 N., Kubouchi M., T. eXPRESS *Polymer Letters* **2009**, Vol.3, No.4 245–255.

[24] Lan T., Pinnavaia T., *Chemistry of Materials*, **1994**, 6, 2216–2219.

[25] Abacha N., Kubouchi M., Sakai T., Tsuda K.: *Journal of Applied Polymer Science,* **2009**, 112, 1021–1029.

[26] Torre L.; Lelli G.; Kenny J. M. *Journal of Applied Polymer Science*, **2004,** 94, 1676-1689.

[27] Costache M.C.; Jiang D.D.; Wilkie C. A. **2005**. *Polymer*, **46**, 6947-6958.

[28] Kashiwagi, T. , Wu M., Winey K., Cipriano B. H., Raghavan S. R., Douglas J. F., **2008** *Polymer*, **49**, 4358.

[29] Danuta KOTNAROWSKA *MATERIALS SCIENCE (MEDŽIAGOTYRA).* **2008**, Vol. 14,No. 4.

[30] Hanim1 H., Zarina1 R., Ahmad Fuad M.Y. , Mohd. Ishak Z.A. and Azman *Malaysian Polymer Journal (MPJ),* **2008**, Vol 3, No.12, p 38-49.

[31] Rong M. Z.; Zhang M. Q.; Ruan W. H., *Materials Science and Technology*, July **2006,** Volume 22, Number 7, pp. 787-796(10).

[32] Lee A.; Lichtenhan J. D. *Macromolecules* **1998**, 39, 4970..

[33] Chuju Y, Matsuki H., Tamki R., *Polym.Prep.Jpn*., **1993**; (42) 2973.

[34] Ziolo R.F, Giannelis E.P.,.Weinstein B.A, O'Horo M.P., Ganguly B.N., Mehrotra V., Russel M.W., Huffman D.R. *Science,* **1992**;(257) 219.

[35] Lyons A.M, Nakahara S, Marcus M.A, Pearce E.M, Waszczak J.V., *J.Phys.Chem*.,**1991**;(95)1098.

[36] Moncada E., Quijada R. and Retuert J., *Nanotechnology*, **2007**,Volume 18 Number 33 .

[37] Schmidt H., Jonschker G., Goedicke S. and Mennig M., *Journal of Sol-Gel Science and Technology*, **2000***,* Volume 19, Numbers 1-3, 39-51.

[38] Brian G. Trewyn, Igor I. Slowing, Supratim Giri, Hung-Ting Chen and Victor S.-Y. Lin *Acc. Chem. Res.*, **2007**, 40 (9)*,* pp 846–853.

[39] Stephen Mann, Sandra L. Burkett, Sean A. Davis, Christabel E. Fowler, Neil H. Mendelson, Stephen D. Sims, Dominic Walsh, and Nicola T. Whilton *Chem. Mater.*, **1997***,* 9 (11), pp 2300–2310.

[40] Radhakrishnan S.; Schultz, J. M., *J. Cryst. Growth* **1992**, 116, 378.

[41] Radhakrishnan S.*, J. Cryst. Growth* **1993**, 129, 191.

[42] Radhakrishnan S., *J. Cryst. Growth* **1994**, 141, 437.

[43] Saujanya, C.; Radhakrishnan S., *J. Mater. Sci.* ***1998***, 33, 1063.

[44] Tchmutin I.A., Ponomarenko A.T., Shevchenko V.G. and D.Yu. Godovski *Synthetic Metals*, 15 September **1994**, Volume 66, Issue 1, Pages 19-23.

[45] Sonawane P.S., Biradar S.S., Radhakrishnan S., Kulkarni B.D., *Materials Chemistry and Physics*, **2007**, Vol.105, No.2-3, 348-353.

[46] Cleo Kosanovi, Giuseppe Falini, and Damir Kralj *Cryst. Growth Des.*, **2011**, 11 (1), pp 269–277.

[47] Mingyuan Gao, Yi Yang, Bai Yang, Fenglan Bian, and Jiacong Shen, *J. Chem. Soc. Commun.*,**1994** pp 2279-2280

[48] Harmer M A, Farneth W.E.,Qun Sun.*J.Amer.Chem.Soc*.,**1996**;(118)7712.

[49] Shen J., Egerton R.. *Langmuir*,**1998**;(14)4343.

[50] Keith M. Bromley, Avinash J. Patil, Annela M. Seddon, Paula Booth, and Stephen Mann, *Adv. Mater*. **2007**, 19, 2433–2438

[51] Byunghoon Yoon, Jennifer L. O'Patchen, Dragos Seghete, Andrew S. Cavanagh, and Steven M. George, *Chem. Vap. Deposition* **2009**, 15, 112–121

52] Kickelbick, G. *Prog. Polym. Sci*. **2003**, *28*, 83.

[53] Liu, T.; Burger, C.; Chu, B. *Prog. Polym. Sci*. **2003**, *28*, 5.

[54] Juangvanich, N.; Mauritz, K. A. *J. Appl. Polym. Sci*. **1998**, *67*, 1799.

[55] Deng, Q.; Moore, R. B.; Mauritz, K. A. *Chem. Mater.* **1995**, *7*, 2261.

[56] Deng, Q.; Jarrett, W.; Moore R. B.; Mauritz, K.A. *Chem. Mater.* **1995**, *7*, 2261.

[57] Deng, Q.; Jarrett, W.; Moore R. B.; Mauritz, K. A. *J. Sol–Gel Sci. Technol.* **1996**,*7*, 177.

[58] Shao, P.L.; Mauritz, K. A.; Moore, R. B. *J. Polym. Sci., Part B: Polym. Phys* **1996**, *34*, 873.

[59] Mauritz, K. A. *Mater. Sci. Eng.* **1998**, *C6*, 121.

[60] Chujo, Y.; Saegusa, T. *Adv. Polym. Sci*. **1992**, *100*, 11

[61] Saegusa, T.; Chujo, Y. *Makromol. Chem. Macromol. Symp.* **1991**, *51*, 1.

[62] Saegusa, T.; Chujo, Y. *Makromol. Chem. Macromol. Symp.* **1992**, *64*, 1.

[63] Tamaki, R.; Chujo, Y. *Appl. Organomet. Chem*. **1998**, *12*, 755.

[64] Landry, C. J. T.; Coltrain, B. K.; Wesson, J. A.; Zumbulyadis, N.; Lippert, J. L. *Polymer* **1992**, *33*, 1496.

[65] Radhakrishnan, S.; Schultz, J. M. *J. Cryst. Growth* **1992**, *116*, 378.

[66] Radhakrishnan, S. *J. Cryst. Growth* **1994**, *141*, 437. Saujanya, C.; Ra

[67] Belfiore, L. A.; Pires, A. T. N.; Wang, Y.; Graham, H.; Ueda, E. *Ma* **1992**, *25*, 1411.

[68] Belfiore, L. A.; Graham, H.; Ueda, E. *Macromolecules* **1992**, *25*, 2935

[69] Belfiore, L. A.; McCurdie, M. P.; Ueda, E. *Macromolecules* **1993**, *26*, 6908.

[70] Bosse, F.; Das, P.; Belfiore, L. A. *Macromolecules* **1995**, *28*, 6993.

[71] Das, P. K.; Ruzmaikina, I.; Belfiore, L. A. *J. Polym. Sci., Part B: Polym. Phys.* **2000**, *38*, 1931.

[72] Belfiore, L. A.; Indra, E.; Das, P. *Macromol. Symp.* **1997**, *114*, 35.

[71] McCurdie, M. P.; Belfiore, L. A. *J. Polym. Sci., Part B: Polym. Phys.* **1999**, *37*, 301.

[71] Belfiore, L. A.; Bosse, F.; Das, P. *Polymer Int.* **1995**, *36*, 165.

[72] Belfiore, L. A.; McCurdie, M. P. *J. Polym. Sci., Part B: Polym. Phys.* **1995**, *33*, 105.

[73] Biswas, M.; Mukherjee, A. *Adv. Polym. Sci*. **1994**, *115*, 89.

[74] Hagihara, N.; Sonogashira, K.; Takahashi, S. *Adv. Polym. Sci*. **1981**, *41*, 141.

[75] Arche R. D. *Coord. Chem. Rev.* **1993**, *128*, 49.

[76] Nguyen, P.; Gomez-Elipe, P.; Manners, I. *Chem. Rev.* **1999**,

[77] Lamba, J. J. S.; Fraser, C. L. *J. Am. Chem. Soc.* **1997**, *119*, 1801.

[78] Collins, J. E.; Fraser, C. L. *Macromolecules* **1998**

[79] McAlvin, J. E.; Fraser, C. L. *Macromolecules* **1999**, *32*, 1341.

[80] McAlvin, J. E.; Fraser, C. L. *Macromolecules* **1999**, *32*, 6925.

[81] Theng, B. K. G. *The Chemistry of Clay-Organic Reactions:* Wiley: New York, 1974.

[82] Brindley, G. W. *Crystal Structures of Clay Minerals and their X-Ray Identification*; Mineralogical Society: London, 1980.

[83] Alexan M.; Dubois, P. *Mater. Sci. Eng*. **2000**, *28*, 1.

[84] Aranda, P.; Ruiz-Hitzky, E. *Chem. Mater.* **1992**, *4*, 1395.

[85] Francis, C. W. *Soil Sci*. **1973**, *115*, 40.

[86] Greenland, D. J. *J. Colloid Sci*. **1963**, *18*, 647.

[87] Zhao, X.; Urano, K.; Ogasawara, S. *Colloid Polym. Sci.* **1989**, *267*, 899

[88] Jimenez, G.; Ogata, N.; Kawai, H.; Ogihara, T. *J. Appl. Polym. Sci.* **1997**, *64*, 2211.

[89] Ogata, N.; Jimenez, G.; Kawai, H.; Ogihara, T. *J. Polym. Sci., Part B: Polym. Phys*. **1997** *35*, 389.

[90] Jeon, H. G.; Jung, H. T.; Lee, S. W.; Hudson, S. D. *Polym. Bull.* **1998**, *41*, 107.

[91] Kawasumi, M.; Hasegawa, N.; Usuki, A.; Okada, A. *Mater. Sci. Eng*. **1998**, *6*, 135.

[92] Usuki, A.; Kawasumi, M.; Kojima, Y.; Okada, A.; Kurauchi, T.; Kamigaito, O. *J. Mater. Res*. **1993**, *8*, 1174.

[93] Messersmith, P. B.; Giannelis, E. P. *Chem. Mater*. **1993**, *5*, 1064.

[94] Pantoustier, N.; Alexandre, M.; Degee, P.; Calberg, C.; Jerome, R.; Henrist, C.; Cloots, R.; Rulmont, A.; Dubois, P. *e-Polymer* **2001**, *9*, 1.

[95] Pantoustier, N.; Lepoittevin, B.; Alexandre, M.; Kubies, D.; Calberg, C.; Jerome, R.; Dubois, P. *Polym. Eng. Sci.* **2002**, *42*, 1928.

[96] Chen, T. K.; Tien, Y. I.; Wei, K. H. *J. Polym. Sci., Part A: Polym. Chem*. **1999**, *37*, 2225.

[97] Wang, Z.; Pinnavaia, T. J. *Chem. Mater.* **1998**, *10*, 3769.

[98] Yao, K. J.; Song, M.; Hourston, D. J.; Luo, D. Z. *Polymer* **2002**, *43*, 1017

[99] Okamoto, M.; Morita, S.; Taguchi, H.; Kim, Y. H.; Kotaka, T.; Tateyama, H. *Polymer* **2000**, *41*, 3887.

[100] Okamoto, M.; Morita, S.; Kotaka, T. *Polymer* **2001**, *42*, 2685.

[101] Akelah, A.; Moet, M. *J. Mater. Sci*. **1996**, *31*, 3589

[102] Doh, J. G.; Cho, I. *Polym. Bull.* **1998**, *41*, 511.

[103] Weimer, M. W.; Chen, H.; Giannelis, E. P.; Sogah, DY. *J. Am. Chem. Soc*. **1999**,*121*, 1615.

[104] Zhu, J.; Morgan, A. B.; Lamelas, F. J.; Wilkie, C. A. *Chem. Mater.* **2001**, *13*, 3774.

[105] Hsu, S. L. C.; Chang, K. C. *Polymer* **2002**, *43*, 4097.

[106] Bergm J. S.; Chen, H.; Giannelis, E. P.; Thomas, M. G.; Coates, G. W. *Chem.Commun.* **1999**, *21*, 2179.

[107] Jin, Y-H.; Park, H-J.; Im, S-S.; Kwak, S-Y.; Kwak, S. *Macromol. Rapid Commun.* **2002**, *23*, 135.

[108] Heinemann, J.; Reichert, P.; Thomson, R.; Mulhaupt, R. *Macromol. Rapid Commun*. **1999,** *20*, 423.

[109] Tudor, J.; Willington, L.; O'Hare, D.; Royan, B. *Chem. Commun*. **1996**, *17*, 2031

[110] Sun, T.; Garces, J. M. *Adv. Mater*. **2002**, *14*, 128.

[111] Ke, Y. C.; Long, C.; Qi, Z. *J. Appl. Polym. Sci*. **1999**, *71*, 1139.

[112] Tsai, T. Y. In *Polymer–Clay Nanocomposites*; Pinnavaia, T. J., Beall, G. W. Eds.;Wiley: London, 2000.

[113] Imai, Y.; Nishimura, S.; Abe, E.; Tateyama, H.; Abiko, A.; Yamaguchi, A.; Aoyama, T.; Taguchi, H *Chem. Mater*. **2002**, *14*, 477.

[114] Messersmith, P. B.; Giannelis, E. P. *Chem. Mater*. **1994**, *6*, 1719.

[115] Wang, Z.; Pinnavaia, T. J. *Chem. Mater*. **1994**, *6*, 468.

[116] Lan, T.; Pinnavaia, T. J. *Chem. Mater*. **1994**, *6*, 2216.

[117] Wang, Z.; Lan, T.; Pinnavaia, T. J. *Chem. Mater*. **1996**, *8*, 2200.

[118] Kornmann, X.; Thomann, R.; Mulhaupt, R.; Finter, J.; Berglund, L. A. *Polym. Eng. Sci*. **2002**, *42*, 1815.

[119] Lan, T.; Pinnavaia, T. J. *Chem. Mater*. **1994**, *6*, 2216.

[120] Wang, Z.; Lan, T.; Pinnavaia, T. J. *Chem. Mater*. **1996**, *8*, 2200.

[121] Kornmann, X.; Thomann, R.; Mulhaupt, R.; Finter, J.; Berglund, L. A. *Polym. Eng. Sci*. **2002**, *42*, 1815.

[122] Vaia, R. A.; Gianellis, E. P. *Macromolecules* **1997**, *30*, 8000. Vaia,

[123] R. A.; Ishii, H.; Giannelis, E. P. *Chem. Mater*. **1993**, *5*, 1694

[124] Ryu, J. G.; Kim, H.; Lee, J. W. *Polym. Eng. Sci.* **2004**, *44*, 119

[125] Vaia, R. A.; Vasudevan, S.; Krawiec, W.; Scanlon, L. G.; Gianne *Mater*. **1995**, *7*, 154.

[126] Liu, L. M.; Qi, Z. N.; Zhu, X. G. *J. Appl. Polym. Sci*. **1999**, *71*, 1133.

[127] Fornes, T. D.; Yoon, P. J.; Hunter, D. L.; Keskkula, H.; Paul, D. R. *Polymer* **2001**, *42*, 9929.

[128] Fornes, T. D.; Yoon, P. J.; Hunter, D. L.; Keskkula, H.; Paul, D. R. *Polymer* **2002,** *43*, 5915.

[129] Hasegawa, N.; Okamoto, H.; Kato, M.; Usuki, A.; Sato, N. *Polymer* **2003**, *44*, 2933.

[130] Usuki, A.; Kato, M.; Okada, A.; Kurauchi, T. *J. Appl. Polym. Sci.* **1997**, *63*, 137.

[131] Hasega N.; Kawasumi, M.; Kato, M.; Usuki, A.; Okada, A. *J. Appl. Polym Sci.* **1998**, *67*, 87.

[132] Nam, P. H.; Maiti, P.; Okamoto, M.; Kotaka, T.; Hasegawa, N.; Usuki, A. *Polymer* **2001**, *42*, 9633.

[133] Liu, X.; Wu, Q. *Polymer* **2001**, *42*, 10013.

[134] Manias, E.; Touny, A.; Wu, L.; Lu, B.; Strawhecker, K.; Gilman, J. W.; Chung, T. C. *Polym. Mater. Sci. Eng*. **2000**, *82*, 282.

[135] Wang, K. H.; Choi, M. H.; Koo, C. M.; Choi, Y. S.; Chung, I. J. *Polymer* **2001**, *42*, 9819.

[136] Davis, C. H.; Mathias, L. J.; Gilman, J. W.; Schiraldi, D. A.; Shields, J. R.; Trulove, P*40*, 2661.

[135] Chisholm, B. J.; Moore, R. B.; Barber, G.; Khouri, F.; Hempstead, A.; Larsen, M.; Olson, E.; Kelley, J.; Balch, G.; Caraher, J. *Macromolecules* **2002**, *35*, 5508.

[136] Kim, S. W.; Jo, W. H.; Lee, M. S.; Ko, M. B.; Jho, J. Y. *Polymer* **2001**, *42*, 9837.

[137]Huang, X.; Lewis, S.; Brittain, W. J.; Vaia, R. A. Macromolecules **2000**, *33* 2000.

[138] Maiti, P.; Yamada, K.; Okamoto, M.; Ueda, K.; Okamoto, K. *Chem. Mater*. **2002**, *14*, 4654

[139] Paul, M-A.; Alexandre, M.; Degee, P.; Henrist, C.; Rulmont, A.; Dubois, P. *Polymer* **2003**, *44*, 443

[140] Sinha Ray, S.; Okamoto, K.; Maiti, P.; Okamoto, M. *J. Nanosci. Nanotechnol*. **2002**, ***2002***, 171.

[141] Sinha Ray, S.; Okamoto, K.; Okamoto, M. *Macromolecules* **2003**, *36*, 2355.

[142] Hergeth W. D.; Peller M.; Hauptmann P. *Acta*. *Polym*. **1986**, *37*, 468.

[143] Hergeth W. D.; Starre P.; Schmutzler K., *Polymer* **1988,** *29*, 1323.

[144] Hergeth W. D.; Steinau U. J.; Bittrich H. J.; Simon G., *Polymer* **1989,** *30*, 254.

[146] Stober W.; Fink A.; Bohn E., *J. Colloid Inter. Sci.* **1968,** *26*, 62.

[147] Badley R. D.; Ford W. T.; McEnroe F. J.; Assink R. A., *Langmuir* **1990**, *6*, 792.

[146] Smith T. W.; Wychick D*., J. Phys. Chem*. **1980,** *84*, 1621.

[147] Hess P. H.; Parker Jr. P. H., *J. Appl. Polym. Sci*. **1966**, *10*, 1915.

[148] Berger M.; Manuel T. A., J. *Polym. Sci. Polym. Chem. Ed*. **1966**, *4,* 1509.

[149] Lee A.; Lichtenhan J. D. *Macromolecules* **1998**, 39, 4970.

[150] Thibeault Jr., George. (2004). Sharing the FPA Experience at FPE's Flexible Packaging. Congress 2004. Retrieved February 18, **2005** from Flexible at http://www.flexpack.org/magazi/aricles/0804%20Articles/FPE.htm.

[151] Butschli. (**2005**, January). *Flexibles outlook is optimistic. Packaging World*, 74.

[152] Pitkethly M.J. "Nanotechnology as building block." *Materialstoday*. Dec. **2003.** 36-42.

[153] Lux research. "Revenue from nanotechnology-enabled products to equal IT and telecom by2014*, exceed biotech* by 10 times." Oct. **2004**.

[154] V. S. Saji and Joice Thomas *CURRENT SCIENCE*, JANUARY **2007**.VOL. 92, NO. 1, 10

[155] Luis F. Hakim, David M. King, Yun Zhou, Christopher J. Gump, Steven M. George and Alan W. Weimer *Adv. Funct. Mater*. **2007**, 17, 3175–3181.

[156] Wang Jincheng, Zheng Xiaoyu, Chen Yuehui, Lu Zhijun And Zhu Zengliang *Journal Of Elastomers And Plastics*, **2009**. Vol. 41

[157] Zak G, Haberer M, Park C B and Benhabib B, *Rapid Prototyping* **2000** , Vol. 6, No. 2, pp. 107-118J.

[158] Shokrieh M.M. and Rafiee R., *Mechanics of Composite Materials* **2010** Volume - 46, Number 2, 155-172.

[159] Shao-rong Lu, Yu-mei Jiang and Chun Wei, *J Mater Sci* **2009** 44:4047–4055.

[160] Li H, Zhang Z, Ma X, Hu M., *Surf Coat Technol,* **2007,** 201:5269.

[161] Takahashi S., Goldberg H.A., Feeney C.A., Karim D.P., Farrell M., O'Leary K. and Paul D.R., *Polymer* Volume 47, Issue 9, **2006**, Pages 3083-3093.

[162] Qunhui Sun, F. Joseph Schork, Yulin Deng *Composites Science and Technology,* **2007**,Volume 67, Issue 9, , Pages 1823-1829.

[163] Chang-Jian Weng, Jane-Yu Huang, Kuan-Yeh Huang, Yu-Sian Jhuo, Mei-Hui Tsai, Jui-Ming Yeh *Electrochimica Acta*, **2010**, Volume 55, Issue 28, 1,Pages 8430-8438.

[164] Fernando R.H. and Sung L.P., *Am.Chem.Soc. Symp. Ser*., **2009,** 1008, p. 448.

[165] Lepoutre P. and Rezanowich A. **1977** *TAPPI*, 60(11): 86-91.

[166] Del B., Rio G. and Rudin A. **2000** *Progress in Organic Coatings*,28: 259-270.

[167] Radhakrishnan S., Saini D.R., *Synth. Met*., **2000**, 58 243.

[168] Radhakrishnan S. and Deshpande S.D., *Sensors* , **2002**, 2 185.

[169] Radhakrishnan S., Santhosh Paul, *Sens. Actuators B*, **2007**. Vol./Iss.: 125, Pages 60-65.

[170] Radhakrishnan S., Saujanya C., Sonar P., Gopalkrishan I. K., Yakhmi J. V. *Polyhedron* 20 (2001), 1489.

[171] Mayne J.E.O., *Official digest*, **1952**, 24 p.127-136,

[172] Nguyen T., Hubbard J.B*., J.M. Pommersheim*, *Nace* **1996**

[173] Deya C., Romagnoli R., del B., Amo *J., Coat. Technol. Res*., **2007**. 4 (2) 167–175,

[174] Romagnoli R., Vetere V.F., *Corros Rev.,* **1995**, 13 (81), 45,

[175] Reinhard G., *Prog. Org. Coat*., **1990,** 18,123,.

[176] Del Amo B., Romagnoli R., Vetere, V.F., *Ind. Eng. Chem. Res*., **1999**,.38 2310

[177] Kumar A., Stephenson L.D., *Coating. World*, June,**2004.** Volume 49, Issue 4, Pages 324-335

[178] Aiken J.D., Finke R.G., *J. Mol. Catal. A: Chem*. **1999,** 145,1-44.

[179] Radhakrishnan S., Sonawane Narendra, Siju C.R., *Progress in Organic Coatings* **2009,** 64, 383–386.

[180] Patil R.C., Radhakrishnan S., *Progress in Organic Coatings* **2006**, 57 332–336.

[181] Radhakrishnan S., Siju C.R., Debajyoti Mahanta, Patil Satish , Giridhar Madras *Electrochimica Acta* **2009**, 54,1249–1254.

[182] Chikara Hayashi, Seiichiro Kashu, Masaaki Oda and Fumio Naruse, *Materials Science and Engineering: A* **1993**, Volume 163, Issue 2, 15, Pages 157- 161.

[183] Wang D., et al*, J. Am. Chem. Soc*., **2011**. Vol. 115(7), 1608- 1615

[184] Sankara T.S.N. Narayanan T.S.N. Sankara Narayanan *Rev.Adv.Mater.Sci.* **2005**, 9, 130-177.

[185] Quanli Hu, Ok Hyoung Lee, Yun Soo Lim, Yong-Sang Kim1, Ju Kyung Shin, Sung-Hyeon Baeck, Hyun Ho 218th ECS Meeting, © **2010** *The Electrochemical Society.*

[186] Ming Hui He, Ai Ping Wang, Shou Gang Chen, Yan Sheng Yin *Advanced*

Materials Research, **2009**, Vol. 79 – 82, pp 939-942.

[187] Hagenmaier R.D. and Grohmann K., *Journal Of Food Science*— **1999,** Volume 64, No. 6,.

[188] Lee H., Neville K., *Handbook of Epoxy Resins*, McGrawHill, Inc., NewYork, **1982.**

[189] Barletta M., Lusvarghi L., Mantini F.P., Rubino G., *Surf. Coat. Technol*. **2007,** 201, 7479–7504

[190] Gopakumar T.G., Patel N.S., Xanthos M., *Polymer Composites*—**2006** 27: 368–380

[191] Sawitowski T., Proceedings of PIRA International Conference: The future of Nanotechnology, Miami, FL, February **2005.**

[192] Danuta *Kotnarowska Materials Science (Medžiagotyra*), **2008**, Vol.14, No. 4.

[193] Tsermaa Galya, Vladimr Sedlark, Ivo Kuritka, Radko Novotny, Jana Sedlarkova, Petr Saha, *Journal of Applied Polymer Science*, **2008**,Vol. 110, 3178–3185.

[194] Knapczyk J. W., In Kirk-Othmer *Encyclopedia of Chemical Technology, 4th ed., edited by J. I.Kruschwitz. John Wiley and Sons, New York*, **1997**, Vol. 24, p. 924.

[195] Blomstrom T. P., *In Encyclopedia of Polymer Science and Engineering*, edited by H. F. Mark, et al.John Wiley and Sons, New York, **1989**, Vol. 17, p.136.

[196] Jacqueline I.K., *Encyclopedia of Polymer Science and Engineering*, John Wiley & Sons, Inc., New York, **1990**, pp. 347–1232.

[197] R.S. Lillard, J. Kruger, W.S. Tait, and P.J. Moran *Corrosion Science* **1995,** Vol.51, No. 4 1995, 251-59

[198] C.H. Tsai and F. Mansfeld *Corrosion Science*, **1993**, Vol. 49, No. 9 september 1993 726-37

[199] Y.Waseda S. Suzuki (Eds.) "Characterization of Corrosion Products on Steel Surfaces" *Advances in materials research*, Springer Berlin Heidelberg New York, December **2005**

CHAPTER – II

EXPRIEMENTAL

CHAPTER 2

2.1 Introduction :

The detailed experimental procedures and various characterisation techniques employed in these studies are documented in this chapter. Three different commercial grade fillers were used viz. calcium carbonate, barium sulphate, iron oxide and synthesized nanoparticles of same by using Polymer Mediated Growth (PMG) technique(1-5) . Our aim is to synthesis the $CaCO_3$, $BaSO_4$, Fe_2O_3 nano particles by using Polyethylene Glycol (PEG) with different molecular weights, different concentration and to blend it with Polyvinyl acetate(PVAc). Characterisation of these nanoparticles is done by X-ray diffraction with Ni filtered CuKα as a radiation source at 2θ scan speed of 2º per minute, Scanning electron microscopy (SEM), transmission emission microscopy (TEM), Thermal Gravametric analysis (TGA), UV-visible spectroscopy, optical polarization microscopy. Applications of these nanoparticulates in PVAc, PVB, and Epoxy polymer to produce a nanocomposite. These nanocomposites are then used to coat on the steel substrate of which the properties are compared with commercial coatings. These coatings applied on stainless steel substrate by using dip coating technique. The optical properties such as gloss, reflectance, transparency, etc. of PVAc and PVB, epoxy containing commercial as well as nanoparticles gave an ample proof of uniform dispersion of the nanoparticles addition in polymer matrix. The second section deals with corrosion properties at various temperatures (45^0C, 55^0C and 65^0C) of PVAc and PVB, epoxy nanocomposites coatings containing nanoparticles were studied by using Electrochemical Impedence Spectroscopy (EIS).

2.2 Materials :

The various chemicals used in the present study along with their grades and make are given in the following table 2.1

Table 2.1 : Materials used

Chemical	Grade	Make
Polyethylene glycol (M.W.= 4000, 60000, 20000 & 35000)	For Synthesis	Merck
Calcium chloride fused	AR Grade	S. D. Fine Chem. Ltd. India.
Potassium carbonate anhydrous	AR Grade	S. D. Fine Chem. Ltd. India
Ferric chloride	AR Grade	S. D. Fine Chem. Ltd. India
Sodium hydroxide	AR Grade	S. D. Fine Chem. Ltd. India
Barium chloride	AR Grade	S. D. Fine Chem. Ltd. India
Potassium sulfate	AR Grade	S. D. Fine Chem. Ltd. India
Methanol	GR Grade	S. D. Fine Chem. Ltd. India
Polyvinyl buatral	LR Grade	Merck
Polyvinyl acetate	LR Grade	Merck
Calcium Carbonate precipitated	Commercial	Merck
Iron Oxide (Fe2O3)	Commercial	Merck
Barium Sulphate	Commercial	Merck
Sodium chloride	LR Grade	Merck
Epoxy Resin(GT 7004)	Commercial	Huntsman
Hardner(HT 2844)	Commercial	Huntsman
Flow Agent	Commercial	CYTEC
Degassing Agent	Commercial	Huangshan

2.3 Preparation of Nanoparticulate Filler by using Polymer Mediated Growth (PMG) technique :

2.3.1 Preparation of Nanoparticles with PEG:

a) Calcium Cabonate ($CaCO_3$)

The nanoparticulate calcium carbonate, barium sulphate, iron oxide filler was prepared by using PEG as a matrix. The PMG method essentially consists of forming a complex of salt of $CaCl_2$ and Polyethylene Glycol (4000, 6000, 20000, 35000) by dissolving the two components in different molar ratios (1:2, 1:4, 1:8, 1:16, 1:32) in methanol (20% solution conc.). This was allowed to digest for 24 hours. Then stoichiometric amount of K_2CO_3 was dissolved in distilled water and then added to the above complex without stirring. The whole mixture was allowed to digest for 24 hours at room temperature. $CaCO_3$ was precipitated in the form as a fine powder. The solution was then stirred vigorously and then filtered properly. It was then washed with distilled water and methanol to remove all PEG and the salt that is KCl. The remaining powder i.e. $CaCO_3$ is then dried.

The reactions involved here are as follows:

$PEG + CaCl_2 \longrightarrow PEG— CaCl_2$ (Complex)

$PEG—CaCl_2$ (Complex) + $K_2CO_3 \longrightarrow PEG---- CaCO_3$ (ppt) + 2KCl

b) Iron Oxide (Fe_2O_3)

We followed the same procedure for synthesis of Fe_2O_3. In this case we prepared first forming complex of ferric chloride ($FeCl_3$) with Polyethelyene glycol (PEG).and then reacting the same with stiochimeteric proportion of sodium hydroxide. Typically, the polymer viz. polyethylene glycol (PEG MW 35000, 20000, 6000, 4000) dissolve in an appropriate solvent(methanol) to make 20 wt% solution. Anhydrous ferric chloride was added to this desired amount i.e. in molar ration of 1:12 with respect to the monomer and the solution allowed to remain at 30^oC for a 24 hrs. so that of iron salt with the polymer was taken in a stoichiometric amount with respect to $FeCl_3$ in an aqueous medium and hole mixture allowed to digest for 24 hrs . The reddish brown fine colloidal precipitate formed.

The reaction is as follows :

$PEG + FeCl_3 \longrightarrow PEG— FeCl_3$ (Complex)

$PEG—FeCl_3$ (Complex) + $3NaOH \longrightarrow PEG\text{----} Fe(OH)_3$ (ppt) + 3NaCl

$PEG\text{----} Fe(OH)_3 \xrightarrow{washinig} Fe(OH)_3 \xrightarrow{\triangle} Fe_2O_3 + H_2O\uparrow$

c) Barium Sulphate ($BaSO_4$)

Preparation of $BaSO_4$ is same as $CaCO_3$ and reaction is as follows :

$PEG + BaCl_2 \longrightarrow PEG— BaCl_2$ (Complex)

$PEG—CaCl_2$ (Complex) + $Na_2SO_4 \longrightarrow PEG\text{----} BaSO_4$ (ppt) + 2NaCl

2.3.2 Preparation of Nanoparticles using PEG–PVAc blending :

$CaCO_3$, Fe_2O_3, $BaSO_4$ nanofillers were prepared by using PEG-PVAc blend. Stock solutions of PEG, PVAc were prepared in methanol in required proportions. This method essentially consists of forming complexes of PEG and $CaCl_2$ $FeCl_3$, $BaCl_2$ by dissolving these two components in different proportions. This PEG- metal complex is then blended with amorphous polymer-PVAc after which the solution is allowed to digest for period of 24 hours. An appropriate stoichiometric amount of K_2CO_3, NaOH, Na_2SO_4 is then added to the above solution without disturbing it. Whole mixture is allowed to digest for 24 hours at room temperature. During this period the metal ions(Ca^+ Fe^{2+},Ba^+) and reactant ions diffused through the matrix and formed a respective gel like precipitate that become powdery over a period of time. This is filtered, washed thoroughly to remove the entire PEG and other reaction products and then dried.

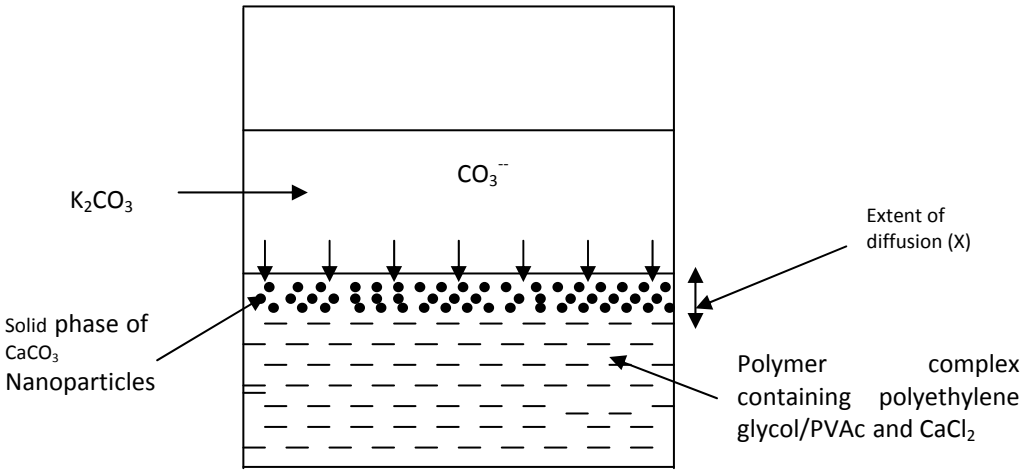

Figure 2.1: Schematic representation of the transport of reactants during polymer mediated growth (PMG) of nano-particulate fillers

The flow chart of the nanoparticles synthesis process of PEG-PVAc blend system

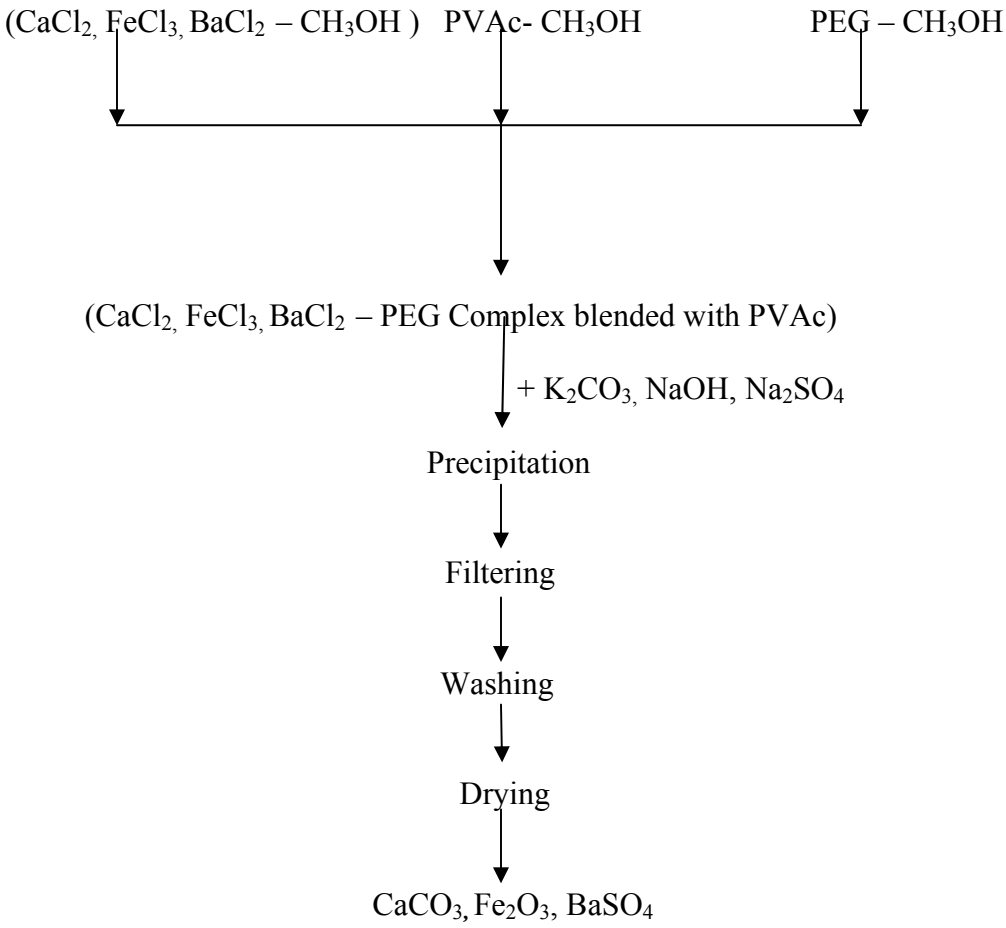

2.4 Preparation of nanocomposite coating with Nanoparticulate of $CaCO_3$, Fe_2O_3, $BaSO_4$:

2.4.1 Coatings with Vinyl Polymers (PVB & PVAc) :

The purpose of this study is to develop special coating for corrosion protection. In particular, the study will focus on the role of special additives such as nano $CaCO_3$, Fe_2O_3, and $BaSO_4$ to thermoplastic or thermoset type coatings. Nanoparticluate especially is expected to impart the enhanced barrier properties are the result of the much greater surface-to-volume ratio of nanofillers that are often characterised by very high aspect ratios.

The coating formulation was made using polyvinyl butyral (PVB), polyvinyl acetate (PVAc) etc. as binder with nano and commercial $CaCO_3$, Fe_2O_3 and $BaSO_4$ as additives at different concentrations. PVB (2g) was dissolved in methanol (20 ml) with continuous stirring for 6hr and then in a sonicator for few hours. The 1%, 3%, 5%, 7% and 10% nanoparticles and 5%, 7%, 10%, 20% and 30% commercial of wt % $CaCO_3$,Fe_2O_3, $BaSO_4$ powder having different compositions was crushed and a slurry was made with small quantity of methanol. The slurry was added and mixed in the PVB, PVAc solutions and subjected to sonication for 24 hours. This yielded a uniform dispersion of the polymers solution with no settling. The stainless steel coupons (50mmx 10mmx 1mm) with rounded corners and edges were polished by C-800 emery paper, washed with acetone and dried. The substrates were dip coated for 30 sec in nanocomposite polymers solution dispersion and dried at room temperature for 30 min followed by baking in air circulating oven at 50^0 C for 4 hours. The samples were cooled and then subjected for measurement of corrosion inhibition properties (6-7). The compositions of the final coatings are given in Table 2.2.

Table 2.2 : Coating compositions of vinyl polymers composite with commercial and nanoparticles

Samples name	PVAC wt. (g) in 20 ml Methanol	Filler Loading wt. (g)
Clear	2.00g	0.0g
Nano1%	2.00g	0.020gm
Nano3%	2.00g	0.060gm
Nano5%	2.00g	0.100gm
Nano7%	2.00g	0.140gm
Nano10%	2.00g	0.200gm
Comm. 5%	2.00g	0.100gm
Comm. 7%	2.00g	0.140gm
Comm.10%	2.00g	0.200gm
Comm.20%	2.00g	0.400gm
Comm.30%	2.00g	0.600gm

2.4.2 Preparation of dispersion coating formulation with PVB + modified PANI :

PVB 2gm was dissolved in methanol by 6 hrs continuous stirring in a sonicator. The 1%, 5% and 10 wt% of different PANI- Fe_2O_3nano powder crushed and a paste was made with methanol. This was added and mixed in PVB solution placed in sonicator for 24 hrs. The stainless steel polished by C-800 emery paper. The SS plate was dip coated in PVB/ PANI-nano dispersion and dried at room temperature followed by baking in air circulating oven at 50º C for 4 hrs. The samples were cooled and then subjected for measurement of corrosion inhibition properties.

2.4.3 Powder coating of Epoxy-Nano-$BaSO_4$ blend :

Epoxy powder coating formulations were made containing Nano $BaSO_4$ additive for better optical, mechanical and chemical properties on steel substrate coated by electrostatic powder coating followed by curing at 180^0C/15min. These coatings will be subjected to accelerated corrosion by immersion test in 3.5% saline

solution and followed by electrochemical characterisation of corrosion resistance using impedance spectroscopy. The standard salt spray test will also be carried out. To evaluate the life time of these coating system at room temperature, accelerated tests at different temperature would be carried out and extrapolated to room temperature [8]. Investigations of actual mechanism taking place in the polymer matrix and /or metal-electrolyte interfaces. These studies will lead to in depth knowledge on corrosion resistant coating which are specially needed for coastal structures, offshore rigs, naval dockyards etc. It can also give deeper understanding of self healing or 'smart' coatings using conducting polymers.

For powder coating, the following paint compositions have been used: Epoxy resin, hardener, flow agents, degassing agent and in that composition nano barium sulphate added as 1%, 3%, 5%, 7%, 10% and commercial 5%, 7%, 10, 20%, 30% of total (phr) respectively. All ingredients homogenously mixed in high speed mixer(rpm-1000) and extruded by Lab model Twin screw extruder at 100-105^{0}C

Figure 2.2 : Lab Model 16 mm Twin Screw Extruder

followed by cooling, grinding and sieving(90micron sive) for obtaining the final powder. Characterisation of these powders carried out by Differential scanning calorimetry (DSC).

Electrostatic spray gun is used for powder coating application, it consists in build cascade which producing the voltage between 0-100KV. For powder coating we were applying 60-80kV. Powder flows by applying the compression air pressure. At

the tip of gun electrode is present which produce high voltage. Powder gets –ve charged and charged powder is stick on the +ve earthen stainless steel plate. And put the coated plate in oven for curing at 180^0C for 15 minutes. After curing, measured the properties of films like gloss and corrosion resistance techniques like Tafel, Impedance and Salt spray testing.

2.5 Characterisation techniques :

2.5.1 FTIR spectroscopy :

Infrared spectroscopy is one of the most powerful techniques which is very useful in nanotechnology for study the dispersion stability, morphology, and structure of the ultrasonic irradiated nanoparticles were characterised by FTIR (Shimadzu FT-IR 8300 spectrometer and analyzed in the range of 400-4000 cm^{-1}).

The transmittance mode technique is the most adapted one in FTIR Spectroscopy. In this techniques, the sample is first diluted with KBr powder to a concentration of ~1% in the solid mixture. Then this mixture is pressed under ~20,000psi pressure to produce a transparent pellet. The infrared spectrum is obtained through exposure of the pellet to an infrared beam and the intensity of the transmitted light is recorded. The transmittance of the sample at given number is then calculated from the transmitted light and the incident light.

2.5.2 UV - Vis spectroscopy :

UV-vis absorption spectroscopy on nanocomposite powders and spectroscopic ellipsometry measurements on thin films and powder was used to study the effect of interfacial morphology, interparticle spacing and finite size effects on optical properties of nanocomposites. Ultraviolet and visible (UV-Vis) spectroscopy is a reliable and accurate analytical laboratory assessment procedure that allows for both qualitative and quantitative analysis of a substance [9]. The spectrophotometer utilizes a DH-2000 deuterium light source and a HR 2000 CG-UV-NIR detector.

2.5.3 Differential Scanning Calorimetry (DSC) :

Differential scanning calorimetric studies on epoxy-$BaSO_4$(different percentage) powder were carried out using DSC Q10(TA instrument, USA). DSC gives an idea about the primary and secondary transition with change in temperature. It gives the exothermic and endothermic change occurring over a particular

temperature range[10-11]. The heating rate was kept constant at 10^0C per minute under N_2 atmosphere. DSC was recorded both heating and cooling cycles. Endothermic changes like melting were recorded during heating cycles, and exothermic changes like crystallization were recorded during cooling. From the glass transition temperature, cross link density of powder was analyzed.Cross link density can be calculated by the following equation,

$$\Delta Tg = Tg\text{-}Tg_{(0)} = 5/(M_c/M_{n)} \text{ x } N_{mt} \qquad (1)$$

Where $Tg_{(0)}$- glass transition temperature of un cross-linked samples, Tg- crosslinked samples, M_c-molecular wt. between cross link, M_n-molecular wt of whole linear chain and N_{mt}- degreee of freedom for rotation of the group between crosslink.

2.5.4 Wide Angle X-ray Diffraction (WXRD) :

Wide-angle X-RAY Diffraction (WXRD) studies [12] were done in order to analyze the structures and crystallite size of synthesized nanoparticles $CaCO_3$, Fe_2O_3, $BaSO_4$ Powder. The incorporation of these nanoparticles is expected to show some structural changes. The various polymeric compositions were investigated by WAXD, using a powder X-ray diffractometer (Rigaku Geigerflex refractometer) using CuKα source and β Ni filter. All the scans were recorded in the 2θ region of 5-50° at a scan rate of 4° per minute. For the amorphous polymeric materials, the average inter chain distance (R) can be estimated from the position of the broad peak seen in the XRD plot by using the relation;

$$R = \{(5/8)\,\lambda / \sin\theta\}. \qquad (2)$$

Where, R is the average interchain separation, λ is the wavelength (1.542 Å) of the X–ray used and θ is the diffraction angle. For the crystalline phase, the *d*- values can be calculated using Brag's equation: $n\lambda = 2d \sin\theta$.

$$d = (n\lambda / 2 \sin\theta) \quad ; \text{where } n = 1 \qquad (3)$$

The crystalline structure and phase was confirmed by comparing the d values with standard reported values for the compound.

The crystallite size (D) is determined from the Sherrer's formula :

$$D = \lambda / [2\,(\Delta\theta) \cos\theta] \qquad (4)$$

where all the symbols have their usual meaning.

2.5.5 Transmission Electron Microscopy (TEM) :

Transmission electron microscopy (TEM) is always the first method used to determine the size and size distribution of nanoparticle samples [13-14]. Once a representative group of images is obtained [15], the next task is to count as many particles as possible, ideally a few thousand, so that good statistics on the size and size distribution present can be obtained. By carefully selecting the orientation of the sample, it is possible not just to determine the position of defects but also to determine the type of defect present [16]. Defects that produce only displacement of atoms that do not tilt the crystal to the Bragg angle (i.e. displacements parallel to the crystal plane) will not produce strong contrast. Nanoparticles selected samples were drop casted on copper grids after dissolving PVB in Methanol and TEM images were taken for the synthesized nanoparticles of $CaCO_3$, Fe_2O_3, $BaSO_4$. TEM Joel model 1200 was employed to take TEM pictures.

2.5.6 Gloss-o-meter :

Gloss is the ratio of specularly reflected light to incident light. For optically smooth surfaces, gloss varies with refractive index and angle of incidence according to Fresnel's law. Gloss is a visual impression that is caused when a surface is evaluated. The more direct light is reflected, the more obvious will be the impression of gloss. The gloss of a surface can be greatly influenced by a number of factors, for example the smoothness achieved during polishing, the amount and type of coating applied or the quality of the substrate. Gloss can also be a measure of the quality of a surface, for instance a drop in the gloss of a coated surface may indicate problems with its cure- leading to other failures such as poor adhesion or lack of protection for the coated surface. Gloss measured by BYK Gardner Tri-angle gloss-o-meter.

2.5.7 Optical Polarizing Microscopy :

A detailed surface morphological analysis of the nanocomposites by using Optical Polarizing Microscopy[17]. Figure 2.3 shows the essential parts of the optical polarizing microscope. It consists of a light source (Tungsten lamp 25 W), a condensor, a polarizer, a sample stage with controlled heating arrangement, objective

assembly, an analyzer and eyepiece/ microphotography arrangement. In another arrangement, the video camera interfaced with a computer was connected in place of the microphotography unit. The image analysis system contained a video camera connected to a computer via the software which provided image grabbing, image

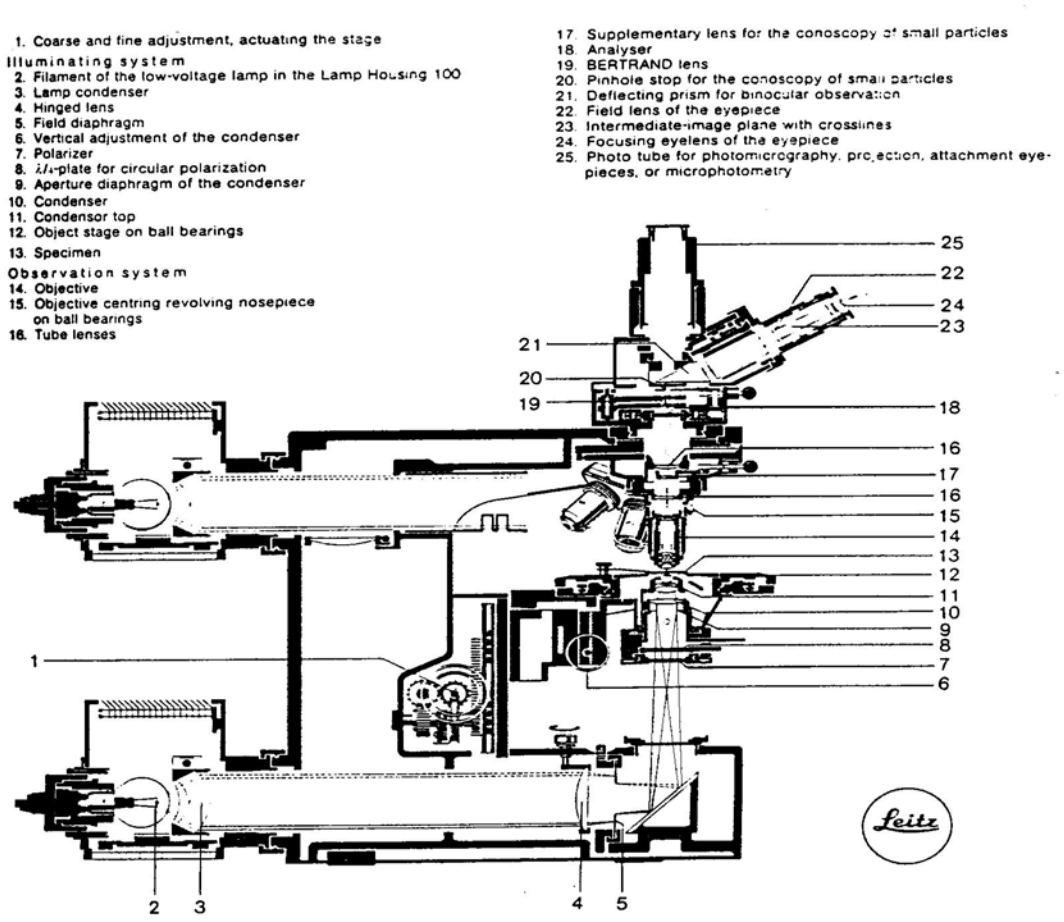

Figure 2.3 : Leitz optical polarizing microscope parts

storage and analysis facilities. The images were continuously recorded during the isothermal crystallization process for every 10 or 30 seconds interval and then analyzed by recording the spot intensity (grey scale) at any given location of the screen. It was possible to direct small changes (up to 1 pixel) occurring at any chosen point, during the crystallization of the matrix. The graphics provided in the software can also used to plot the intensity of transmitted light under the cross-polar condition

with respect to real time. This gives essentially the study of surface morphology, defect on surface and dispersion of nanoparticles in the coating .

2.6 Techniques used in corrosion studies :

2.6.1 Salt spray test :

Salt spray test is a standardized test method (ASTM B117) used to check corrosion resistance of coated samples. Salt spray test is an accelerated corrosion test that produces a corrosive attack to the coated samples in order to predict its suitability in use as a protective finish. The appearance of corrosion products (oxides) is evaluated after a period of time. Test duration depends of the corrosion resistance of the coating, the more corrosion resistant of the coating is the longer period in testing without showing signs of corrosion. There is no co-relation between the duration in salt spray test and the expected life of a coating, since corrosion is a very complicated process and can be influenced by many external factors[18-19].

The apparatus for testing consists of a closed testing chamber, where a salted solution (mainly, a solution of sodium chloride) is sprayed by means of a nozzle. This produces a corroding environment in the chamber and thus, parts in it are attacked under this severe corroding atmosphere. Typical volumes of these chambers are of 400 L, but they can be constructed larger. Tests performed with a solution of NaCl are known as NSS (neutral salt spray). Results are represented generally as testing hours in NSS without appearance of corrosion products .Salt spray test conducted on 5% NaCl solution spray on epoxy- $BaSO_4$ powder coated samples solution in a chamber at 1000 hours and analyzed.

2.6.2 Set-up for EIS Experiment :

Electrochemical tests are normally carried out in a single compartment cell which is shown in figure 2.3.

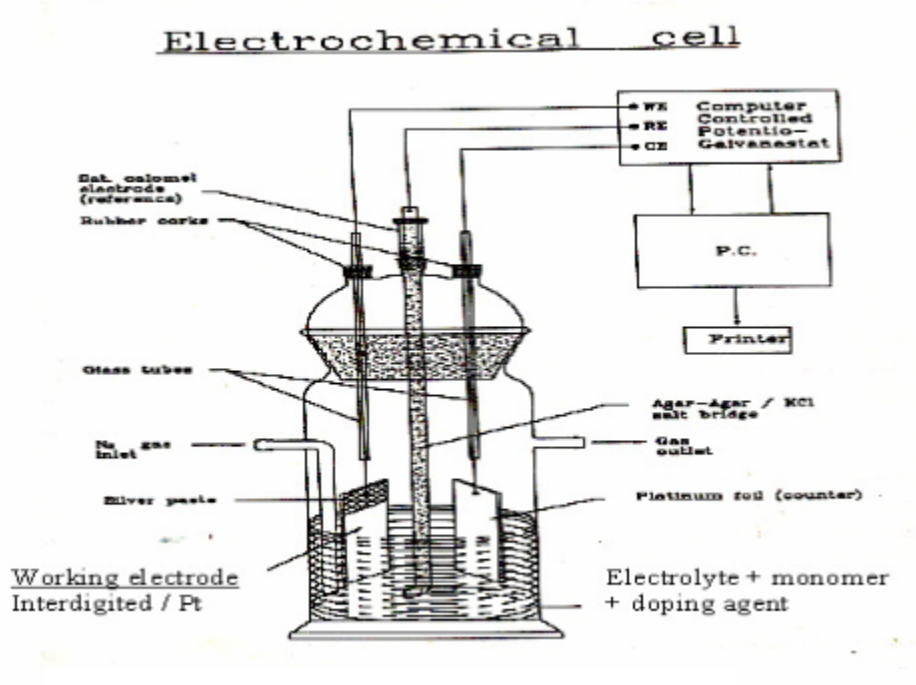

Figure 2.4 : Electrochemical cell for EIS experiment

The electrochemical cell for an EIS experiment conventionally consists of three electrodes, which are immersed in an electrolyte. The working electrode is the corroding metal. The working electrode is grounded, usually through an operational amplifier that is part of a current to voltage converter. The counter electrode is made from an inert metal (graphite electrode was used in my experiment). The counter electrode is connected to a potential control device called a potentiostat. The potentiostat applies to the counter electrode whatever voltage and current are necessary to maintain the potential that is desired between the working and reference electrodes. The reference electrode is constructed so that it has a negligible contact potential regardless of the environment in which it is placed. The reference electrode is connected to a potentiometer. Both Harrison solution and 3.5 wt% sodium chloride were used as electrolytes.

The potentiostat was connected to the computer with appropriate software which gave directly the data in terms of potential scan, frequency scan, current, real and imaginary part of impedance. The data analysis was carried out by the software as desired: Tafel, Bode, Niquist plots from which the corresponding parameters viz. corrosion potential, corrosion current, equivalent circuit elements etc. could be determined.

2.7 References :

[1] Saujanya C, Ashamol S, Padalkar S, Radhakrishnan S. *Polymer* **2001**, 42, 2255.

[2] Saujanya C, Radhakrishnan S. *Polymer* , **2001**, 42, 6723.

[3] Saujanya C, Radhakrishnan S. *J. Mat. Sci.* **1998**, 33, 1063.

[4] Radhakrishnan S., Saujanya C, Sonar P., Gopalkrishan I. K., Yakhmi J. V. *Polyhedron*, **2001**, 20,1489.

[5] Sonawane PS, Biradar SS, Radhakrishnan S, Kulkarni BD *Materials Chemistry and Physics,* **2007**, Vol.105, No.2-3, 348-353,

[6] Patil R.C., Radhakrishnan S. , *Progress in Organic Coatings* , **2006**, 57, 332–336.

[7] Radhakrishnan S., Siju C.R., Mahanta Debajyoti, Patil Satish , *Madras Giridhar Electrochimica Acta* , **2009**, 54, 1249–1254

[8] Radhakrishnan S. , Sonawane Narendra, Siju C.R. *Progress in Organic Coatings,* **2009**, 64, 383–386

[9] Meeten G. H. *Optical Properties of Polymers*; Elsevier Applied Science Publishers: London, **1986.**

[10] *Thermal Characterization of Polymeric Materials*, 2nd ed.; Turi, E. A., Ed.; Academic Press: San Diego, **1997**; Vol. 1.

[11] Turi E. A. *Thermal Characterization of Polymeric Materials*; Academic Press: London, **1981**.

[12] Alexander L. E. *X-Ray Diffraction Methods in Polymer Science*; John Wiley: New York, **1969**.

[13] Williams D. B., Carter C. B. *Transmission Electron Microscopy*: A Textbook for Materials Science; Plenum Press: New York, **1996**; Vol. 1.

[14] Hayat M.A., "*Basic techniques for transmission electron microscopy*", Orlando, Academic Press, **1986**.

[15] Williams D.B. and Carter C.B., "*Transmission electron microscopy: a textbook for materials science".* New York, Plenum Press, **1996**.

[16] McLaren, "Transmission electron microscopy of minerals and rocks", Cambridge, Cambridge University Press, **1991**

[17] Sawyer L. C., Grubb D. T. *Polymer Microscopy*; Chapman and Hall: London, **1987**

[18] Bandyopadhyay N. T, Jha G., Singh A.K., Rout T.K., Rani Nitu, *Surface & Coatings Technology*, **2006**, 200, 4312– 4319.

[19] Eva Fekete , B´ela Lengyel *Progress in Organic Coatings*, **2005**, 54, 211–215.

CHAPTER – III

Effect of $CaCO_3$ Nanoparticles Addition on Optical and Corrosion Properties of PVAc and PVB nanocomposite Coatings.

CHAPTER 3

3.1 Introduction :

Calcium carbonate is a white or transparent salt with a very low solubility in water. It reacts with acids forming the corresponding calcium salt and carbon dioxide. At around 900^0C solid calcium carbonate dissociates into calcium oxide and carbon dioxide. In aqueous solution solid calcium carbonate is formed by a simple precipitation reaction [1].

$$Ca^{2+}Cl_2 + K_2CO_3^{2-} \rightarrow CaCO_3(s) + 2KCl \qquad (1)$$

Calcium carbonate, which can be found in five crystalline polymorphic phases and in one amorphous phase in biominerals, is abundant in nature. Calcium carbonate appears in three water-free modifications: calcite, aragonite, and vaterite, with calcite being the most thermodynamically stable, and vaterite the most unstable.

Table 3.1 : Crystallographic and physical data of the different calcium carbonate phases

Property	**Calcite**	**Aragonite**	**Vaterite**	**Monohydro-calcite**	**Ikaite**
Formula	$CaCO_3$	$CaCO_3$	$CaCO_3$	$CaCO_3.H_2O$	$CaCO_3.6\ H_2O$
Space group	*R* 3*c*	*P mcn*	*P* 6_3/mmc	*P* 3_1	*C*2/c
Crystal system	trigonal	orthorhombic	hexagonal	hexagonal	monoclinic
Lattice constants/Å	a=b=4.991 c=17.062 γ =120º	a=4.959 b=7.964 c=5.738 α=β=γ=90º	a=b=4.130 c=8.490 γ=120º	a=b=10.5536 c=7.5446 γ=120º	a=8.792 b=8.312 c=11.021 β=110.53º
Density/g.cm³	2.71	2.93	2.65	2.43	1.83
Abundance	very common	common	rare	rare	very rare
ICDD-Reference	81-2027	76-0606	72-0506	83-1923	75-1733

Calcium carbonate exhibits other solid forms besides its three true polymorphs. Clarkson and coworkers [2] have, for instance, dealt with the spontaneous precipitation of calcium carbonate from highly supersaturated solutions. Their findings indicate that during precipitation an amorphous form of calcium carbonate is invariably formed. They also found evidence of $CaCO_3.6H_2O$ forming

under certain conditions. This is consistent with observations made by Brecevic and Nielsen [3] who report on formation of an amorphous form of calcium carbonate during spontaneous precipitation at relatively high supersaturations.

Calcium carbonate ($CaCO_3$) is a mineral with diverse applications; it is applied widely as fillers in the areas of plastics, rubbers, paints, papermaking, textiles, pigments, ceramics, medicine, pharmacy and so on, in virtue of its different physical and chemical properties and many of its important technological applications [4—11]. As widely and efficiently used processing additives in industrial end products, the anion surfactants are used the particular interest in the growth of calcium carbonate. In recent years, there have been a number of studies found on the precipitation methods in the literature [12-21]. It has been demonstrated that the characteristics of particles, such as the morphology and the particle size of $CaCO_3$, depend heavily on the preparation methods and experimental conditions. It is well known that the synthesis of $CaCO_3$ was followed by basic synthetic routes.

Among the various applications of $CaCO_3$ filled composites in paints, pigments etc., the corrosion inhibition of the coatings containing this filler is not studied extensively. There are few reports on $CaCO_3$ filled thermoset and thermoplastics and their respective anticorrosion properties [22-24]. However, the reduction in the particle size of $CaCO_3$ is very important so that low loading of the same can be employed in any polymer matrix which in turn increases the barrier and optical properties. The crystallite/particle size reduction of $CaCO_3$ can be had by High energy ball milling [25-27], Sol-Gel processing routes etc.. Each route has its own merits and demerits and hence polymer mediated growth (PMG) technique for the reduction of particle size of $CaCO_3$ becomes important. PMG technique has been successfully used for the past several years for synthesizing and controlling the shape and size of various materials especially nano particulate fillers [28-31]. In the PMG route, one of the reactant is complexed and bound to the polymer matrix while the second reactant is allowed to enter from external solution. Although the synthesis of nanoparticles by this method especially using partially miscible polymer blends has been successfully demonstrated, the underlying phenomena are yet to be clear. For example, the diffusion and transport of ions through the polymer medium depends

upon the nature of ions i.e. their size, charge etc., the free volume in the polymer which also depends on its glass transition temperature, degree of interaction with the polymer medium, molecular weight of polymer medium, solvent concentration used for polymer dissolution, etc. are to be studied exhaustively. A special emphasis on anticorrosion coating formulations with different particles sizes of $CaCO_3$ synthesized by PMG technique in polymer matrices such as PVB and PVAc is given in the present chapter.

3.2 Synthesis of Nanoparticles of Calcium Carbonate using PEG with Different Molecular Weights :

The diffusion behaviour for a given polymer-penetrant system varies with change in molecular weights of polymers. This behavior depends on the free volume within the polymer, end groups on the chains and on the segmental mobility of the polymer chains [32]. Thus, it is aimed here at generating nanoparticles of calcium carbonate and to investigate the role of PEG with different molecular weights was used as a polymer medium for the synthesis of nanoparticles of calcium carbonate. The calcium chloride is arrested in the PEG solution and potassium carbonate is left free to move through the gel. The white layer of calcium carbonate particles grows with time.

Table 3.2: Change in crystallite size of synthesized $CaCO_3$ with different molecular weight of PEG

Sample	PEG Molecular weight	Crystallite Size(nm)
A	6000	45
B	20000	18
C	35000	17

The particles formed from solutions of different molecular weights were subjected to XRD analysis and data of which was used to find out the particle size was calculated by using scherrer's formula as reported earlier [28-31]. The crystallite

size was calculated with Scherrer's formula suing the XRD data.. As shown in Table 3.2, A, B and C are corresponding to calcium carbonate nanoparticles synthesized using PEG with molecular weights such as 6000, 20000 and 35000 (gm/mol), respectively. From Table 3.2 we observed that with the increase in molecular weights of PEG, particle size of $CaCO_3$ decreases. It was also observed that as the concentration of PEG of same molecular weight increases, the particle size of calcium carbonate decreases. This is discussed later in the chapter.

The molecular weight of PEG will control the viscosity of the medium and the diffusion of ions. As shown in the Chapter-2, the process of PMG involves binding of one ion (in this case Ca^{++}) and diffusion of the reactive ions to form the final compound. The diffusivity is found to increase with decrease in molecular weight of PEG. If the molecular weight of PEG is less, the length of polymer chains is small and tends to stay away from each other, due to which path for freely moving carbonate ions in the solution gets easier. Thus, the resistance to the movement of carbonate ions is less. As a result, the $CaCO_3$ is formed throughout and which can then come together to form large particles. If the molecular weight of PEG is higher, the viscosity is higher, chain movement is restricted and diffusion of ions is also lower. In this case, the Ca^{++} ions are bound within the matrix and there is slow diffusion of carbonate to form calcium carbonate in localized region. Due to close packing of polymer chains and entanglement there is no free movement of the calcium carbonate formed which therefore remain in nano-particle form.

3.3 XRD Characterisation of $CaCO_3$ nanoparticles :

XRD scans of calcium carbonate nanoparticles synthesized using PEG as a polymer medium with different molecular weight is shown in Figure 3.1. All the peak positions were analyzed and the d-values estimated. In all cases, the crystalline phase of $CaCO_3$ was found to be Vaterite type [33]. It is found that the XRD patterns are becoming more broadened with increase in MW of PEG. This suggests that the crystallite size reduces with the increase in PEG molecular weight. These results have been discussed in the above section. The particle size has been reduced from 45 to 17 nm by increasing molecular weight of PEG from 6000, 20000 and 35000. Figure 3.2 shows the dependency of particle size of calcium carbonate particles on the molecular

weight of PEG used for the synthesis of nanoparticles. It is found that the particle size has decreased with the increase in the molecular weight of PEG medium. Thus, it can be established from the above findings that the synthesis of nanoparticles of calcium carbonate using PEG medium with different molecular weights is an also diffusion controlled process.

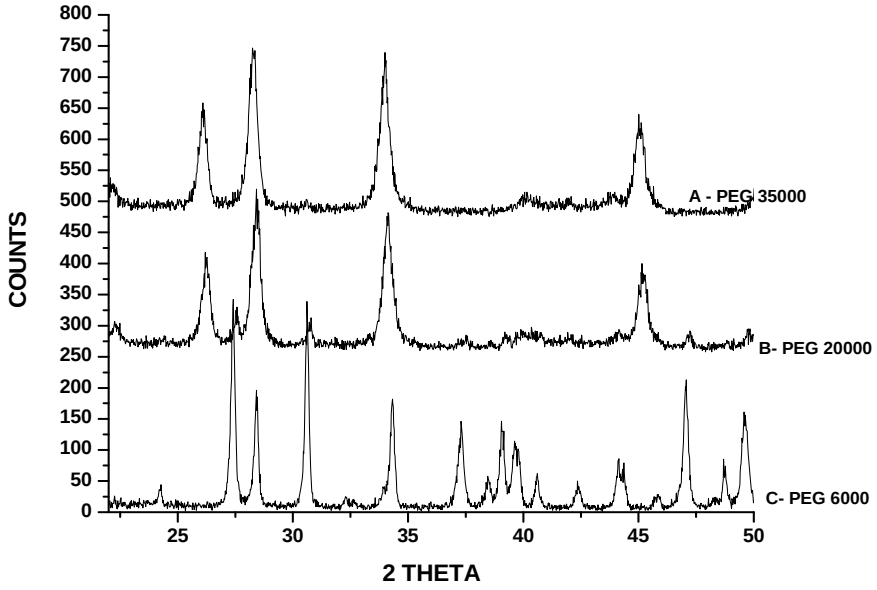

Figure.3.1 : X-ray diffraction scan of $CaCO_3$ A) PEG 6000 B) PEG 20000 C) PEG 35000

In order to confirm the above findings, some of the samples were examined by TEM. Figure 3.2 shows a typical electron micrograph obtained for $CaCO_3$ synthesized using PEG. From TEM micrograph we can be seen that the tiny particles of 25nm particles are embedded in PEG matrix are clearly visible.

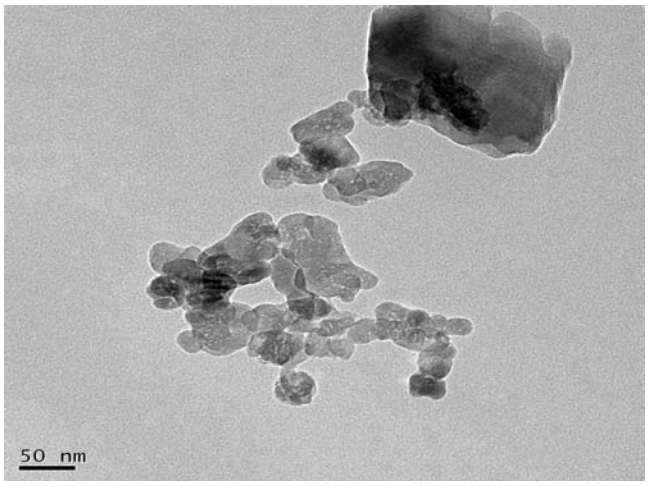

Figure.3.2 : Transmission electron microscopy (TEM) image of $CaCO_3$ synthesized by using PEG of molecular weight 35000 with 16:1 concentration

3.4 Effect of Different Molar Ratio of PEG and Reactant on the Synthesis of Nanoparticles of Calcium Carbonate :

The calcium carbonate nanoparticles synthesis was carried out using different molar ratio of PEG and $CaCl_2$ to prepare dilute to viscous liquids and then added K_2CO_3. This would bring out the effect of viscosity as well as complex formation (due to co-ordinate bond between Ca^{++} and oxygen of the monomer unit) on the particle size. Calcium chloride was dissolved using methanol solvent along with PEG at different polymer molar ratios such as 1:2, 1:4, 1:8, 1:16 and 1:32. As the polymer molar ratio increases, the Ca^{++} ions get more bound within PEG medium. The stability of the complex formed between the particle and the surrounding polymer matrix and the slow diffusion of reacting species are the most important criteria for the formation of nanoparticles. The surrounding polymer matrix should be able to hold the metal atom at a particular place e.g. at the -O- atoms in PEG and should not allow it to break away from the matrix. That is the reason why in the present experiment we allowed the complex to digest for specified time. Since $CaCl_2$ is first complexed with PEG, the $CaCl_2$ molecules are strongly held within the polymer chains. Each molecule of $CaCl_2$ is then shared by molecules of PEG to form a complex of PEG - $CaCl_2$. Due to this sharing of $CaCl_2$ the domain for the subsequent reaction with K_2CO_3 is reduced. That is why we get drastic reduction in particle size

XRD was also run for the $CaCO_3$ nano particle and particle size analysis was also calculated using Scherrer's formula as reported earlier [28-31]. Figure 3.5 shows the XRD scans of calcium carbonate particles synthesized by PMG technique using PEG as a polymer medium with different molar ratio with different molecular weight. It is found that the particle size was decreased upto 16.5 nm using viscous liquids.

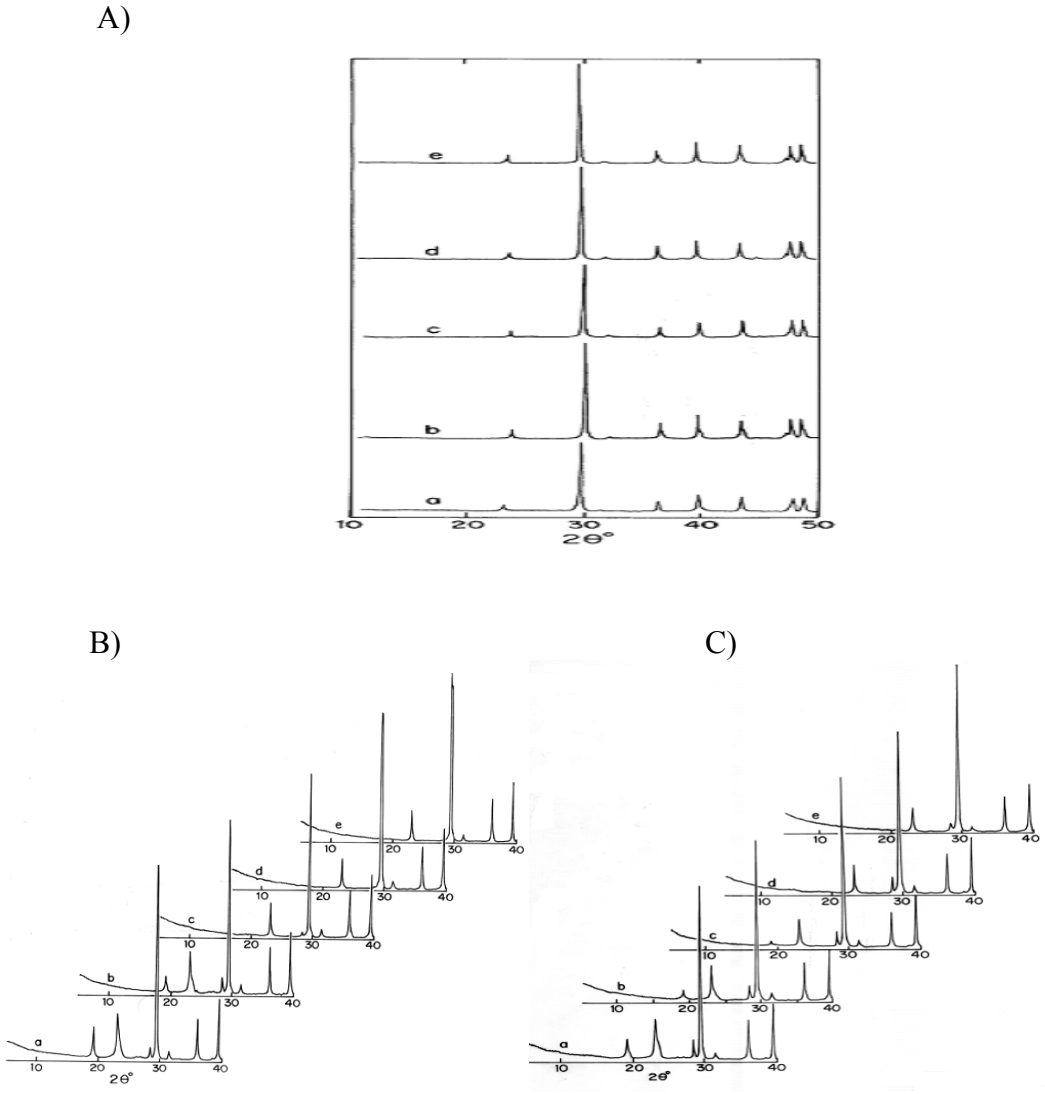

Figure 3.3 : XRD scans of $CaCO_3$ with different concentration of PEG: Reactant a) 2:1 b) 4:1 c) 8:1 d) 16:1 e) 32:1 A) PEG 6000 B) PEG 20000 C) PEG 35000

From Table 3.3 we can be seen that as molar ratios of polymer increases the particle size going down to nano levels. In the cases where PEG 6000 was used, the effect of $CaCl_2$ to polymer ratio at 1:2 and 1:4 on crystallite size is not much as compared to 1:16 and 1:32. This may be because the polymer molecular weight is less and dilution of media is also less so the stability of complex is not much. On the other hand as the molecular weight of polymer increases the viscosity increases leading to higher stability of complex. As molecular weight of PEG increases the distance between functional groups which forms complex will be more stable. As the viscosity of the reaction medium increases with increase in molecular weight, which in turn reduces the diffusion of K_2CO_3, the reaction will be slow leading to reduction of the particle size of calcium carbonate.

Table 3.3 : Crystallite size variation of $CaCO_3$ synthesized by using different molecular weights and concentration of PEG

	Calculated crystallite size (nm) with different reactant ratio					
PEG MW	**1:32**	**1:16**	**1:8**	**1:4**	**1:2**	**1:0**
6000	45	72.1	72	72.1	80	90.168
20000	18	27.7	45	51.5	60.1	90.168
35000	16.5	25.7	28.8	36	45	90.168

From Table 3.3 it is seen that calcium carbonate nanoparticles synthesized using PEG with molar ratio such as 1:2, 1:4, 1:8, 1:16 and 1:32 decreases in for all molecular weights but for higher molecular weight (MW 35000), the change is more prominent. Thus, both viscosity and the molar ratio play important role in bringing down the particle size of the $CaCO_3$ synthesized by PMG route.

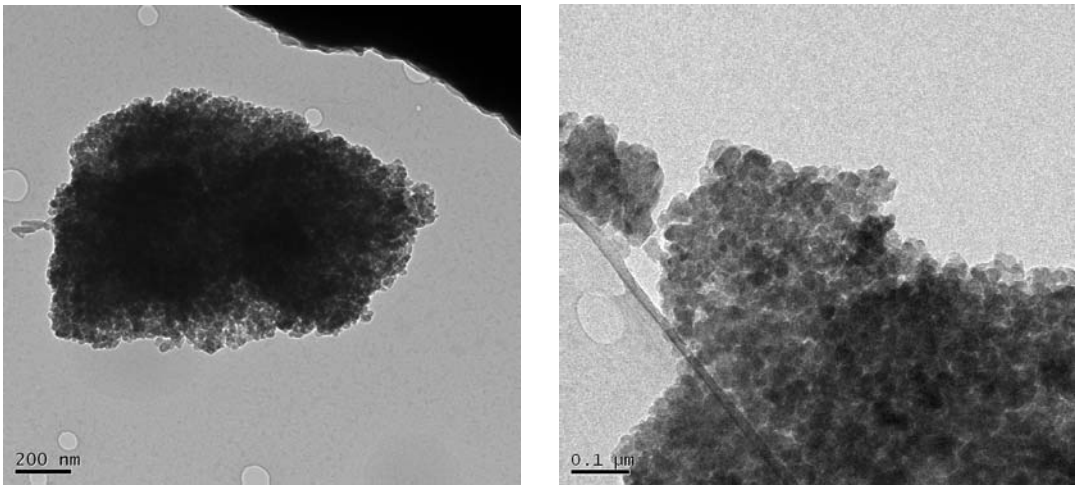

Figure 3.4 : TEM image of nano $CaCO_3$ synthesized by A) PEG 20000 B) PEG 35000

3.5 Synthesis of Nanoparticles of Calcium Carbonate using PEG-PVAc Blend :

In yet another technique, nano-sized filler particles were prepared in-situ using a blending technique that gave further reduction in particle size. The PEG-$CaCl_2$ complex was blended with an amorphous polymer like PVAc, which led to further reduction in particle size.

From table 3.4 it is seen that the particle size reduces with increase in concentration of PVAc. The complex of PEG/$CaCl_2$ is immiscible with PVAc as a result the domain size of dispersed phase is small due to form a complex structure around PEG/ $CaCl_2$ through additional hydrogen bonding. The hydrogen bonding is responsible for stable complex, and which becomes smaller with increasing concentration of PVAc. Thus smaller particles are obtained in this method as compared to the particle we get in only PEG matrix systems mentioned previously. This is also observed in X-Ray Diffraction scan. In Figure 3.5 PEG system the width of the XRD scan is greater than that in commercial system. Also the width of the peak goes on increasing with increasing proportion of PVAc-PEG blending.

Table 3.4: Change in crystallite size of synthesized $CaCO_3$ with different ratios of PVAc blend with PEG-35000 (Polyethylene Glycol)

PEG MW	Reactant Ratio	PVAc Concentration (%)	Calculated Crystallite size(nm)
PEG – 35000	1:16	5	23.46
		10	20.81
		20	19.75
		30	17.615

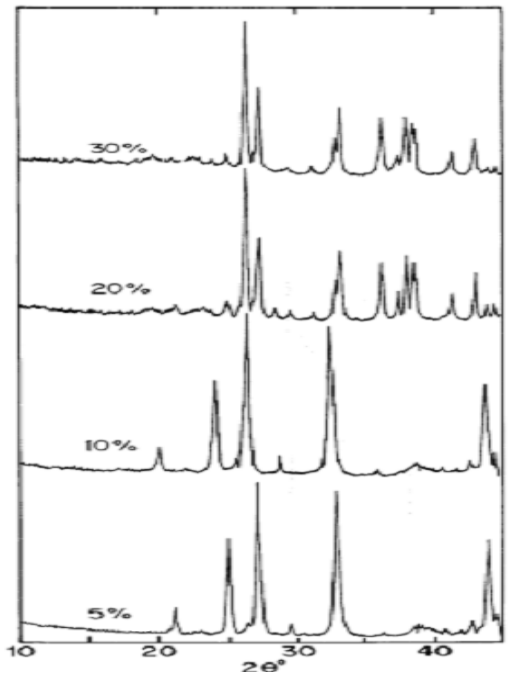

Figure 3.5 : XRD scans of $CaCO_3$ with PEG-35000 blended with PVAc with different concentration

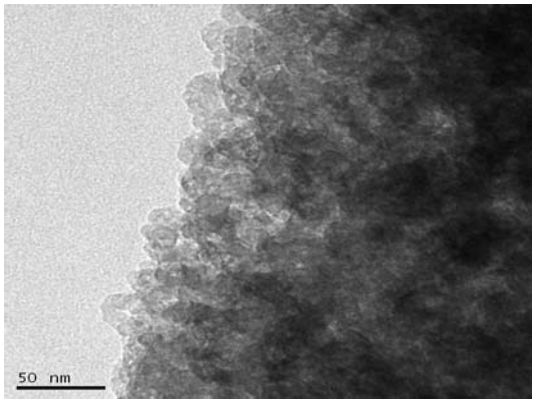

Figure 3.6: TEM image of nano $CaCO_3$ synthesized by PEG 35000: PVAc 20% blend

3.6 Large Scale Synthesis of Nano-$CaCO_3$ with PEG– PVAc Blend:

PMG route was used for synthesis of higher quantity of nano $CaCO_3$ (250 gms) so that it can be used for formulating coatings with different polymers. These were characterized to confirm the nano-particle size and crystalline structure. Figure 3.7 shows the XRD of the large scale batch of nano $CaCO_3$ and Figure 3.8 indicates the TEM for the same.

PEG MW	Reactant Ratio	PVAc Concentration (%)	Calculated Crystallite size(nm)
PEG – 35000	1:16	20	16.723

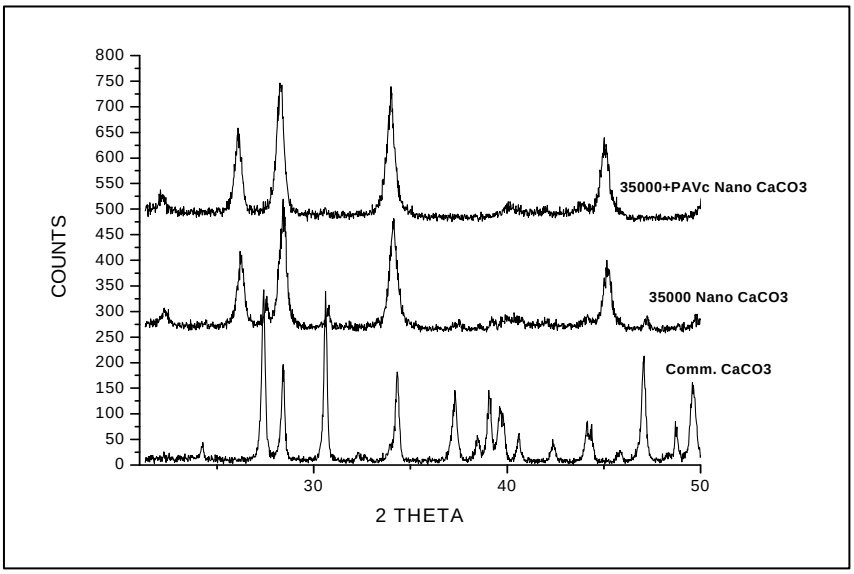

Figure 3.7 : XRD scans of $CaCO_3$ synthesized by using A) PEG 6000 B) PEG 20000 C) PEG 35000

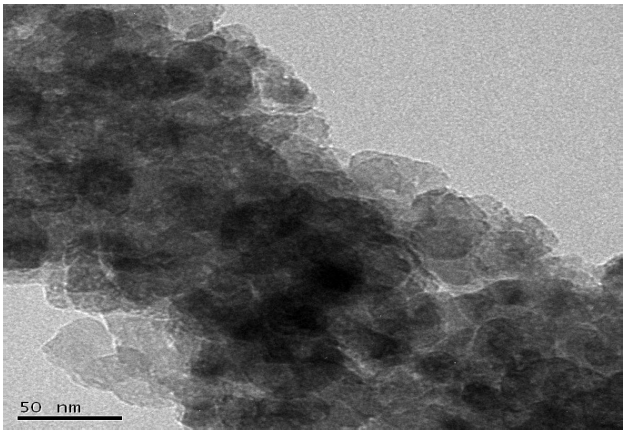

Figure 3.8: TEM image of nano $CaCO_3$ synthesized by PEG 35000: PVAc 20% blend

3.7 Absorbance spectra of Nano $CaCO_3$:

The nano-particle $CaCO_3$ has attracted more and more research interest because of its broad applications in industrial fields. Many researchers tried to explain the abnormal characteristics of nano-material from the viewpoint of the crystal structure and crystal interfacial volume fraction. This contraction (or expansion) of crystal grains results in the distortion of the crystal lattice [34], which is normally called size effect, and further influences the physicochemical properties such as infrared assimilation behavior. For most of the nano-materials, blue shift and broadening of the absorption peaks will occur with the diminution of particle size [35]. For most of the nano-materials, blue shift and broadening of the absorption peaks will occur with the diminution of particle size [36]. However, some nano-materials show both blue shift and red shift of the infrared absorption peaks under the influence of the crystal expansion and hydrogen bonds [33, 35].

In addition to their highest refractive index, strong UV adsorption up to visual wavelength, and transparency at the visible wavelength, which render nanocomposites attractive for making optical materials. Transparency, an increase in refractive index, and other optical gains resulted in to investigation of nanocomposites with the polymer matrices including PMMA [37-44].

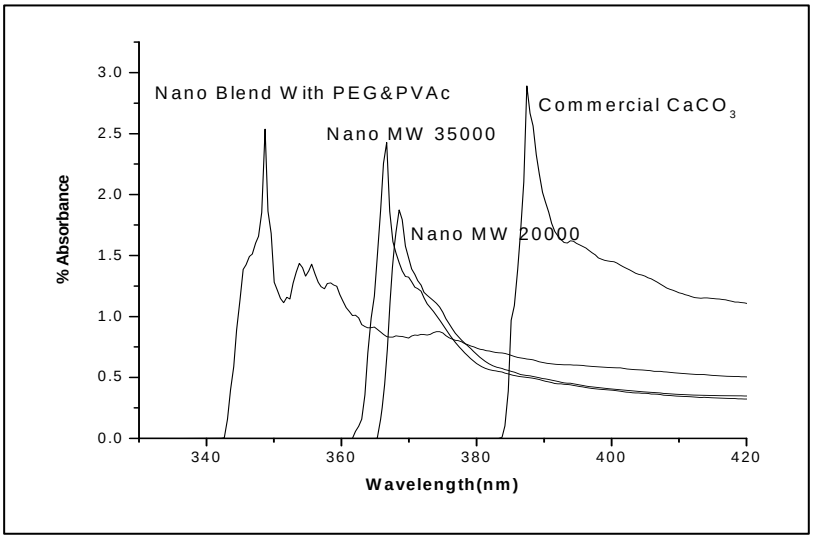

Figure 3.9 : Absorbance spectra of lab synthesized nano $CaCO_3$ in the UV region with peak absorption

The absorbance spectra of $CaCO_3$ of nano and macro particle size are shown in Figure 3.9. Two important features could be noted from the Figure: 3.9 as the crystallite size increases from 17 to 90 nm for $CaCO_3$, the absorbance in the visible region decreases and the absorption peak shows shift toward ultraviolet region from 392 nm for macrosize to 348 nm for nanosize $CaCO_3$. The blue shifting of λ_{max} due to smaller particle size is expected because of the size effect with corresponding change in band gap. The decrease in the overall absorption in the visible region is because of decrease in light scattering (diffuse) and more transparency with lower particle size.

3.8 Preparation of PVAc-$CaCO_3$ nanocomposite coating for optical and corrosion studies

A nanoparticulate material finds applications in various fields. In one such application, the effect of the presence of $CaCO_3$ nanoparticles in the polyvinyl coating as well as the influence of their concentration on the evaluation of the coating behavior in corrosive environment (3.5% NaCl) was studied. Electrochemical impedance spectroscopy, corrosion potential, corrosion current density (Tafel) and optical properties of coating (i.e. gloss and reflectance). The aim of this work is to study the effect of concentration of nanoparticles on the corrosion performance of steel specimens. Coating formulation was made using $CaCO_3$ nanoparticles with using polyvinyl butyral (PVB), polyvinyl acetate (PVAc) etc. as binder. This coating formulation was coated on stainless steel substrates by dip coating followed by heating at moderate temperature.

3.8.1 Optical properties of Nano $CaCO_3$/ PVAc Nanocomposite coating :

Optical properties are function of the properties at the interface. The magnitude of the difference in refractive index across an interface determines, in part, the light-scattering efficiency. Other factors include the size of the scattering species relative to the light wavelength. Air voids included in the film act as additional scattering centers, improving the “dry hiding” in paint films. In a given system, the light scattering coefficient was found to be linearly proportional to coating porosity.

3.8.1.1 Gloss :

Gloss is the ratio of specularly reflected light to incident light. For optically smooth surfaces, gloss varies with refractive index and angle of incidence according to Fresnel's law. Gloss is a function of roughness, an increasing roughness degrades gloss. del Rio and Rudin (1996) showed for a TiO_2 paints with different lattices (particle size ranging from 200 to 1200 nm) the development of gloss for different incidence angles. A minimum in gloss was found at the critical pigment volume concentration (CPVC). However, the CPVC values were found to be different for different incident angles, depending on surface roughness. According to them an incident angle of 85° was found to correlate best with the CPVC.

Size distribution of particles influences the packing structure. A narrow distribution results in a bulky structure whereas a polydisperse pigment packs with a higher density. Brightness and opacity are function of the coating's light scattering ability.

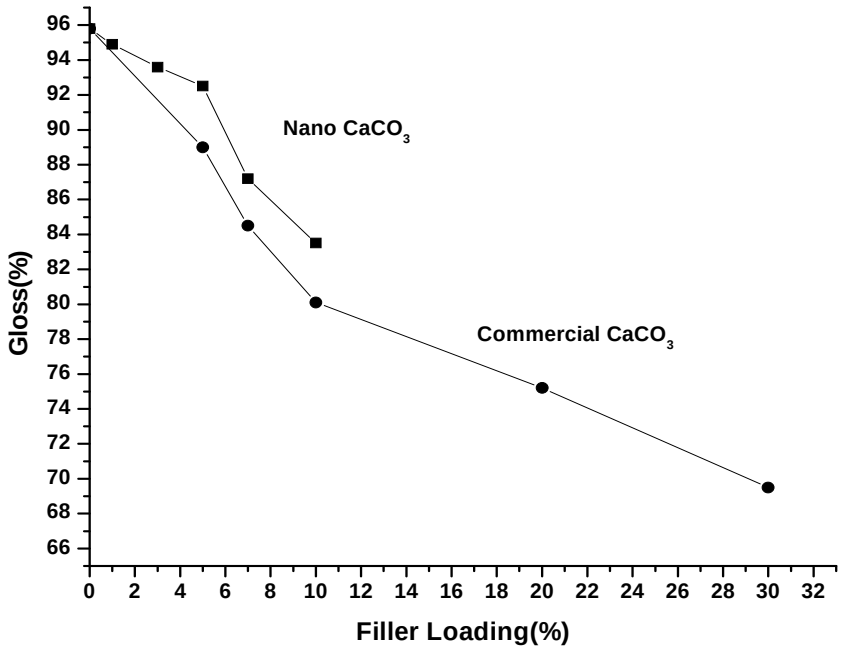

Figure.3.10 : Comparison of gloss between commercial and nanoparticles of $CaCO_3$ in PVAc coating at 60^0 angle

3.8.1.2 Transparency :

It is observed that small $CaCO_3$ nanoparticles size leads to homogeneous dispersion in the polymer matrix which in turn give less surface roughness and hence much higher gloss. On the other hand, the transparency of the coating also improves in presence nano $CaCO_3$ (Fig. 3.11). This is due to reduction in optical scattering as well as individual particle transparency. Both these factors are contributing to improved optical properties of the nanocomposites.

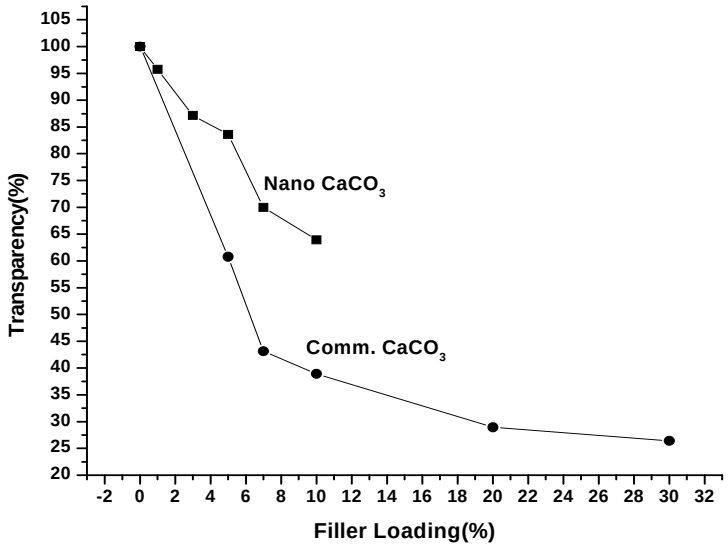

Figure 3.11: Transparency variation with filler concentration of synthesized $CaCO_3$ in PVAc - $CaCO_3$ nanocomposite coating

3.8.2 Corrosion resistance investigation of PVAc - nano $CaCO_3$ Coatings :

Protective coatings are organic polymers applied to a surface, primarily to protect it from oxidation, weathering, and corrosion. In addition, the protective coatings are usually very insulating so that they effectively block the flow of corrosion currents. The largest fraction of protective coatings for field application is mainly organic coating used for corrosion protection of metal substrate. These

coatings are made from formulations containing polymers with fillers and other additives which give corrosion protection. The application of nanocomposite coating is a typical example of such barrier protection. These types of coating will be the focus of our discussion. An active corrosion cell requires the presence of an oxidant at the metal surface as well as a mechanism for ion movement along the surface between the anodic and cathodic site of the corrosion cell. Such ion movement at the interface usually occurs within a thin layer of electrolyte that forms on the metal surface. Coating reduces the rate of corrosion by reducing the rate of access of these essential ingredients to the interface. The coatings also serve to increase the resistance of ion movement at the interface, which also contributes to a reduction in corrosion rate. Eventually, water, oxygen, and ions from the environment penetrate the coating and reach the metal interface and corrosion take place.

Defects in coating expedite the process of corrosion. Molecular adhesion between organic polymer and the metal surface is an important parameter that determines the barrier quality of coating. It is confirmed experimentally that barrier coating having high ionic conductivity afford poor corrosion protection. The coating properties which decrease the permeability of films to water and oxygen enhance the barrier effect. For example, low free volume concentration, high crosslinking, thick film, high crystallinity and proper ratio of pigment volume concentration to critical pigment volume concentration (PVC/CPVC) will help film corrosion protection. Water permeating through an intact film with poor wet adhesion could displace some area of contact from the metal and water with dissolved oxygen would then be in direct contact with the metal surface. The fillers and additives enhance the barrier properties and it is now well known that nano-particulate additives give better barrier resistance than the macro-particulate fillers. In the present work, the effect of organic coating and the presence of $CaCO_3$ nanoparticles in the coatings as well as the influence of their concentration on the evaluation of the coatings' behavior in a corrosive environment (3.5% NaCl) was investigated.

Electrochemical impedance spectroscopy (EIS), Open Circuit potential (OCP), Potentiodynamic polarization (Tafel plot) measurements were performed to investigate the corrosion resistant behavior of the coating. Experiments were

performed with respect to time and temperature of exposure to corrosive environment.

3.8.2.1 Polarization measurement (Tafel Plot)study of PVAc-$CaCO_3$ coating :

The corrosion of steel substrate was estimated for each type of coated specimen by monitoring the open circuit potential (OCP) versus the exposure time to the corrosive environment. Plots of this evaluation with reference to a saturated calomel electrode (SCE) are given for specimens coated with pure PVAc, composites of PVAc with $CaCO_3$ nanoparticles and PVAc with commercial $CaCO_3$.

Figure 3.12 shows Tafel plots of PVAc coating containing nano and commercial $CaCO_3$ having different concentration. The open circuit potential determined from these plot recorded after different time of exposure to hot 3.5 % NaCl solution are indicated Figure 3.13. It is seen that the OCP is initially high and more anodic in all cases with respect to bare steel (-0.6V SCE). Further, the OCP is more anodic in the case of nano-particulate filled coatings than the unfilled or macro-particle filled composite coatings. This suggests that nanocomposites have better corrosion resistance than ordinary coatings. After prolonged exposure the OCP progressively shifts to more cathodic regions in all cases. This is due to increasing penetration of the corrosive ions into the coating and reaching the metal-polymer interface, where the corrosion reaction takes place. Increase in penetration can be due to defect formation, breakdown of barrier and diffusion of ions. It can be seen that in case of pure PVAc the OCP is initially -0.05V SCE but after 50 hrs it shifts to -0.4V SCE (closer to bare steel). In the coatings containing commercial $CaCO_3$, there is similar shift but it depends on the concentration of the filler. At 7% of $CaCO_3$, the shift is seen but it is more anodic than pure PVAc. On the other hand for higher concentration of $CaCO_3$, it is even lower than pure polymer and takes place within 40 hrs. This suggests that more number of defects created and also the structure is more pervious to ion penetration. This can arise from non-uniform distribution of particles and aggregate formation. It is interesting to note that for nano-particle $CaCO_3$, the shift of OCP is much less and quite anodic as compared to the pure PVAc as well as PVAc + commercial $CaCO_3$. It is evident that the nanocomposite coatings have much

better barrier properties and do not allow the corrosive ions / water to permeate through. The shift in the OCP to the potential more noble than the original bare steel increases with the increase in the concentration of nanoparticles.

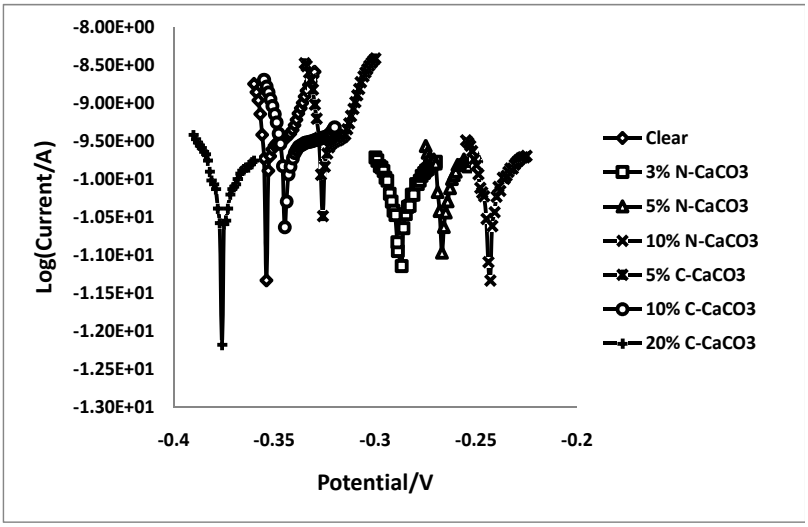

Figure 3.12 : Potentiodynamic polarization plots (Tafel) for different composition of PVAc – $CaCO_3$ coating after 135 hrs at 45^0 C exposed to 3.5% NaCl solution

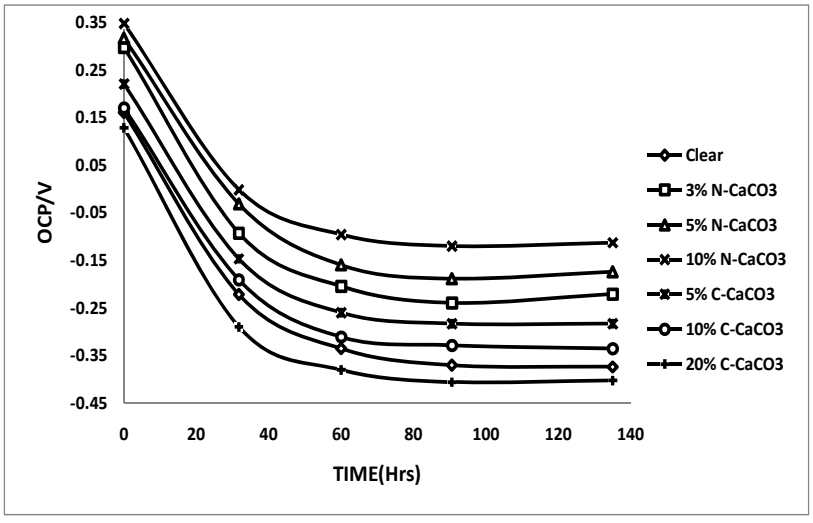

Figure 3.13 : Time dependence of corrosion potential of PVAc - $CaCO_3$ coating at 45^0 C immersed in 3.5% NaCl solution

High OCP value compared to the plain PVAc as well as commercial $CaCO_3$ coating clearly indicate the high corrosion protection provided by the nano $CaCO_3$ coating. This is due to formation of more compact micro-structure of the coating as compared to commercial $CaCO_3$ coating.

Table 3.5 : Study of OCP of different composition of PVAc - $CaCO_3$ nanocomposite coating at various temperatures like 45^0 C and 55^0C

	Composition	Clear	Nano3%	Nano5%	Nano10%	Comm5%	Comm10%	Comm20%
TEMP.°C	TIME(Hrs)							
45	0	0.16	0.35	0.35	0.35	0.22	0.17	0.13
	30	-0.22	-0.04	0.00	-0.12	-0.18	-0.20	-0.25
	60	-0.35	-0.19	-0.14	-0.25	-0.28	-0.31	-0.36
	90	-0.36	-0.23	-0.18	-0.27	-0.30	-0.33	-0.37
	135	-0.35	-0.27	-0.24	-0.29	-0.33	-0.35	-0.38
55	0	0.045	0.15	0.166	0.125	0.082	-0.03	0.069
	30	-0.29	-0.26	-0.29	-0.32	-0.41	-0.36	-0.44
	60	-0.38	-0.3	-0.35	-0.31	-0.34	-0.38	-0.26
	90	-0.33	-0.3	-0.29	-0.31	-0.34	-0.35	-0.44
	135	-0.38	-0.32	-0.28	-0.33	-0.36	-0.39	-0.43

In order to accelerate the corrosion process, the studies were carried out at different temperatures. Table 3.5 gives the values for, the OCP of pure PVAc , nano and commercial $CaCO_3$ coating exposed to saline electrolyte at different temperature and time . It indicates that as temperature is increased, the OCP shifted towards more cathodic side for all compositions. The OCP remains more anodic side for nano coating whereas it is shifting towards more cathodic side of pure PVAc and commercial $CaCO_3$ coating. The variation of OCP with temperature and time which is shown in figure The change in OCP with pure PVAc, nano and commercial $CaCO_3$ at different temperature (45° C and 55° C) shows that OCP decreases as the temperature increases. Since the glass transition temperature of PVAc is about 55° C, there is large change in the OCP and corrosion current as the temperature is increased beyond Tg. The fillers, especially nanoparticle fillers like $CaCO_3$ raise effectively Tg due to physical crosslinking and reduction in free volume. In such cases there is more compactness of the coating and less temperature variation of these properties.

Commercial macro-particles on the other hand, are coarse and form aggregates, defects more easily which leads to poorer performance.

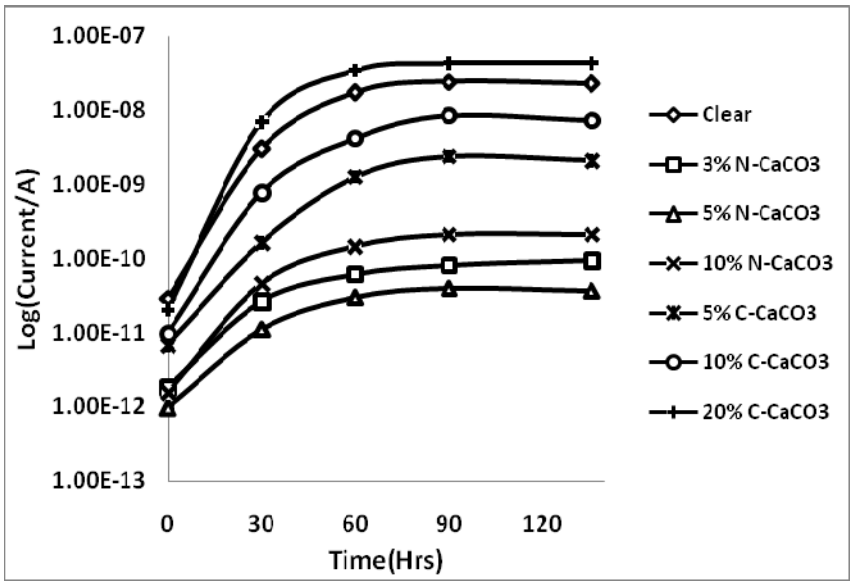

Figure 3.14 : Time dependence of corrosion current of PVAc - $CaCO_3$ coating at 45^0C immersed in 3.5% NaCl saline solution

The corrosion current (I_{corr}) was determined from the Tafel plots for pure PVAc, nano and commercial $CaCO_3$ containing coatings and its variation with time indicted in Figure 3.14. The initial value of I_{corr} for all coating which is low, in the range of 10^{-11} to 10^{-12} increases rapidly of unfilled and commercial $CaCO_3$ filled coatings after exposure to corrosive saline conditions. On the other hand for nanoparticle filled coatings there is little change in the I_{corr} value especially for filler content of 5%. Interesting to note that in some of these nano-composite coatings, there appears to be some self healing effect as well i.e. the I_{corr} value decreases after exposure to saline condition (see 10% nano $CaCO_3$ curve). This may be due to ion exchange between the nano $CaCO_3$ and the -OH groups of PVAc which are invariably present in this polymer. This in turn helps in the formation of protective coating at the metal – polymer interface.

Table 3.6 : Study of corrosion resistivity by corrosion current with different compositions of PVAc - $CaCO_3$ nanocomposite coating at different temperatures like 45^0 C and 55^0 C

Composition / TEMP.(°C)	TIME (Hrs)	clear	Nano3%	Nano5%	Nano10%	Comm5%	Comm10%	Comm20%
45	0	2.52E-13	4.96E-12	2.90E-11	2.02E-11	3.42E-12	9.61E-12	0.00E+00
	30	6.00E-10	5.65E-11	2.75E-11	9.19E-13	2.93E-11	5.04E-12	5.99E-08
	60	1.72E-08	7.46E-11	1.00E-11	1.79E-10	6.67E-10	5.25E-10	1.44E-08
	90	2.44E-08	2.12E-10	2.67E-11	1.82E-11	3.19E-10	1.54E-08	3.15E-08
	135	2.29E-08	2.13E-10	2.21E-11	4.49E-11	1.42E-09	3.98E-09	2.83E-08
55	0	5.13E-12	4.57E-12	1.04E-10	2.16E-11	5.65E-11	1.00E-11	1.50E-11
	30	1.36E-10	4.17E-10	8.96E-09	7.61E-11	3.26E-10	2.41E-09	3.89E-08
	60	2.02E-10	8.71E-11	2.27E-09	1.81E-09	1.14E-10	2.48E-09	4.94E-09
	90	1.38E-09	5.25E-10	5.42E-09	2.82E-09	9.86E-09	4.44E-09	5.52E-08
	135	2.13E-08	6.59E-09	6.95E-09	3.91E-09	1.45E-09	2.41E-08	9.58E-09

3.8.2.2 Electrochemical impedance study of PVAc-$CaCO_3$ coating :

For any anticorrosion coating, the charge transport mechanism is very important and critical to lead to barrier formation, especially electrostatic potential barrier at the interfaces, grains etc. The real part of impedance of the coating (/Z/) give the information on these internal charge transport phenomena.

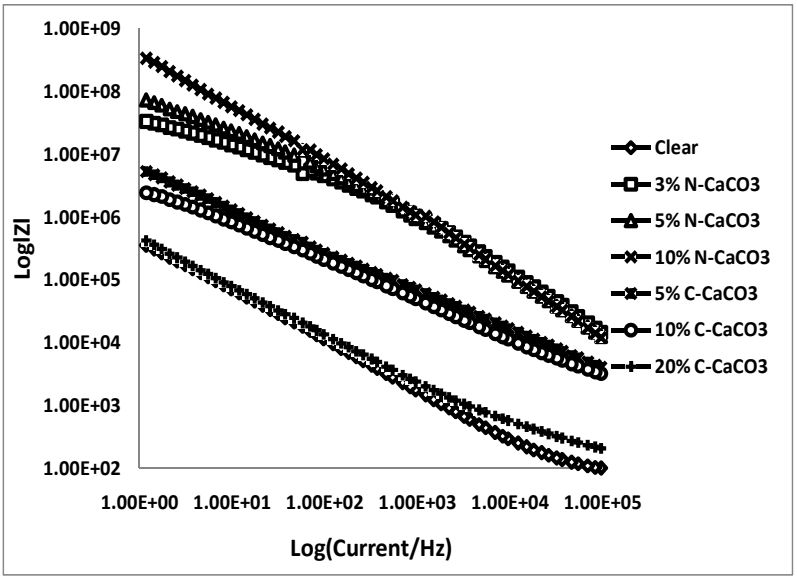

Figure 3.15 : Frequency dependence of impedance log /Z/ for different composition nano and commercial PVAc - $CaCO_3$ coatings after 135 hrs.

Nano $CaCO_3$ coating has higher resistance than the coatings with pure PVAc especially at low frequency which is associated with ionic transport through the film. All coatings have a higher impedance on initial immersion in the electrolyte close to 10^9 Ω as shown in Table 3.7. However as immersion time increases the pure PVAc and commercial $CaCO_3$ degrades more quickly than that of the nano $CaCO_3$ coating and after around 90 hours the pure PVAc and commercial coated substrates show similar resistance, around 10^5 Ω . One possible reason for this continued corrosion protection via the nano $CaCO_3$ coating due to the coating having compact nanostructure sealing and penetration of corrosive species is very difficult so that after 100 hours the coating resistance is $>10^8$ Ω . This also suggests that there is much lower ionic conductivity in the nano-composites than macro-particle composite coatings. Here again, the self healing effect is seen i.e. the impedance decreases slightly first but on prolonged exposure, the impedance again increases which indicates there is a protective layer created within the matrix and or near the interface due to the chemical reaction between the ions and internally liberated calcium ions. This effect is very much pronounced in the nano-particle $CaCO_3$ filled coatings with >5% fillers.

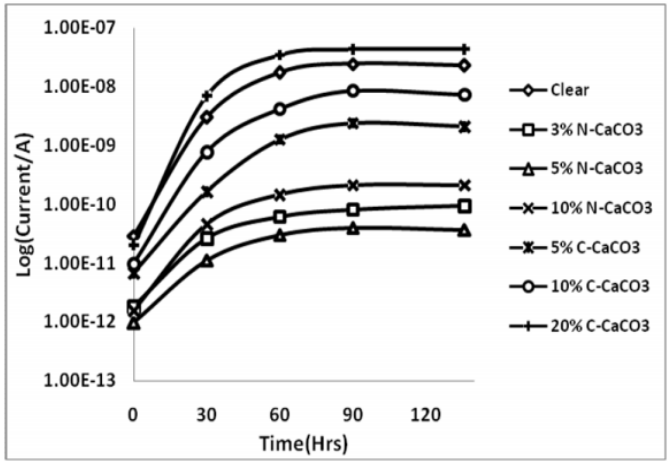

Figure 3.16 : Time dependance of impedance of PVAc - $CaCO_3$ coating at 45^0 C immersed in 3.5% NaCl solution

Nano ccoating has higher resistance than the coatings with pure PVAc especially at low frequency which is associated with ionic transport through the film. All coatings have a higher impedance on initial immersion in the electrolyte close to 10^8 Ω as shown in Table 3.7. However as immersion time increases the pure PVAc and commercial $CaCO_3$ degrades more quickly than that of the nano $CaCO_3$ coating and after around 90 hours the pure PVAc and commercial coated substrates show similar resistance, around 10^5 Ω . One possible reason for this continued corrosion protection via the nano $CaCO_3$ coating may be due to the fact that coating having compact nanostructured sealing and penetration of corrosive species is very difficult so that after 90 hours the coating resistance is 10^{08} Ω .

Table 3.7 : Study of corrosion resistance by bode plot of different compositions of PVAc - $CaCO_3$ nanocomposite coating at various temperatures like 45 ^{o}C and 55^{o}C

composition		clear	nano3%	nano5%	nano10%	Comm5%	comm10%	comm20%
TEMP.(°C)	TIME (Hrs)							
45	0	9.74E+08	3.82E+08	6.16E+08	5.69E+08	9.28E+08	7.15E+08	8.10E+08
	30	5.76E+06	2.18E+08	3.62E+08	1.67E+08	5.36E+08	1.07E+08	1.64E+05
	60	2.45E+05	3.65E+08	4.97E+08	6.58E+08	8.73E+08	1.96E+08	4.76E+08
	90	3.74E+05	2.98E+08	1.03E+08	3.86E+08	2.01E+07	1.45E+05	4.73E+05
	135	3.52E+05	2.21E+08	7.25E+07	3.36E+08	5.28E+06	2.45E+06	2.45E+06
55	0	1.41E+08	1.36E+08	7.18E+08	1.81E+08	5.32E+08	7.30E+08	9.85E+08
	30	4.95E+06	1.13E+07	7.60E+06	3.86E+06	2.44E+06	6.36E+05	1.96E+05
	60	1.19E+05	9.17E+06	5.13E+06	5.44E+06	1.81E+06	1.68E+06	8.50E+05
	90	4.27E+05	6.96E+06	2.41E+06	1.63E+06	1.25E+06	7.43E+05	2.22E+05
	135	6.04E+05	6.60E+06	2.15E+06	3.35E+06	1.58E+06	7.58E+05	7.60E+05

Nano $CaCO_3$ coating has higher resistance than the coatings with pure PVAc especially at low frequency which is associated with ionic transport through the film. All coatings have higher impedance on initial immersion in the electrolyte close to 10^{08} Ω as shown in Table 3.8. However as immersion time increases the pure PVAc and commercial $CaCO_3$ degrades more quickly than that of the nano $CaCO_3$ coating and after around 90 hrs the pure PVAc and commercial coated substrates show similar resistance, around 10^5 Ω . One possible reason for this continued corrosion protection via the nano $CaCO_3$ coating may be due to the fact that coating having

compact nanostructured sealing and penetration of corrosive species is very difficult so that after 90 hours the coating resistance is 10^{08} Ω .

Amongst the various mechanisms for deterioration of barrier coatings, physical defect formation during prolonged exposure to corrosive atmosphere is very important factor. In order to investigate these effects by impedance spectroscopy, the Bode plot is generally used. Figure 3.17 shows the phase angle with frequency for coatings containing various concentration of nano and macro particulate $CaCO_3$ filler after exposure to saline conditions at 45°C for 135 hrs. The increase of phase angle at high frequency region is indicative of defect formation in the coating. Figure 3.18 shows the variation of phase angle at high frequency with respect to time of exposure to corrosive conditions . This is very evident in the coatings containing macro-particle $CaCO_3$ where the phase angle rapidly shifts to upper side giving a broad band peak while there is no such change in the nano-particle containing coatings which remain intact.. The ease of defect formation in the macro-particle filled coatings is due to large amount of fillers as well as aggregate formation leading voids and micro-cracks which expand during aging / corrosion testing.

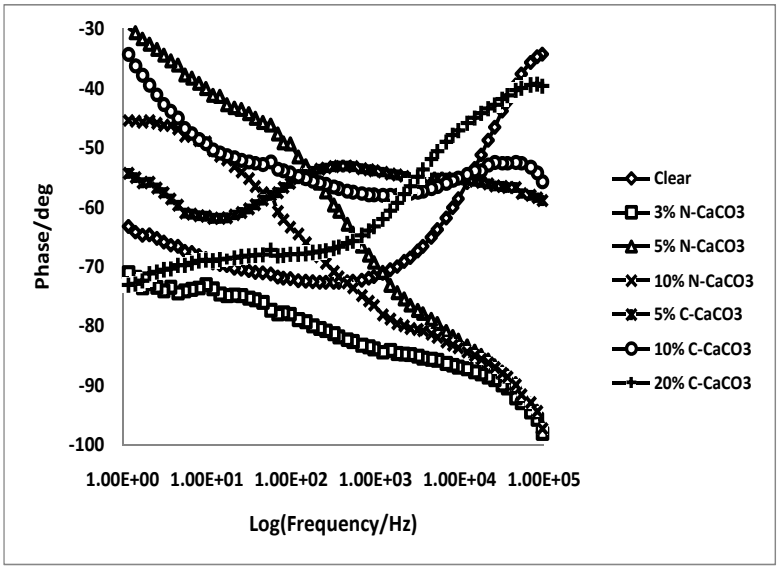

Figure 3.17 : Frequency dependance of phase of different composition of nano and commercial PVAc - $CaCO_3$ filled coatings after 135 hrs.

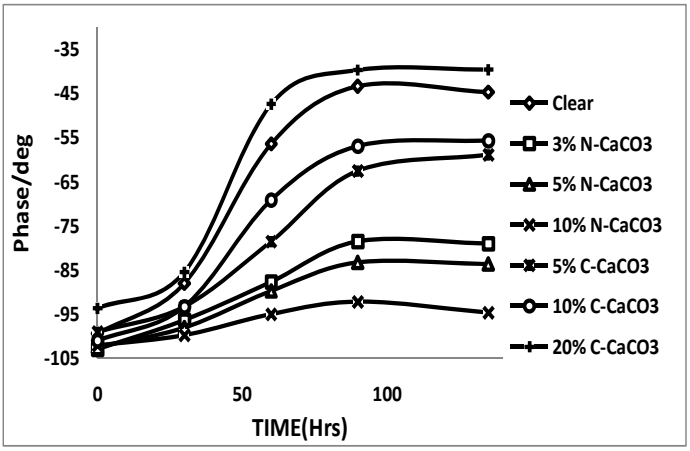

Figure 3.18 : Time dependance of phase of PVAc - $CaCO_3$ coating at 45^0 C immersed in 3.5% NaCl solution

Table 3.8: Study of coating degradation by phase angle of different compositions of PVAc - $CaCO_3$ nanocomposite coating at different temperatures like 45 ^{o}C and 55 ^{o}C

Composition		clear	nano3%	nano5%	nano10%	Comm5%	comm10%	comm20%
TEMP.(°C)	TIME (Hrs)							
45	0	-101.8	-102.9	-102.4	-102.1	-102.5	-102.4	-102.2
	30	-97.2	-99.2	-99.2	-98.1	-98.9	-97.9	-46.2
	60	-33.8	-99.8	-99.6	-99.3	-97	-98.5	-46.2
	90	-32.6	-98.8	-95.9	-97.8	-96.4	-42.9	-45.1
	135	-34.3	-98.3	-97.3	-98.1	-58.9	-55.7	-39.6
55	0	-106.7	-106	-104	-103.7	-105.7	-105.4	-105.1
	30	-93.4	-89.8	-79.4	-86.3	-98.5	-98.5	-74.9
	60	-38.9	-90	-77.5	-64.6	-70.4	-98.4	-56.2
	90	-34.5	-87.4	-66.1	-56.6	-70.2	-74.9	-30.9
	135	-40.7	-76.5	-64.8	-64.7	-62.7	-41.4	-35

Effect of temperatures on coating stability was studied for different particle size and concentration as shown in Table 3.8. It was observed that with increase in temperature phase angle value is increases and changes in phase angle value was more with increase in size of particles and with increase in temperature. At higher temperature, effect of particle size on phase value nullifies and phase value varies drastically. This could be attributed to sudden increase in mobility of charge tranport suggesting defect formation and ion penetration in the film.

3.8.3 Optical Microscopy study of PVAc- $CaCO_3$ nanocomposite coating:

Optical microscope reflectance mode images of coatings are shown in Figure 3.19 for Nano 3% and macro-particle 10%. Extensive damage of the latter after exposure to corrosive conditions is seen. However, nanoparticle composite coatings remain intact with very small micro-defects under similar conditions of corrosive atmosphere. These results corroborate the above conclusions as regards defect formation

Nano 3% Comm. 10%

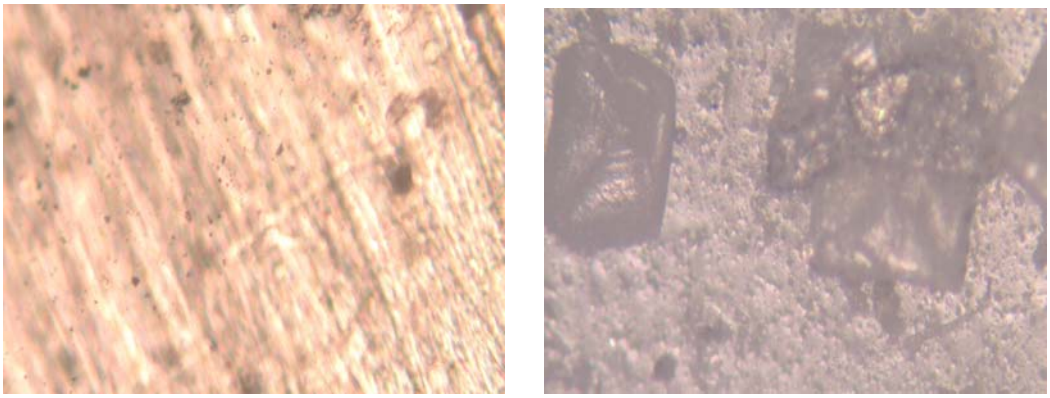

Figure 3.19 : Optical microscope images of PVAc - $CaCO_3$ coating after 135 hrs at 45^{o} C exosed in 3.5% saline solution

3.9 Preparation of PVB-$CaCO_3$ nanocomposite coating for optical and corrosion studies :

Poly (vinyl butyral) (PVB) is a member of the class of poly (vinyl acetal) resins. It is derived by condensing poly (vinyl alcohol) (PVA) with butyraldehyde in the presence of a strong acid. PVA reacts with the aldehyde, to form six-membered rings primarily between adjacent, intra molecular hydroxyl groups, Furthermore, PVB has excellent adhesive properties with many materials such as glass, metal, plastics and wood. Resistance to penetration by natural wood oils, film clarity, heat sealability, adhesion to a variety of surfaces, chemical and solvent resistance, physical toughness [45-47]. Thus, PVB is widely used as paint, an adhesive agent, a printing paste and a film sandwiched in a safety glass for automobiles [48]. Wash primer, Foil Coatings [49], Wood Paints [50], Leather Paints [51], Stoving Paints [52], Printing Inks, Hot-melt Adhesives, Ceramic Binders, transfer Paper for Textile, Powdery Paints, and Adhesives [53].

Fu et al. prepared silica/PVB hybrid material and used as a support of ternary europium complexes and phenanthroline [54]. A new type of coating for manufacturing DNA chips was constructed of the basis of an organic-inorganic nanocomposite based on the polyvinylbutyral-tetraethoxysilane copolymer. The organosilicon composite was functionalized by introduction of ethanolamine vinyl ether copolymers, which contain amino groups and anchor vinyloxide units capable of reacting with silanol groups of the nanocomposite [55]. In the case of PVB, there is a possibility to deteriorate its good optical and adhesive properties [56]. Excess noise in a drop-coated poly (vinyl butyral) carbon black nanocomposite gas sensitive resistor [57].

3.9.1 Optical properties of PVB- $CaCO_3$ nanocomposite coating:

Among the optical properties for coating, gloss plays very crucial role. Gloss property is depend on surface of the coating. The particle size distribution of particles influences the packing structure. A narrow distribution results in a bulky structure whereas a polydisperse pigment packs with a higher density. Figure 3.20 shows the variation of gloss at 60 of nano $CaCO_3$-PVB coating. It was observed that the gloss of commercial $CaCO_3$-PVB coating dropped with increase filler loding. Compared the result with nanocomposite coating, we seen that with gloss level of nano $CaCO_3$ coating much better than commercial $CaCO_3$ coating. When we compared 7% loading both nano and commercial, the gloss dropped drastically in commercial but in nano$CaCO_3$ it has been higher side, due to better dispersion of nanoparticle in coating. But in case of commercial $CaCO_3$, due to higher particle size and rough surface of particles having more porosity and surface roughness.

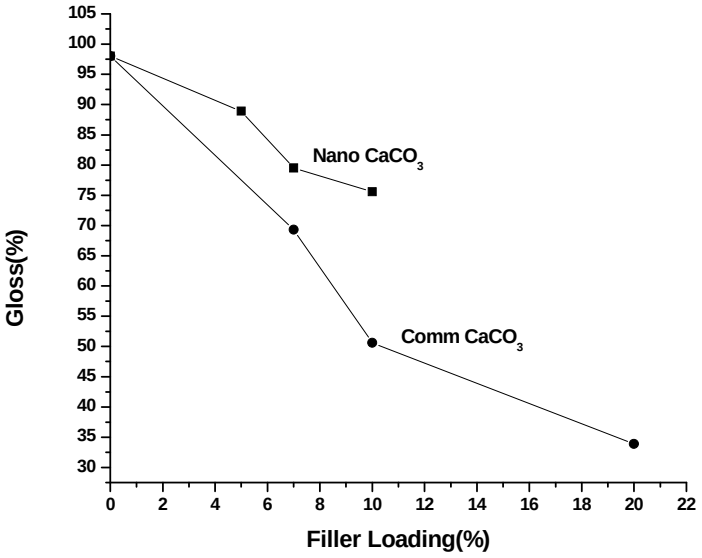

Figure 3.20 : Comparison of gloss between commercial and nano $CaCO_3$ - PVB coating at 60^0 angle

We found smoothness of nanocomposites coating due to reduced down porosity. Porosity is depending on compactness of film, which is affect by particle size and loading of nanoparticles. Comparison between nanocomposite coating films with commercial was studied. We observed that the gloss level decreased drastically above than 5% loading of nanoparticles because of agglomeration of nanoparticles. In case of commercial filler due to higher particle size the surface smoothness is uneven and porosity is high so gloss level is decreased.

3.9.2 Corrosion resistance investigation of PVAc - nano $CaCO_3$ Coating :

PVB-nanocomposite coating was prepared by different percentage loading of $CaCO_3$ nanoparticles. We studied the barrier properties of coating. The barrier properties studied by electrochemical method, which include polarization measurement and electrochemical impedance spectroscopy.

3.9.2.1 Polarization measurement (Tafel Plot) study of PVB-$CaCO_3$ coating :

In Figure 3.21, i.e. in the tafel plot, which shows open circuit potential of PVB coating. Effect of particle size after 300 hrs was observed by OCP, The measurements were carried out at an accelerated temperature at 45^0 C and compared with commercial particulates.

The Tafel plot show that the nanocomposite coating shows potential at anodic side (0.051V, -0.106V and -0.136V) indicating the good barrier properties even after 300 hrs. In case of coating without filler loading, OCP is more negative as compare to nanocomposite coating (-0.269V). Commercial coating is totally shifted towards more negative (cathodic side) which indicating poor barrier properties of the coating (-0.324,-0.354, -0.340) which is shifted towards to that of bare steel (-0.5V).

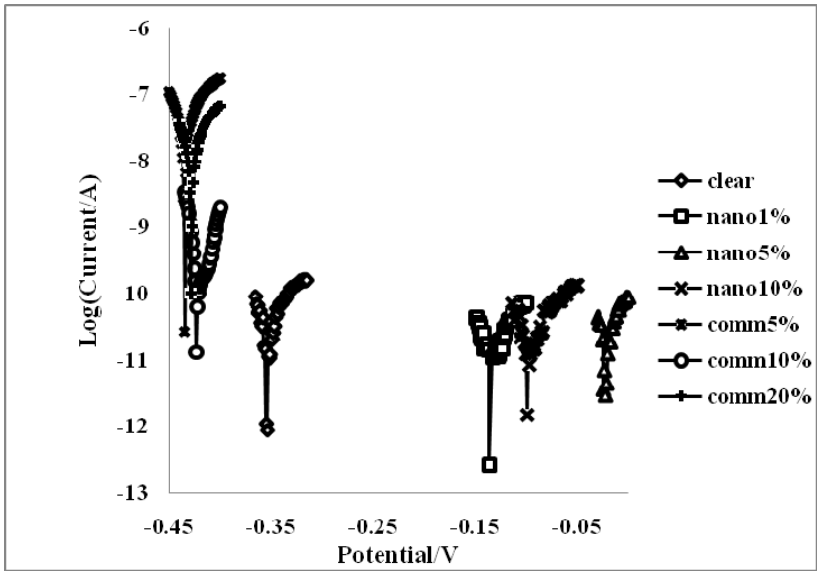

Figure 3.21 : Potentiodynamic polarization plots (Tafel) for composition of PVB – $CaCO_3$ coating after 150 hrs immersion at 45^0C exposed to 3.5% NaCl solution

OCP w.r.t. time of clear epoxy, commercial $CaCO_3$ and nanocomposite coating shows in Figure 3.22. The OCP gradually decreases after 40 hrs and remains constant thereafter however commercial further drops gradually above 125 hrs. Coating without any filler follows similar trend with time as observed in commercial coatings. In nanocomposite coating the OCP dropped initially very nominal till 75 hrs and remain steady thereafter upto 150 hrs also indicating nanocomposite coating exhibits good compact structure which restricts transport of the corrosive ions through the coating. This trend was observed in case of 1% to 10% loading of nanoparticles. Though trend of corrosion resistance observed was similar but from Figure 3.22 it appears that resistance to corrosion of nano 1% is less than nano 5% but better than commercial particulates and coating without any fillers. Lower resistance nano 1%

than nano 5%; could be because of less effectiveness nanoparticles due to less no. nanoparticulates present in per square unit area of coating. However if nanoparticulates loading when increased upto 10%; corrosion resistance slightly decreases which might be because of exceeding critical pigment volume concentration (cpvc).

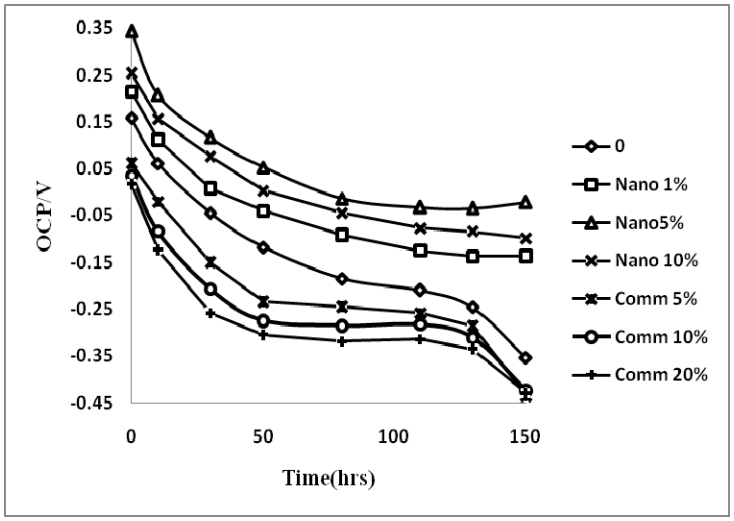

Figure 3.22 : Time dependence of corrosion potential of PVB - $CaCO_3$ coating at 45 ^{0}C exposed to 3.5% NaCl solution

3.9.2.2 Electrochemical Impedance analysis of PVB - $CaCO_3$ coating:

The corrosion properties of the PVB coating was characterize by EIS. The test was carried out for over 150 hrs at 45^{o}C with 3.5% NaCl solution for different percentage loading of nanoparticulate and commercial micro particulates, which was compared with clear or coating without any fillers. It was observed that particle size plays very crucial role in corrosion properties as shown in Figure 3.23

Comparison between nanocomposite coating films with commercial was studied, and it was found that the coating with nano fillers with 1%, 5% and 10% loading overall corrosion properties are improved i.e., initial resistance. But as can be seen from Figure 3.23, at nano 1%, corrosion resistance is improved compared to clear coating (i.e., without any fillers) and commercial coating; nano 5% coating shows better resistance than nano 1% when further loading was increased i.e., upto nano 10%, its resistance decreased but still exhibited better properties than commercial and clear coatings.

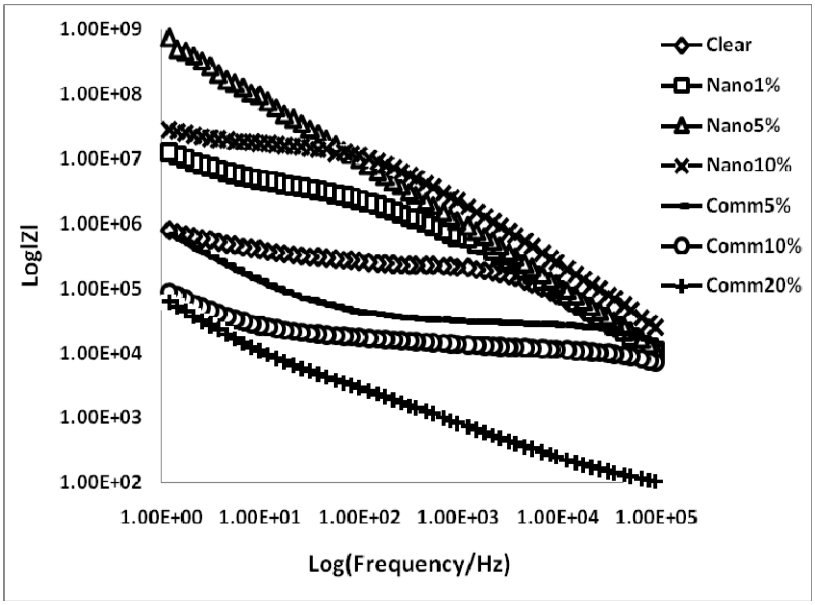

Figure 3.23 : Frequency dependence of impedance log /Z/ for different composition nano and commercial PVB - $CaCO_3$ coatings after 150 hrs.

Whereas in case of commercial coating comm. 5%, exhibited similar properties as that of clear coating, here added advantage over clear coating is that while maintaining the corrosion properties, cost of the coating can be reduce, however when loading was further increased to comm. 10%, resistance decreased, which could be attributed to effect of large particle size. We found that nanocomposites coating increases resistance due to reduced down porosity, which again depends on compactness of film, which is affected by particle size and percentage loading of nanoparticles.

The coating impedance with time (Figure 3.24) was somewhat stable over this time period in clear and commercial coating. There was a gradual decrease upto 50 hrs for the solution resistance, which is consistent with time till after 150 hrs.

The drop is believed to be due to micron size of commercial filler, which allows the corrosive ion to penetrate due to high porosity. About coating containing nanocomposite all plot exhibited high resistance of coating at low frequencies. Since these higher impedance values correlate to the coating resistance. The overall trend for the coating resistance is decreasing.

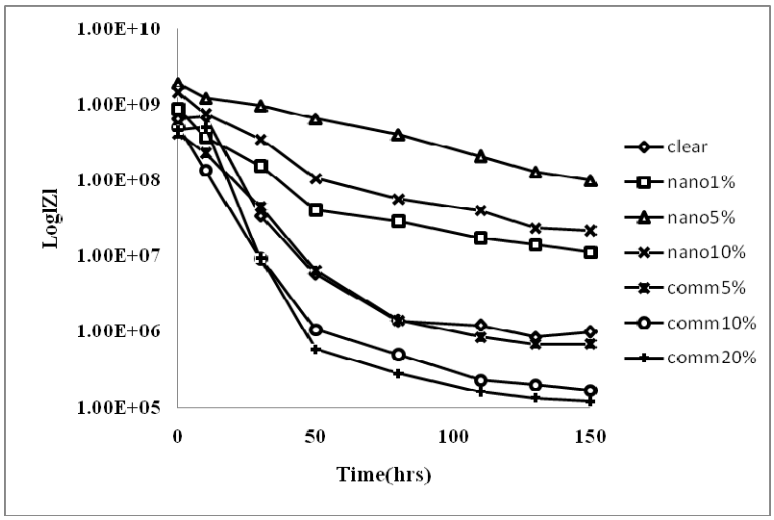

Figure 3.24 : Time dependence of impedance of PVB-$CaCO_3$ coating at 45 ^{0}C immersed in 3.5 % NaCl Solution

The coating resistance of PVB-$CaCO_3$ has higher side than the coatings with pure PVB especially at low frequency, which is associated with ionic transport through the film. So it seen in Figure 3.24 with time, all coatings have higher impedance on initial immersion in the electrolyte close to 10^{09} Ω. However as immersion time increases the pure PVB and commercial $CaCO_3$ degrades more quickly than that of the nano $CaCO_3$ coating and after around 90 hrs the pure PVB and commercial coated substrates show similar resistance, around 10^{06} and 10^{05} Ω respectively. One possible reason for this continued corrosion protection via the nano $CaCO_3$ coating may be due to the fact that coating having compact nanostructured sealing and penetration of corrosive species is very difficult so that after 90 hrs the coating resistance is 10^{08} Ω.

The phase angle shows that the degradation of film due to attack of corrosive species from figure 3.25, it shows that phase value at initial stage is -90^o to -95^o for all compositions including clear PVB and commercial $CaCO_3$ continuing same experiment up to 150 hrs,

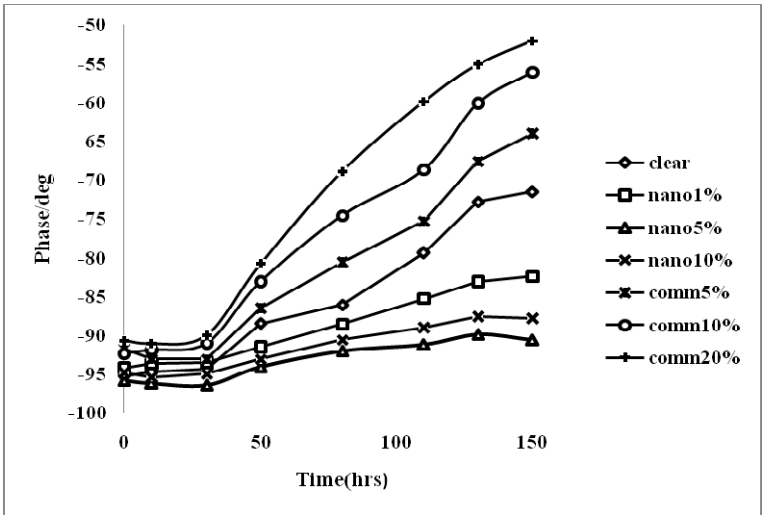

Figure 3.25 : Time dependance of phase of PVB-$CaCO_3$ coating at 45 ^{0}C immersed in 3.5% NaCl solution

We observed that after 90 hrs phase value changes drastically in case pure PVB and commercial coatings were -70 and -80^o respectively, which shows the degradation of the film considerably. Similar pattern was observed when continued upto 150 hrs. In case of nano $CaCO_3$, 5% loading, it was observed that after 90 hrs phase values were around -90^o and after 150 hrs -88^o which shows the coating resistance against corrosive species is more because the film of $CaCO_3$ nanocomposite coating is still not degraded.

3.10 Conclusion :

Calcium carbonate nanoparticles have been synthesized using polymer mediated growth technique. These have been characterized for their structure, particle size and optical properties. The effect of polymer molecular weight, molar ratio with the initial reactant, blending on the calcium carbonate produced has been studied. There is clear shift in the particle size to nano region with increasing molecular weight of PEG used and blending this with PVAc further reduces the calcium carbonate size which is formed in the matrix. The coatings incorporating this nanoparticulate calcium carbonate exhibit much superior optical properties in terms of gloss and whiteness. These coating also have much higher corrosion resistance than the coatings containing commercial calcium carbonate.

3.11 References :

[1] Schroter W.; Lautenschlage K.H.; Bibrack H. *Taschenbuch der Chemie.* **1990**, Thun: Verlag Harri Deutsch.

[2] Clarkson J. R.; Price T. J.; Adams C. J. *Journal of the Chemical Society Faraday Transactions,* **1992**, 88, 243-249.

[3] Kralj D.; Brecevic L.; Nielsen A. E. *Journal of Crystal Growth*, **1990**,104, 793-800.

[4] Silva A. L. N., Rocha M. C. G., Moraes M.A. R., Valente C. A. R., and Coutinho F.M.B., *Polym. Test.*, **2002,** 21, 57.

[5] Osman M. A., Atallah A., and Suter U. W, *Polym.***, 2004,** 45,1177.

[6] Pukanszky B. and Fekete E., *Advances in Polymer Science*, **1999**, Vol. 139, pp 110- 153

[7] Rothon R.N., *Advances in Polymer Science*, **1999**.vol 139, pp. 251

[8] Roussel M. D., Guy A.R., Shaw L.G. and Cara J.E.,Inc.61 Main St. Proctor, VT 05765.

[9] Guy A.R., *TAPPI Polymers, Laminations, and Coatings Conference, Proceedings* **2004**, Indianapolis, IN.

[10] Ruiz F.A.,*TAPPI Polymers, Laminations & Coatings Conference Proceedings TAPPI Press,* **1994,** p.89 – 95.

[11] Bartzcak Z., Argon A.S., Cohen R.E., and Weinberg M., *Polymer*, **1999**, 40, 2347.

[12] Mann S., Heywood B. R., Rajam S., Birchall J. D. *Nature*, **1988,** 334, 692—695.

[13] Hari B., Ding X. F., Guo Y. P., Deng Y. H., Wang C. Y., Li M. G., Wang Z. C. *J Mater Lett*, **2006**, 60, 1515—1518.

[14] Keum D. K., Kim K. M., Naka K., Chujo Y., *J. Mater Chem,* **2002**, 12, 2449—2452.

[15] Wei H., Shen Q., Zhao Y., Zhao Y., Wang D. J., Xu D. F., *J Cryst Growth,* **2004**, 26, 511—516.

[16] Tong H., Ma W. T., Wang L. L., Wan P., Hu J. M., Cao L. X. *Biomaterials,* **2004**, 25: 3923—3929.

[17] Ueno Y., Futagawa H., Takagi Y., Ueno A., Mizushima Y. *J Controlled Release,* **2005**,103, 93—98.

[18] Domingo C., Carmona J. G., Loste E., Fanovich A., Fraile J., Morales J.G. *J Crystal Growth,* **2004,** 271, 268—272.

[19] Li Z., Guo S., Song W., Yan Y., *J Polym Sci Part B: Polym Phys,* **2002,** 40, 1804—1812.

[20] Zeshan Hu, Yulin Deng and Qunhui Sun, *Colloid Journal*, **2004**,Vol. 66, No. 6, pp 745-750.

[21] Yu Dong, Chu Ying, Dong Li-hong and Zhuo Yu-Jiang *Chem. Res. Chinese Universities*, **2010**, 26(5), 678—682.

[22] Olad and Rashidzadeh A. *Iranian, Journal of Chemical Engineering*, **2008**, Vol. 5, No. 2 (Spring), IAChE

[23] Haojie Yu, Li Wang, Quan Shi, Song Jiang, Guohua Jiang, *Journal of Applied Polymer Science*, August **2006**, Volume 101, Issue 4, pages 2656–2660, 15

[24] Hare C.H., *Mod. Paint and Coatings,* November **1993**. Volume 83 (12).

[25] Lam C., Zhang Y.F., Tang Y.H., Lee C.S., Bello I. and Lee S.T., *Journal of Crystal Growth,* December **2000**,Volume 220, Issue 4, , Pages 466-470.

[26] Takuya Tsuzuki, Kellie Pethick and Paul G. McCormick, *Journal of Nanoparticle Research*, **2001**, Volume 2, Number 4, 375-380

[27] Devarajan A., Abdul Khadar M. and Chattopadhyay K. *Materials Science and Engineering: A*, 15 April **2007**, Volumes 452-453, Pages 395-400

[28] Saujanya C., Ashamol S., Padalkar S., Radhakrishnan S. *Polymer*, **(2001)**, 42, 2255.

[29] Saujanya C., Radhakrishnan S. *Polymer*, **2001**, 42, 6723.

[30] Saujanya C., Radhakrishnan S. *J. Mat. Sci*., **1998**, 33, 1063.

[31] Saujanya C., Radhakrishnan S. *J. Mat. Sci.,* **(1998)**, 33, 1069.

[32] Brown W. R., Park G. S. J., *Paint Tech*., **(1970)**, 42, 16.

[33] Radhakrishnan S., Saini, *J.Cryst.Growth,* **(1993)**, 129,191

[34] Ye B., Del Genio A.D., and Lo K.K.W., *J. Climate*, **1998**, 11, 1997-2015.

[35] Yue Lin-hai, Shui Miao and Xu Zhu-de, *Journal of Zhejiang ,University* -

Science A **2000**, Volume 1, Number 2, 178-183.

[34] Ren Y.L., Wang X., Shui M. and Li R.S., *Journal of Thermal, Analysis and Calorimetry*, **2010**, Volume 91, Number 3, 867-871.

[37] Agag T., Tsuchiya H., Takeichi T., *Polymer*, **2004**, 45, 7903.

[38] Carotenuto C., Her Y.S., Matijevic E., *Ind. Eng Chem. Res*., **1996**, 35, 2929.

[39] Chang C. C., Chen W. C., *J. Polym. Sci,* **2001**, 39, 3419.

[40] Chen G., Chen X., Yao K., *J. Mater. Sci. Lett.,* **1999**, 18, 1761.

[41] Lee L. H., Chen W. C., *Chem. Mater.,* **2001**, 13, 1137.

[42] Yang B. D., Yoon K. H., *Synth. Metals***, 2004**, 142, 21.

[43] Wang B., Wilkes G. L., McGrath J. E., *Macromolecules,* **1991**, 24, 3449.

[44] Gerardo del Rio and Alfred Rudin, *Progress in Organic Coatings*, August **1996**, Volume 28, Issue 4, Pages 259-270

[45] Knapczyk, J. W. In *Kirk-Othmer Encyclopedia of Chemical Technology*, 4th ed.,Edited by J. I. Kruschwitz. John Wiley and Sons, New York, **1997**, Vol. 24, p. 924.

[46] Blomstrom, T. P. In *Encyclopedia of Polymer Science and Engineering*, edited by H. F. Mark, et al. John Wiley and Sons, New York, **1989**, Vol. 17, p.136.

[47] Lavin, E., and J. A. Snelgrove. In *Kirk-Othmer Encyclopedia of Chemical Technology*, 3d ed., edited by J. I. Kruschwitz. John Wiley and Sons, New York, **1983**, Vol. 23, p. 798.].

[48] Blomstrom, T. P. *Concise Encyclopedia of Polymer Science and Engineering*", Edited by Kroschwitz, J. I. John Wiley & Sons, Inc., N.Y. (**1990**).]

[49] Zbigniew S. Rak and Janusz,Walter *Journal of Materials Processing Technology* **2006**, Volume 175 Issues 1-3, Pages 358-363

[50] H. K. Jeong, M. Rooney, D. J. David, W. J. MacKnight, F. E. Karasz, T. Kajiyama *Polymer*, Volume 41, Issue 15, **2000**, Pages 6003-6013

[51] Sina Ebnesajjad *Handbook of Adhesives and Surface Preparation*, **2011**, Pages 137-183.

[52] Barbara Biegaǹska and Edward Ś̀mieszek *Progress in Organic Coatings* **1982**, Vol 10, 3**,** Pages 215-234

[53] Allen K. W. *Encyclopedia of Physical Science and Technology (Third Edition)* **2004** Pages 237-250

[54] Fu, L., Zhang, H., Wang, S., Meng, Q., Yang, K. and Ni, J. *J. Sol-Gel Sci. Tech.*, **1999** 15 49-55.

[55] Annenkov VV, Levina AS, Danilovtseva EN, Filina EA, Mikhaleva EA, Zarytova VF. *Russian Journal of Bioorganic Chemistry,* **2006,** Vol. 32, No 5, pp.460-467,

[56] Pistek K. Merinska D., Dujkova, tupy *M SENSIG '10/MATERIALS'10 Proceedings of the 3rd WSEAS international conference on Advances in sensors, signals and materials,* **2010** pp-26-29

[57] Arshak K.I., Cavanagh L.M. and Cunniffe C. *Thin Solid Films*, **2006**, Vol 495, Issues 1-2, Pages 97-103

CHAPTER – IV

Effect of Fe_2O_3 nanoparticle Addition on Optical and Corrosion Properties of PVAc and PVB nanocomposite Coatings.

CHAPTER 4

4.1 Introduction :

Iron being one of the transition elements, exhibits very peculiar characteristics, due to various oxidation states, because of which various transitions occurs, which further affects on its magnetic and structural polymorphism. Iron is available in abundance, it comprises of more than 80% of the metals available.

The iron oxide (Fe_2O_3), the most common oxide of iron comprises some important magnetic properties. The existence of amorphous Fe_2O_3 and its four types of polymorphs (alpha, beta, gamma and epsilon) is well established [1]. The most frequent polymorphs structure "alpha" (hematite) possesses a structure in the form of rhombohedra-hexagonal. Prototype corundum structures and cubic spinel structure "gamma" (magnetite) have been found in nature. Hematite has strongly antiferromagnetic properties. Gamma Fe_2O_3 (magnetite) is the ferromagnetic cubic form of Fe (III) oxide and it differs from the inverse spinel structure of magnetite by having vacancies on the cation sublattice. In time, at room-temperature, the maghemite turns into hematite crystalline structure.

Magnetic nanoparticles have been attracting much interest as a labeling material in the fields of advanced biological and medical applications such as drug delivery, magnetic resonance imaging and array-based assaying [2]. Iron oxides often form only minute crystals, both in natural environments and when produced industrially. They have, therefore, a high specific surface area, often > 100 m^2/g, at which the so called functional groups are exposed; this makes them effective sorbents for a large range of dissolved ions, molecules and gases [3].

The use of nanosized inorganic iron oxide particles is particularly attractive with the aim of improving the properties of polymers such as appearance, chemical, mechanical etc. by controlling the degree of interaction between the polymer and the nanofiller [4]. Coating properties can be markedly improved by replacing conventional pigments with nanosized particles, thus improving properties. In contrast to micron Fe_2O_3, nano-Fe_2O_3 added coatings not only improves their coloring

ability, transparency, and UV resistance but also results in new properties, including antibacterial and self-cleaning properties. However, little research has been carried out on the effect of nano-Fe_2O_3 on barrier properties [2].

Nanoparticles are prone to aggregate because of the high surface area-to volume ratio, which affect their application. The synthesis of inorganic nanoparticles with controlled morphology has attracted great interest due to its important application in various fields. Use of iron-oxide nanoparticles is particularly interesting, due to the excellent hiding power and long-term outdoor exposure properties. Iron oxide is characterized as being lightfast and by its excellent chemical resistance. Iron oxide pigments with extremely small particle diameters are used in metallic-effect coatings and transparent paints [5].

The electrochemical testing of coated mild steel substrates indicated that the nano-scale additive imparted high corrosion resistance of the coating relative to the commercial grades. In one of the examples, the coating containing the nano-scale additive withstood a harsh chloride-laden environment at 50° C even for 8 hours, whereas the coating containing the commercial-grade additive failed immediately within 1 hour.

4.2 Synthesis of Nanoparticles of Iron Oxide using PEG with different Molecular Weights :

The polymer mediated growth technique (PMG) is a versatile route to obtain functionalized nanoparticles that involves a two-step processes, whereby polymer (PEG)-protected nanoparticles are initially synthesized followed by partial or complete exchange with the functionalized ligands in subsequent steps [6-10]. The first step allows controlling the particle size through the stoichiometry of the metal salt and the capping ligand (such as PEG 4000, 6000, 20000 and 35000). In the second step, incorporation of second reactant forms relevant metal oxide and sodium hydroxide solution is added to form Fe_2O_3 nanoparticles.

The nano-particle of ferric oxide was initially prepared by forming complex of ferric chloride ($FeCl_3$) with Polyethelyene glycol (PEG) in molar ratio of 1:12 and then reacting the same with stiochiometeric proportion of sodium hydroxide.

Typically, the polymer viz., polyethylene glycol (PEG MW 35000, 20000, 6000, 4000) and stiochiometry ratio is defined with Fe^{3+} which will be reacted with monomer of polymer (1:1, 1:3, 1:6, 1: 12.1:24).

From Table 4.1 it can be seen that the particle size of Fe_2O_3 decreases with increasing molecular weight of PEG. As molecular weight increases, the diffusivity was observed to decreasing. Lower the molecular weight of polymer, smaller the length of polymer and hence tends to stay away from each other. The path for freely moving sodium and hydroxyl in the solution gets easier. Thus, the resistance to the movement of sodium and hydroxyl is less. As a result, sodium and hydroxyl ions diffuse more freely and hence diffusivity is more. The viscosity and binding of the Fe(III) ions within the matrix are important in the formation of the particles in the PMG process. Higher the molecular weight, more is the viscosity and slower is the diffusion of the reactive OH- ions. The molar ratio and the segmental motion decide the tight binding of Fe(III) in the PEG matrix. If the molecular weight is less, there is greater movement of these ions and the probability of their agglomeration leading to bigger particle size formation becomes high. This is evident from the variation of particle size with molecular weight of the polymer used.

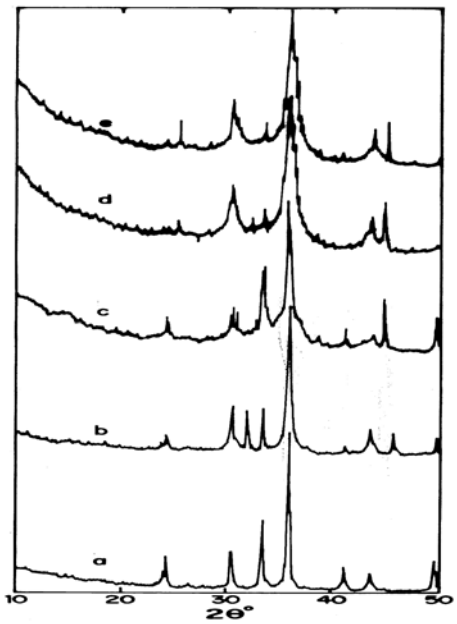

Figure 4.1 : X-ray Diffraction scans of Fe_2O_3 a) Precipitated Fe_2O_3 b) PEG4000 c) PEG6000 d) PEG 20000 e) PEG 35000

Table 4.1 : Change in crystallite size of synthesized Fe_2O_3 for different molecular weights of PEG

Sample	PEG Molecular weight	Crystallite Size(nm)
A	4000	16.5
B	6000	10.5
C	20000	7.5
D	35000	6.2
E	Commercial Fe_2O_3*	78.2

*The commercial grade mentioned in the table is the precipitated grade used for coatings.

4.3 XRD Characterisation of Fe_2O_3 nanoparticles :

The size of ferric oxide can be reduced to nanoscale by properly adjusting the concentrations of polymer and the reactant. More the molecular weight of the polymer, the particle size of Fe_2O_3 is decreased to a considerable extent. The synthesis procedure is discussed in chapter-2.

Figure 4.1 shows the XRD scans of Fe_2O_3 synthesized using different molecular weight polyethylene glycol. The curves (a), (b), and (c) correspond to commercial, PEG 20000 and PEG 35000 respectively, and curve (a) is for commercial Fe_2O_3 having the α-phase. In case of (b) and (c), the molecular weight of PEG is different but composition of the complex remained the same, i.e. 12:1 prior to the reaction with $FeCl_3$. All the peaks were identified as those originating from alpha ferric oxide. These have been indexed as shown in the figures later. The peak intensities of XRD pattern change with amount of PEG used and its molecular weight in the PMG route but the major peaks (110) remain the same. It is clear that the crystalline phase of Fe_2O_3 depends on the synthesis route and the polymer matrix used.

The prominent peak is considered for crystallite size calculation which is done through Scherrer's equation. It is clear from the scan that the FWHM of is increased with increase in the molecular weight of PEG. This is a reflection of reduction in the crystallite size of Fe_2O_3. It can also be seen from the Figure 4.1 that the FWHM of peak of commercial ferric oxide is lesser than the one synthesized by PMG technique. Table 4.1 describes the crystallite size / particle size reduction of ferric oxide with increase in the MW of PEG. The crystallite size decreases from 17 nm to 6 nm when the molecular weight of PEG is increased from 4000 to 35000 for a fixed polymer to reactant ratio i.e. 1:12.

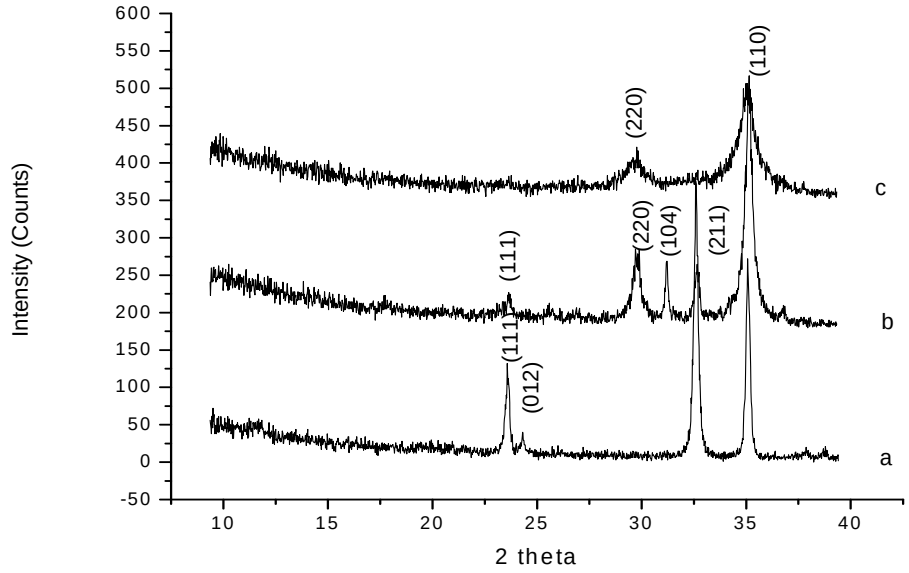

Figure 4.2 : X-ray diffraction scans of Fe_2O_3 with different of molecular weight of PEG a) Commercial b) 20000 c) 35000

In order to confirm the above findings, Fe_2O_3 synthesized by using PEG of molecular weights 20,000 and 35,000 was examined by TEM. Fig. 4.3 depict typical electron micrograph obtained for Fe_2O_3 synthesized using 35000 PEG. The tiny particles (black spots) of the order of 7 nm embedded in the PEG matrix are clearly visible. Higher magnifications could not be used due to instability of the polymer matrix under high-energy electron bombardment.

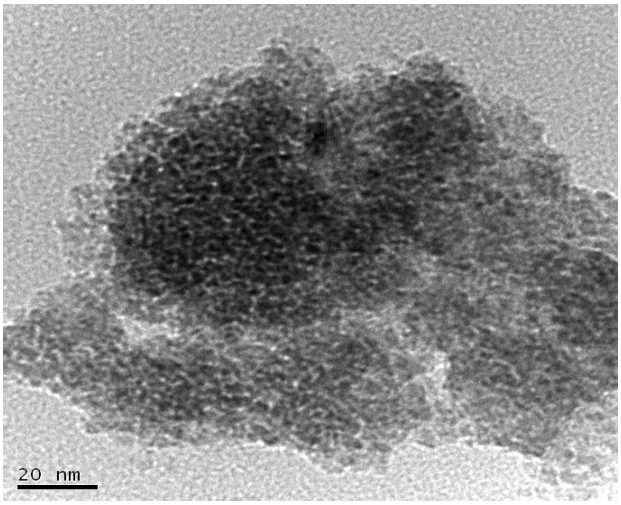

Figure 4.3 : Transmission electron microscopy(TEM) image of nano Fe_2O_3 synthesized by using PEG 35000

The influence of the polymer on the formation of the particular crystalline phase of the material formed has been reported previously in several cases [24,25]. In the present case, the PEG forms a complex with $FeCl_3$ in which the Fe^{3+} ions are held by the oxygen atoms in the chain by a co-ordination bond. Since the Fe atoms are placed only at certain fixed distances, the complex formation governs the subsequent growth of the oxide formed after the reaction with alkali. Further, the number of Fe atoms available within the nearest neighbour distance depends on the Fe/monomer ratio, and hence the particle size of Fe_2O_3 formed is also influenced by the molecular weight of PEG which is shown in Figure 4.4. Increasing the molecular weight of PEG results in the reduction of Fe_2O_3 particle size.

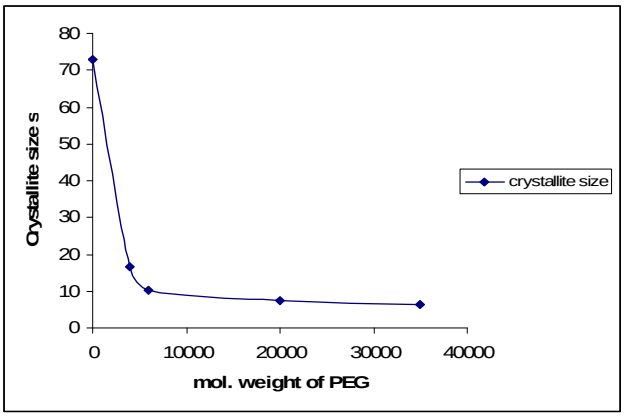

Figure 4.4 : Plot of particle size vs. different molecular weight of PEG (4000, 6000,

20000, 35000)

4.4 Synthesis of Nanoparticles of Iron Oxide using PEG-PVAc Blend :

The synthesis of nano Fe_2O_3 using PEG has been outlined in Chapter-2. With increasing molecular weight of PEG, the distance between the hydroxyl groups which are responsible for making complex with $FeCl_3$ is increased. Upon addition of second reactant; NaOH, $Fe(OH)_3$ molecules are well separated and on heating, agglomeration of nano Fe_2O_3 is prevented. The agglomeration can further be avoided by blending PEG with PVAc as the acetate group further stabilizes the complex formed with $FeCl_3$ and hence $Fe(OH)_3$ molecules are well separated resulting in formation of fine nano Fe_2O_3 particles. PEG to PVAc ratio is maintained at 20 wt% and the reactant concentration with PEG is maintained at 12:1. Figure 4.5 shows the XRD scans of Fe_2O_3 with PEG of 35,000 molecular weight, with or without addition of PVAc. It is evident from the XRD that with PVAc, FWHM of the more prominent peak is increased suggesting more reduction in the crystallite size of Fe_2O_3. Further the TEM picture in Figure 4.6 clearly reveals that the particle size of Fe_2O_3 with PVAc is reduced when compared to Figure 4.2 which is the TEM picture of nano Fe_2O_3 synthesized without PVAc.

Table 4.2: Change in crystallite size of synthesized Fe_2O_3 with 20% PVAc blended with PEG-35000

Sample	Polymer used	Crystallite Size(nm)
a	Without PEG Fe_2O_3	78.2
b	PEG 35000+ 20% PVAc Blend	5-6

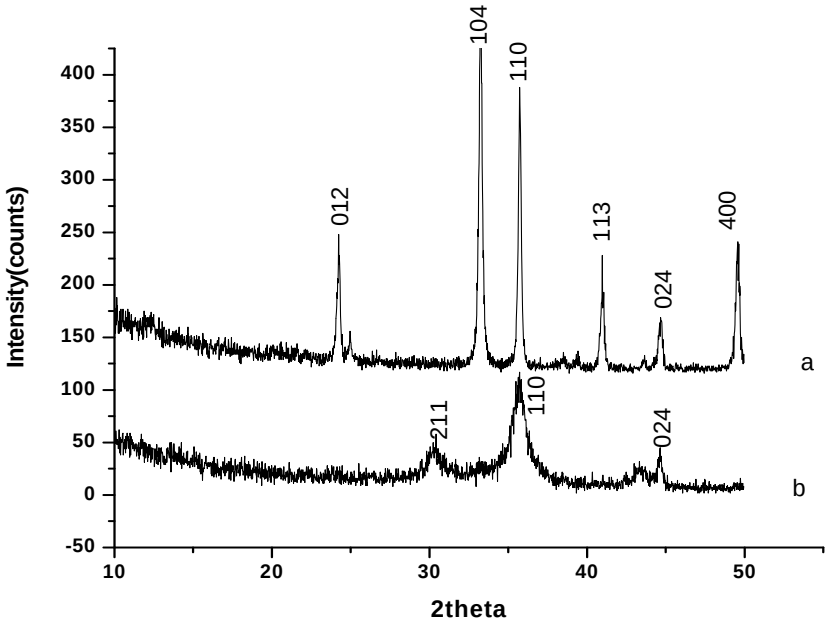

Figure 4.5 : X-ray diffraction scan of Fe_2O_3 a) Without PEG b) PEG 35000 +20% PVAc blend

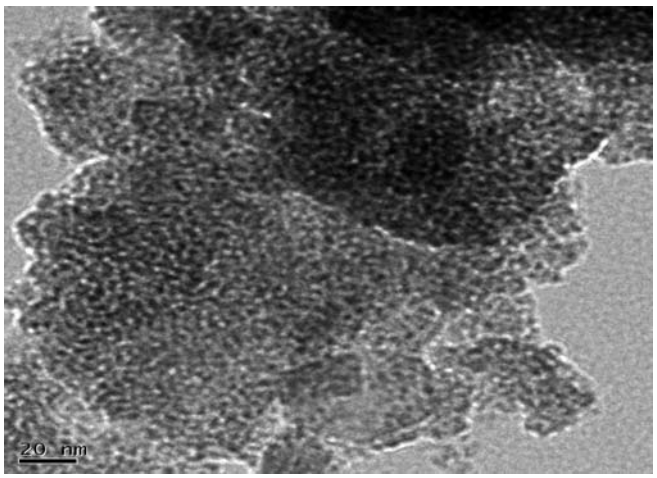

Figure 4.6 : TEM image of nano Fe_2O_3 synthesized by PEG 35000:PVAc 20% blend

4.5 Reflectance spectra of Nano Fe_2O_3 :

The reflectance spectra of nano Fe_2O_3 synthesized by PMG technique with different molecular weights of PEG were studied and results are compiled in Figure 4.7. It can be seen that, increasing the molecular weight of PEG results in better

reduction in the particle size of synthesized nano Fe_2O_3. Table 4.3 shows clearly that the maximum reflectance is higher in the case of nano Fe_2O_3 synthesized with PEG of 35,000 molecular weight.

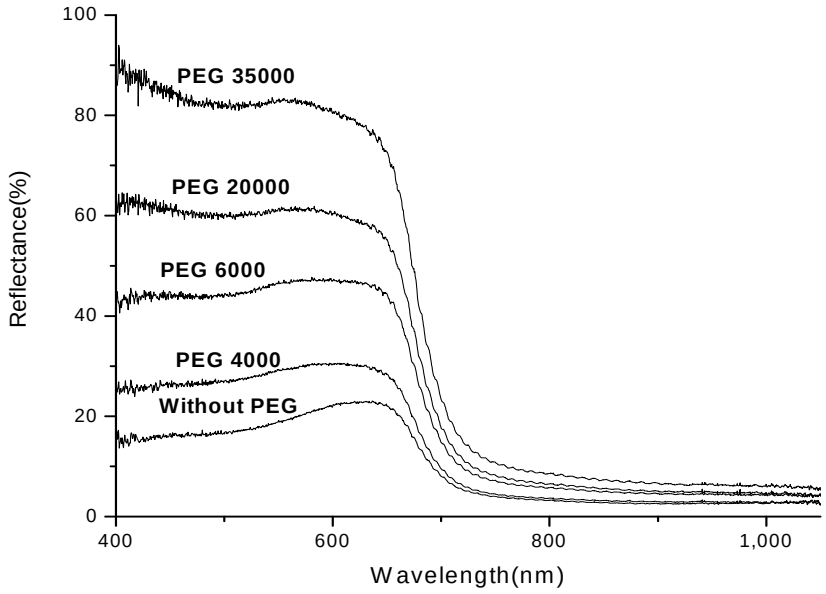

Figure 4.7 : Reflectance spectra of commercial and synthesized nano Fe_2O_3 with different molecular weights of PEG

This is due to more reduction in the particle size of Fe_2O_3 resulting in increase in surface area. This study thus proves that with increasing molecular weight of PEG, particle size of Fe_2O_3 can be reduced to a greater extent.

Table 4.3: Maximum reflectance value of different Fe_2O_3 nanoparticles synthesized by PEG technique

PEG M.W.	Particle size	Maximum reflection
35000	6.2	83.5
20000	7.595	61.8
6000	10.44	47.62
4000	16.51	30.60
Without PEG	72.8	23.4

4.6 Synthesis of PVAc-Fe_2O_3 nanocomposite coating for optical and corrosion studies :

4.6.1 Optical properties of PVB- $BaSO_4$ nanocomposite coating :

4.6.1.1 Colour :

One of the optical properties of materials namely the colour changes with the particle size of those materials. In the case of synthesized Fe_2O_3 with different molecular weight of PMG, the colour is changed. This reflects that the particle size of Fe_2O_3 has pronounced effect in the colour. As discussed in Figure 4.3, PMG of 35000 results in more reduction in particle size. Thus Figure 4.8 clearly shows the colour of Fe_2O_3 becomes more red (yellower) when the particle size reduction is more.

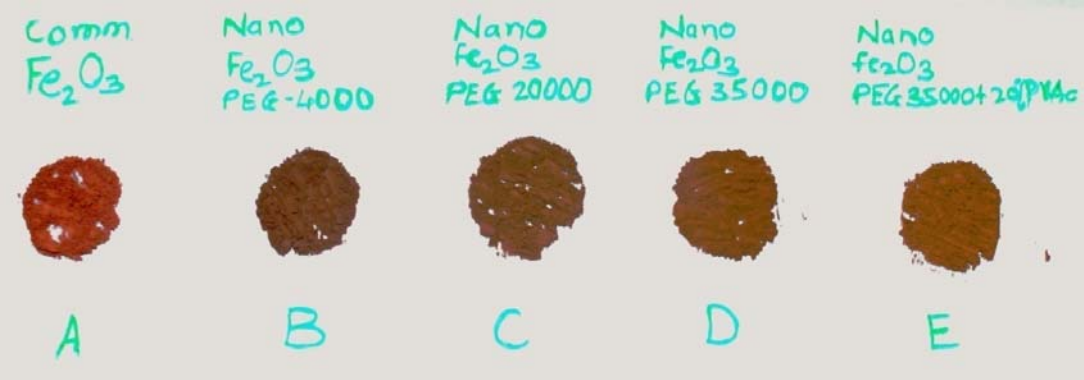

Figure 4.8 : Colour change of Fe_2O_3 w.r.t.change in particle size

4.6.1.2 Gloss :

Among the optical properties for coating, gloss plays very crucial role in appearance. Figure 4.9 shows the variation of gloss at 60 degrees for nano Fe_2O_3-PVAc coating and comparison with commercial grade Fe_2O_3 filled coating.

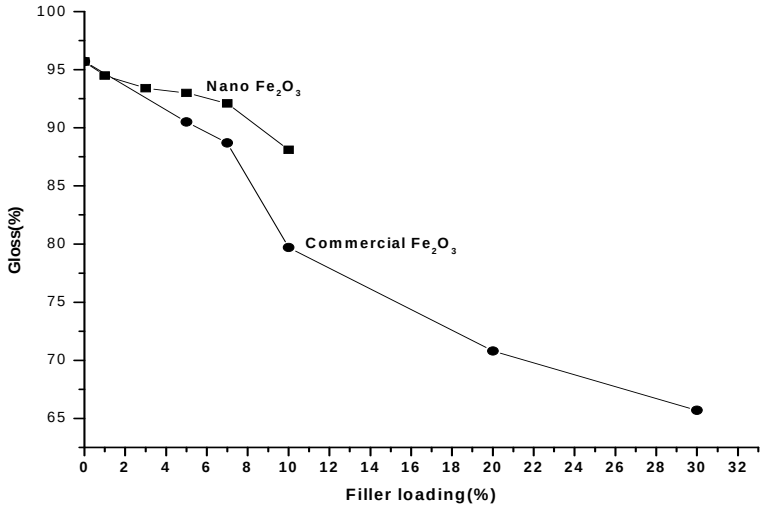

Figure 4.9 : Comparison of gloss between commercial and nanoparticles of Fe_2O_3 in PVAc coating at 60^o angle

With the increase of loading of nano Fe_2O_3 (average particle size of nano Fe_2O_3 is 6 to 7 nm), gloss at 60^o decreases slightly while there is drastic reduction of gloss in macro particle containing coatings. It was observed that the coloration of commercial Fe_2O_3-PVAc coating becomes lighter than that of synthesized nano Fe_2O_3-PVAc coating for low filler loading. In nano composite coating, dispersion of nano particles is better than commercial Fe_2O_3, the particle size affects the surface smoothness and porosity as well as coloration tint of the coating.

4.6.2 Corrosion inhibition study of PVAc-Nano Fe_2O_3 composites :

Protective coatings which are essential for preventing corrosion of steel normally are made of insulating polymers. When nanocomposites are used as protective coatings, the high aspect ratio nano fillers act as barrier for the alkaline solution and hence the base steel is protected from corrosion. The corrosion inhibition is checked through electrochemical impedance spectroscopy by measuring the impedance of the coated steel time to time. If the real part of impedance, decreases with increasing time of exposure to saline medium, then coating becomes perforated by the salt solution and hence the steel will be corroded [11-12]. Due to incorporation of nanoparticles of Fe_2O_3, the barrier performance of PVAc coatings

can be enhanced. The uniform dispersion of nanoparticle in the coating is responsible for decreasing the porosity and zigzag path for the diffusion for corrosive species. The incorporation of nanoparticles into coating offers environmentally benign solutions to enhancing the integrity and durability of coatings, since the fine particles dispersed in coatings can fill cavities and cause crack bridging, crack deflection and crack propagation [11-13,14]. The small size of the nanoparticles is advantageous since it enables their penetration into "ultra-small holes, indentation and capillary areas at surface of the metallic subject".

4.6.2.1 Polarization Measurement (Tafel Plot) :

The corrosion of the steel substrate was estimated for each type of coated specimen by monitoring the oxidation potential versus the exposure time to the corrosive environment. Plots of this evaluation referred to a saturated calomel electrode are given for steel coupons coated with composites of pure PVAc, PVAc with Fe_2O_3 nanoparticles and PVAc with commercial Fe_2O_3. Figure 4.10 shows Tafel plots of PVAc coating containing nano and commercial Fe_2O_3 having different concentrations. The open circuit potential determined from these plot recorded after different time of exposure to hot 3.5% NaCl solution are indicated in Figure 4.11. Open circuit potential (OCP) can be used as a measure of the spontaneity of the reaction and an indication of tendency to corrode [15]. It is seen that the OCP is initially high and more anodic in all cases with respect to bare steel (-0.56V SCE). Initially at 0.0 hrs, the OCP of the nano-Fe_2O_3 modified coatings remain in noble direction (anodic) as compared to the neat coating and commercial Fe_2O_3 coatings . In nanocomposite coating it was observed that after 40hrs the OCP value dropped down from -0.16 to -0.200V at 60 hours but after that the OCP value again came up to -0.16V. This is attributed to formation of some porosity in coating but Fe_2O_3 nanoparticle act as corrosion inhibitor which give so called self healing properties of nanocomposite coating. This self healing behaviour is more pronounced at 1% and 3% nano Fe_2O_3 while for higher concentrations (>10%) this behaviour is decreased and the coating is more or less like macro-particle type. This is associated with pigment loading > CPVC and agglomeration of particles.

The OCP values for the nanocomposite coatings remain on anodic side of other coatings even after 145 hours of exposure. (see Figure 4.10) This clearly suggests that nanocomposites have better corrosion resistance than ordinary coatings. After prolonged exposure the OCP progressively shifts to more cathodic regions in all cases. It may be due to the diffusion of corrosive species which leads to electrochemical process and hence shift in the OCP values towards the active direction [16,17]. This phenomenon can be attributed to increasing penetration of the corrosive ions into the coating and reaching the metal-polymer interface, where the corrosion reaction takes place. Increasing penetration can be due to defect formation, breakdown of barrier and diffusion of ions. It can be seen that in the case of pure PVAc the OCP is initially 0.26V SCE but after 40 hrs it shifts to -0.33V SCE (shift towards bare steel). In the coatings containing commercial Fe_2O_3, there is similar shift but it depends on the concentration of the filler. At 1% of Fe_2O_3, the shift is seen but it is more anodic than pure PVAc. On the other hand for macro-size Fe_2O_3 especially at higher concentrations, the OCP is even lower than pure polymer and takes place within 40 hours. This is associated with the defects / porosity in the inter-particulate regions which can lead to ease of diffusion of corrosive ions. The more compact microstructure of the nanocomposite coating does not allow this process and hence it is more stable as compared to commercial Fe_2O_3 coating.

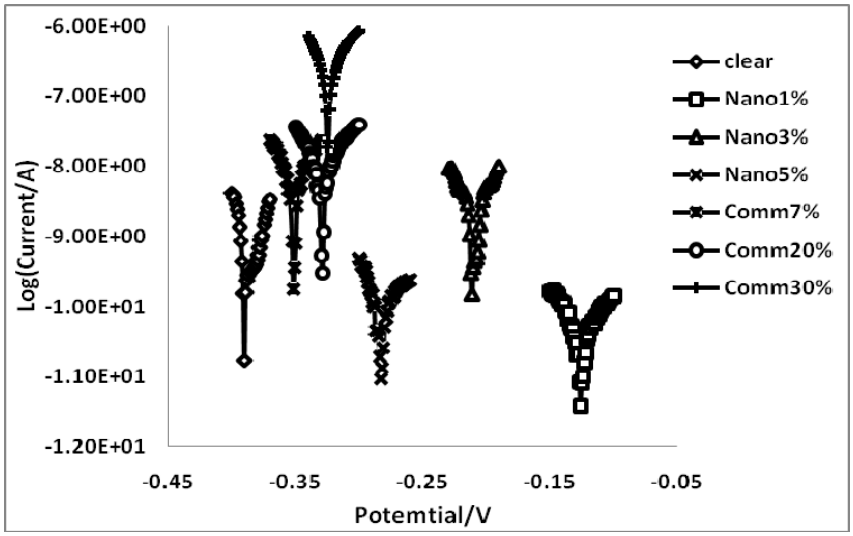

Figure 4.10 : Potentiodynamic polarization plots for composition of PVAc – Fe_2O_3 coating after 145hrs immersion at 45^o C exposed to 3.5% NaCl solution

From these results the amount of nanoparticles was also found to be relevant to the protective characteristic of the film. Thus, with lower quantity of nanosized particles incorporated into the PVAc coating, higher protective properties of the film are obtained. The most interesting features of these coatings are that these exhibit a self healing behaviour as regards corrosion protection.

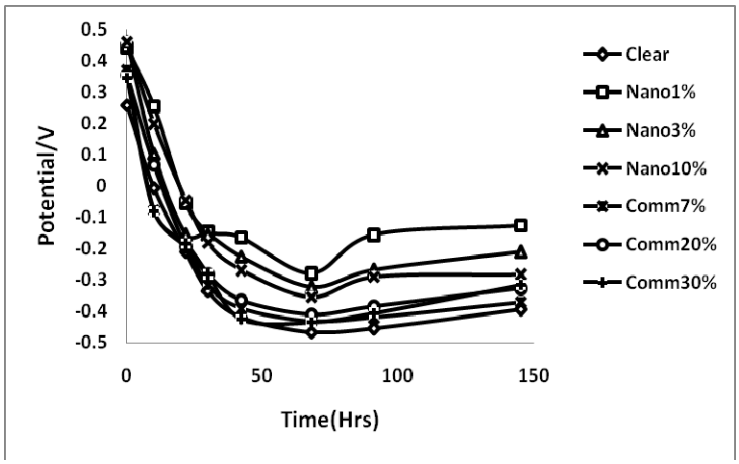

Figure 4.11: Time dependence of corrosion potential of PVAc- Fe_2O_3 coating at 45^0 C immersed in 3.5% NaCl solution

Table 4.4: Study of OCP of different composition of PVAc - Fe_2O_3 nanocomposite coating at different temperatures like 45^o C and 55^o C

	Composition	**Clear**	**1%N Fe_2O_3**	**3%N Fe_2O_3**	**10%N Fe_2O3**	**7%C Fe_2O_3**	**20%C Fe_2O_3**	**30%C Fe_2O_3**
Temp.(°C)	Time(Hrs)							
45	0	0.259	0.443	0.463	0.463	0.371	0.496	0.347
	10	-0.023	0.256	0.105	0.2	-0.056	0.276	-0.14
	30	-0.334	-0.144	-0.154	-0.1084	-0.316	-0.315	-0.2
	68	-0.384	-0.198	-0.231	-0.116	-0.454	-0.468	-0.3
	91	-0.362	-0.155	-0.236	-0.127	-0.417	-0.405	-0.322
	145	-0.32	-0.125	-0.242	-0.144	-0.407	-0.391	-0.317
55	0	-0.042	0.24	0.372	0.278	-0.121	-0.017	-0.03
	10	-0.25	-0.122	0.197	-0.286	-0.228	-0.25	-0.2505
	30	-0.272	-0.125	-0.1538	-0.226	-0.412	0.041	-0.379
	68	-0.166	-0.146	-0.174	-0.253	-0.459	-0.281	-0.36
	91	-0.265	-0.1978	-0.1442	-0.1834	-0.4389	-0.3144	-0.3754
	145	-0.324	-0.172	-0.268	-0.175	-0.446	-0.28	-0.333

The corrosion current (I_{corr}) was determined from the Tafel plots for pure PVAc, nano and commercial Fe_2O_3 containing coatings and its variation with time indicated in Figure 4.12. The initail value of I_{corr} for all coating is low; in the range of 10^{-11} to 10^{-12} A which increases rapidly after exposure to saline conditions, for unfilled and commercial Fe_2O_3 filled coatings. On the other hand, for nanoparticle filled coatings there is little change in the Icorr value especially for filler content of <5%. It is interesting to note that in some of these nano-composite coatings, there appears to be some self healing effect as well i.e. the Icorr value decreases after exposure to saline condition (see 1% nano Fe_2O_3 curve). This may be due to ion exchange between the nano Fe_2O_3 and the -OH groups of PVAc which are invariably present in this polymer. This in turn helps in the formation of protective coating at the metal – polymer interface.

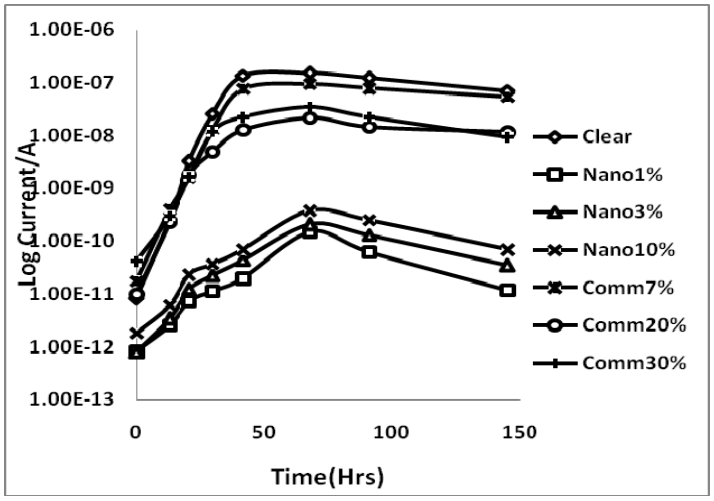

Figure 4.12: Time dependance of corrosion current of PVAc - Fe_2O_3 coating at 45^0 C immersed in 3.5% NaCl saline solution

Table 4.5 : Study of I_{corr} of different composition of PVAc - Fe_2O_3 coating at different temperatures like 45° C and 55° C

	Composition	Clear	1%N Fe_2O_3	3%N Fe_2O_3	10%N Fe_2O_3	7%C Fe_2O_3	20%C Fe_2O_3	30%C Fe_2O_3
Temp.(°C)	Time(Hrs)							
45	0	6.02E-11	5.71E-12	6.04E-14	1.37E-11	1.77E-11	2.79E-11	4.09E-11
	10	1.33E-10	3.39E-10	3.31E-11	3.83E-12	9.02E-08	3.51E-10	7.81E-10
	30	6.35E-08	4.46E-11	1.05E-10	2.11E-11	7.72E-08	1.29E-08	2.69E-09
	68	5.10E-08	7.21E-11	1.83E-10	6.23E-11	9.49E-08	2.20E-08	3.45E-09
	91	5.75E-08	3.06E-10	1.78E-10	6.23E-11	7.94E-08	1.48E-08	3.73E-09
	145	5.11E-08	3.85E-10	3.47E-11	2.58E-10	5.42E-08	1.16E-08	6.20E-08
55	0	2.31E-10	5.13E-11	2.24E-10	5.56E-10	9.18E-10	6.47E-09	5.23E-07
	10	3.57E-10	4.36E-11	2.45E-10	1.84E-10	6.49E-08	2.64E-09	7.65E-07
	30	4.02E-10	7.92E-11	1.69E-10	8.12E-10	1.37E-08	2.33E-09	1.25E-06
	68	2.50E-10	1.21E-10	3.35E-10	4.34E-10	4.45E-09	2.17E-09	1.61E-06
	91	2.97E-08	9.22E-10	3.28E-10	7.08E-10	6.57E-09	3.69E-09	2.99E-06
	145	1.34E-08	6.51E-10	8.80E-10	4.95E-10	5.29E-09	4.95E-09	3.06E-06

4.6.2.2 Electrochemical Impedance spectroscopy (EIS) :

The impedance value of the initial 0.0 hrs exposure for neat coating and the nano- Fe_2O_3 modified coatings remained high at low frequency as shown in Figure 4.13 and Figure 4.14. Also, the coating resistance which is associated with the uptake of water by the coatings has been found to increase during initial stage of immersion. Nano Fe_2O_3 coating has higher resistance than the coatings with pure PVAc especially at low frequency which is associated with ionic transport through the film. All coatings have higher impedance on initial immersion in the electrolyte close to 10^8 Ω as shown in Table 4.6. However as immersion time increases the pure PVAc and commercial Fe_2O_3 degrade more quickly than that of the nano Fe_2O_3 coating and after around 90 hours the pure PVAc and commercial coated substrates show similar resistance, around 10^5 Ω . One possible reason for this continued corrosion protection via the nano Fe_2O_3 coating due to the compact nanostructure sealing of the coating and penetration of corrosive species is very difficult so that after 100 hours the coating resistance is $>10^7$ Ω . This also suggests that there is much lower ionic conductivity in nanocomposites than macro-particle composite coatings. Here again, the self healing effect is seen i.e. the impedance decreases slightly first but on prolonged exposure, the impedance again increases which indicates there is a protective layer created within the matrix and or near the interface due to the

chemical reaction between the ions and internally liberated Fe^{3+} ions. This effect is very much pronounced in the nano-particle Fe_2O_3 filled coatings with 5% fillers.

The excellent anticorrosion protection of nano-Fe_2O_3 incorporated coating is attributed to their small size and large surface area of the nanoparticles. In addition, the coating resistance of the neat coating and nano-Fe_2O_3 modified coatings after 145hrs of exposure showed a decrease in their values 10^6 Ω and 10^7 Ω respectively. However, this suggests that nano- Fe_2O_3 due to their small size allow large amount of resin to get adsorbed on it and reduces the free space between the particle and resin thereby delays the diffusion of electrolyte to the coating and increases the resistance of the coating.

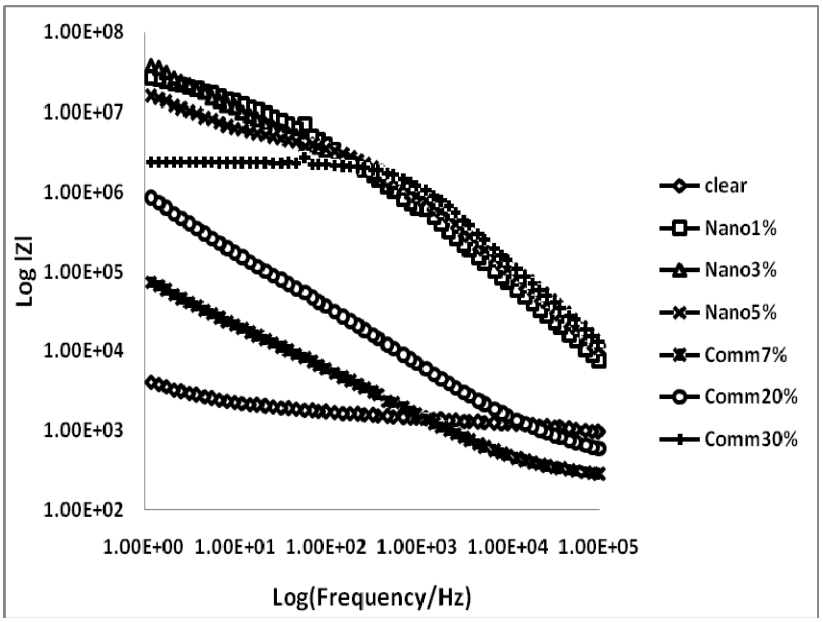

Figure 4.13 : Frequency dependence of impedance log *lZl* for different composition nano and commercial PVAc - Fe_2O_3 coatings after 145 hrs

It can be concluded from Table 4.6 that the corrosion rate at different temperatures for commercial and neat coating is higher than that of nano-Fe_2O_3 coating. This is attributed to increased compactness of nano-Fe_2O_3 which all act as a barrier for the electrolytes to inhibit corrosion [12, 16, 17, 18].

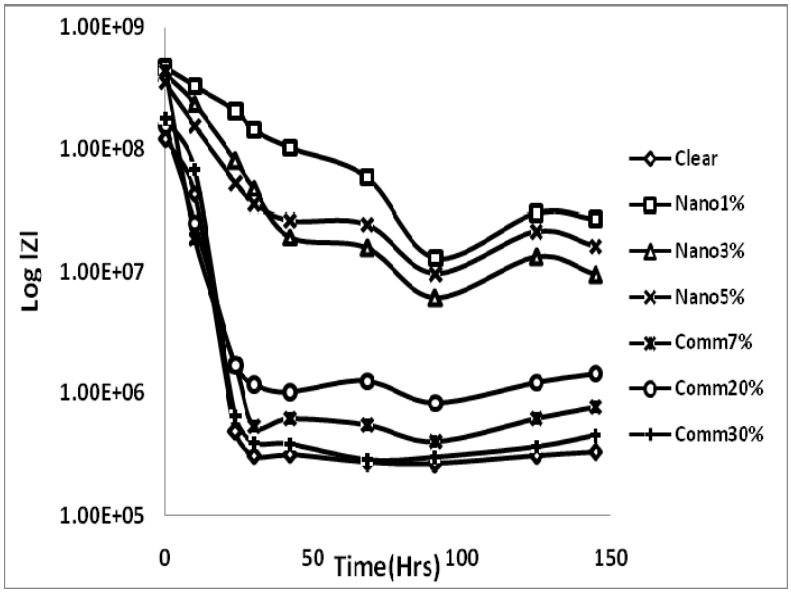

Figure 4.14 : Time dependence of impedance of PVAc - Fe_2O_3 coating at 45^0 C immersed in 3.5% NaCl solution

Table 4.6 : Study corrosion resistance(lZl) of different composition of PVAc - Fe_2O_3 coating at different temperatures like 45^o C and 55^o C

Composition		Clear	1%N Fe_2O_3	3%N Fe_2O_3	10%N Fe_2O_3	7%C Fe_2O_3	20%C Fe_2O_3	30%C Fe_2O_3
Temp.(°C)	Time (Hrs)							
45	0	3.81E+08	2.26E+07	8.40E+07	2.35E+08	4.39E+08	4.14E+07	1.02E+08
	30	1.04E+08	6.24E+07	4.69E+07	1.22E+07	5.34E+05	5.77E+06	1.65E+06
	68	1.02E+07	7.07E+07	8.95E+07	1.01E+07	6.69E+05	1.86E+06	1.40E+05
	91	1.49E+07	3.86E+07	5.43E+07	1.11E+07	7.54E+05	8.15E+05	1.24E+05
	125	8.14E+06	2.99E+07	4.70E+07	2.14E+07	8.30E+05	1.27E+05	1.37E+05
	145	2.41E+06	2.71E+07	3.81E+07	1.61E+07	8.59E+05	7.39E+04	1.57E+05
55	0	6.04E+08	3.13E+08	3.33E+06	1.88E+06	5.09E+08	1.83E+08	1.11E+06
	30	1.35E+06	4.14E+07	1.73E+07	3.22E+06	4.44E+04	8.85E+06	1.74E+04
	68	3.98E+06	2.50E+07	2.90E+07	3.46E+06	1.06E+06	4.58E+06	6.20E+03
	91	5.15E+06	2.41E+07	1.72E+07	3.60E+06	2.14E+06	4.35E+06	4.49E+03
	125	3.16E+06	1.46E+07	1.81E+07	5.84E+06	2.39E+06	6.36E+06	4.24E+03
	145	3.56E+06	9.78E+06	6.91E+06	4.71E+06	7.75E+05	5.63E+06	4.46E+03

Coating film degradation was studied from Bode plots, as shown in Figure 4.15 and Figure 4.16, which represent the bode plot of coating exposed for 145 hrs and time based analysis in 3.5% NaCl solution, respectively. Bode plot shows major degradation of the polymer (0 filler) coating and commercial Fe_2O_3 coating of PVAc, which indicate that there was substantial electrolyte to penetration. The phase values

of nano- Fe_2O_3 modified coatings were high as compared to other coatings, suggesting that the coatings with nano-Fe_2O_3 contain no diffusion path for penetration of electrolyte.

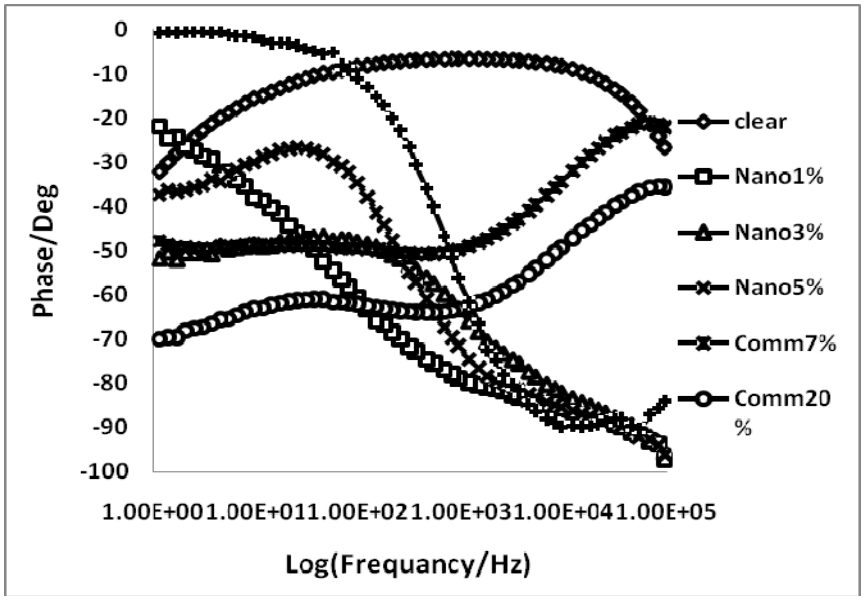

Figure 4.15 : Frequency dependance of phase of different composition of nano and commercial PVAc - Fe_2O_3 filled coatings after 145 hrs

Amongst the various mechanisms for deterioration of barrier coatings, physical defect formation during prolonged exposure to corrosive atmosphere is very improtant factor. In order to investigate these effects by impedance spectroscopy, the Bode plot is generally used. Figure 4.15 shows the phase angle with frequency for coatings containing various concentration of nano and macro particulate Fe_2O_3 filler after exposure to saline conditions at 45° C for 135 hrs. The increase of phase angle at high frequency region is indicative of defect formation in the coating. Figure 4.16 shows the variation of phase angle at high frequency with respect to time of exposure to corrosive conditions. This is very evident in the coatings containing macro-particle Fe_2O_3 where the phase angle rapidly shifts to upper side giving a broad band peak. It may be attributed that the coating might had undergone some structural deformation due to uptake of saturated electrolyte during long exposure to the test solution. This results into electrochemical process on the metallic interface leading to the loss of coating adhesion. While addition of nano-Fe_2O_3 provides longer diffusion paths in the

film for the water and corrosive ions to arrive at the substrate and maintains the integrity of the coatings [20–21], there is no such change in the nano-particle containing coatings which remain intact. The ease of defect formation in the macro-particle filled coatings is due to large amount of fillers as well as aggregate formation leading voids and micro-cracks which expand during aging / corrosion testing.

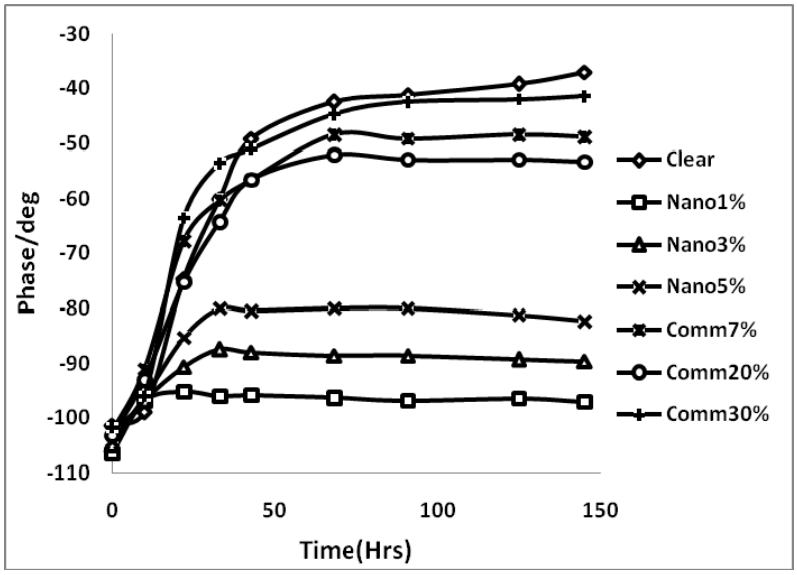

Figure 4.16 : Time dependance of phase of PVAc-Fe_2O_3 coating at 45^0 C immersed in 3.5% NaCl solution

From Table 4.7 coating tested after exposure to saline at temperature 45 and 55^o C, it is seen that there is enhanced corrosion protection effect of PVAc/nano-Fe_2O_3 coatings on the metallic surface as compared to the pure PVAc based coatings might probably resulting from the enhancement of the adhesive strength of nano-Fe_2O_3 modified coatings on the mild steel substrate relative to that of neat coating[22].

For any anticorrosion coating, the charge transport mechanism is very important and critical to lead to barrier formation, especially electrostic potential barrier at the interfaces, grains etc. The real part of impedance of the coating (/Z/) give the information on these internal charge transport phenomena.

Table 4.7 : Study of degradation of coating (Phase) of different composition of PVAc - Fe_2O_3 coating at different temperatures like 45° C and 55° C

Temp.(°C)	Composition Time(Hrs)	Clear	1%N Fe_2O_3	3%N Fe_2O_3	10%N Fe_2O_3	7%C Fe_2O_3	20%C Fe_2O_3	30%C Fe_2O_3
45	0	-101.4	-106.6	-105.1	-104.3	-96.2	-94.7	-101.8
	30	-94.9	-96	-96	-95.1	-56.9	-57.2	-48
	68	-89.1	-96.4	-96.2	-96.3	-43.1	-37.4	-42.6
	91	-87.3	-96.9	-96.1	-96.1	-44.1	-36.2	-43.3
	125	-84.1	-96.5	-96	-96.3	-45.6	-34.9	-39.8
	145	-74	-97.1	-95.5	-96.1	-50.5	-38.2	-37.1
55	0	-96.8	-105.3	-105.1	-106.7	-95.1	-103.2	-72.9
	30	-58.8	-97	-96.4	-89.9	-86	-95.7	-60.3
	68	-65.3	-94.8	-95.6	-96.1	-66.9	-86.8	-35.6
	91	-78.1	-95.9	-94.9	-94.6	-69.1	-84.3	-38.5
	125	-76.4	-95.5	-94	-94.3	-75.4	-87	-48.5
	145	-69.5	-95.6	-93.9	-94	-57.5	-86.5	-32.5

4.6.3 Optical Microscopy study of PVAc-Fe_2O_3 nanocomposite coating :

Optical microscope images were studied for nanocomposite coatings analysis at different loading, representative images of coatings are shown in Figure 4.17 for nano 5% and Commercial 7%. Extensive damage was observed for commercial 7 % nanocomposite coating when exposed to corrosive conditions. However, nanoparticle composite coatings remain intact with very small micro-defects under similar conditions of corrosive atmosphere. These results correlate the above conclusions as defect formation.

5% Nano Fe_2O_3 7% Commercial Fe_2O_3

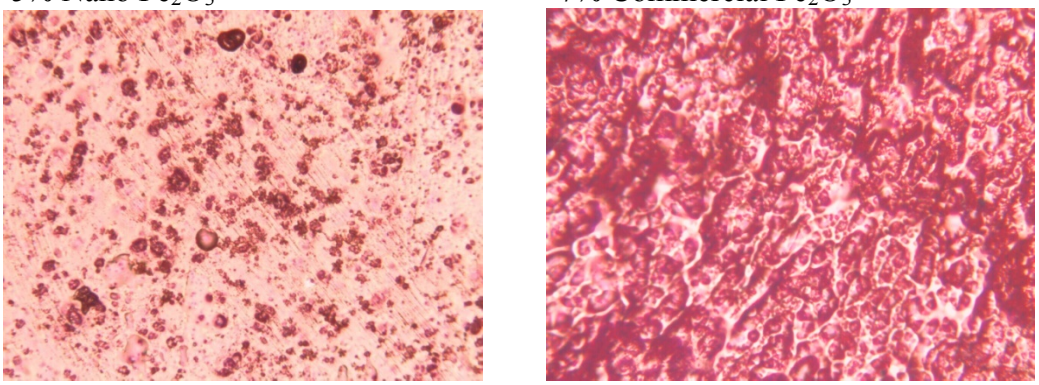

Figure 4.17 : Optical microscope images of PVAc - Fe_2O_3 coating after 145 hrs at 45° C exposed in 3.5% saline solution

4.7 Corrosion inhibition study of PVB-Nano Fe_2O_3 composites :

4.7.1 Open Circuit Potential(OCP) of PVB- Fe_2O_3 Coating:

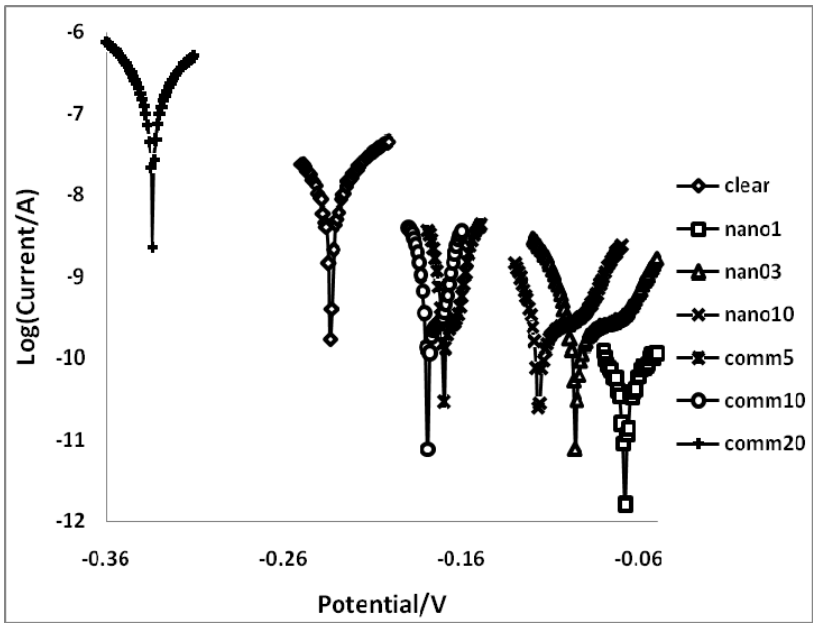

Figure.4.18 : Potentiodynamic polarization plots (Tafel) for composition of PVB – Fe_2O_3 coating after 174 hrs immersion at 45^0 C exposed to 3.5% NaCl solution

Figure 4.18 shows the Tafel plots of PVB-Fe_2O_3 composites coating on steel substrate. It can be clearly seen that addition of nano Fe_2O_3 in PVB enhances the corrosion protection as the OCP is shifted to more anodic side. Addition of 10 wt% nano Fe_2O_3 increases corrosion protection where as commercial Fe_2O_3 containing PVB composite coating exhibits lesser protection than that of synthesized Fe_2O_3-PVB coatings. This is attributed to the fact that reduction in the particle size of Fe_2O_3 increases and compactness where by the penetration of electrolyte is hindered and hence corrosion protection is enhanced i.e., the barrier property of the composite coating is increased.

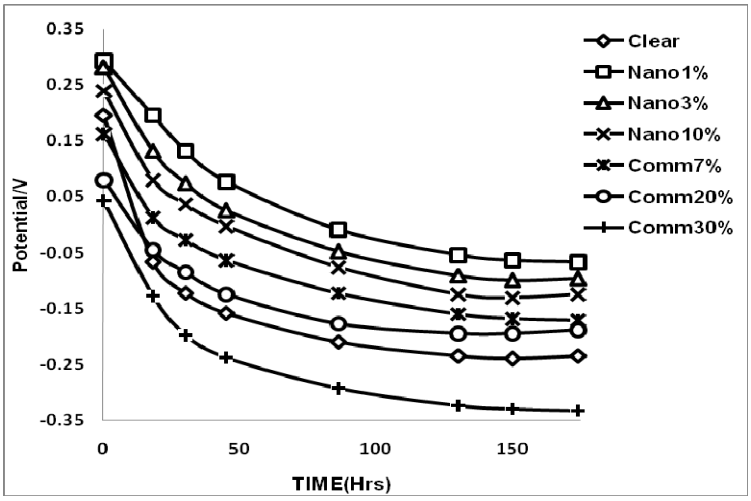

Figure 4.19 : Time dependance of corrosion potential of PVB-Fe_2O_3 coating at 45^0 C immersed in 3.5% NaCl solution

Change in OCP with time of exposure to the electrolyte determines the stability of the coating material. Figure 4.19 shows the OCP variation of PVB-Fe_2O_3 coatings with respect to time. The OCP is decreased with time for all the coatings in the PVB-Fe_2O_3 system. However addition of nano Fe_2O_3 in the concentration range 1-10 wt% in PVB show superior performance as at all time of exposure since the OCP is much higher on anodic region than that of commercial Fe_2O_3 filled PVB coatings. The OCP of 3 and 10 wt% Fe_2O_3 addition in PVB results in lesser OCP compared to that of 1 wt% addition probably due to agglomeration of nanoparticles. It may be noted that in this PVB-Fe2O3 case, there is very little self healing behaviour observed which was distinctly seen for the PVAc-Fe2O3. This may be due to absence of the functional groups which are responsible for co-ordinate bond formation with Fe atom and /or formation of FeO via OH groups which leads to passivation layer.

4.7.2 Electrochemical impedance study of PVB-Fe_2O_3 coating :

Impedance is a versatile tool to understand the corrosion behaviour of coatings. When the coating on bare steel starts deteriorating in the presence of electrolyte, the impedance decreases which can be due to penetrating ions. The variation of impedance with frequency for PVB-nano Fe_2O_3 and PVB-commercial Fe_2O_3 are presented in Figure 4.20. One can easily guess that impedance decreases

with increasing frequency as the coating is pierced by the electrolyte at higher frequency. With nano Fe_2O_3 added PVB exhibits higher impedance than other loadings as the dispersion of Fe_2O_3 is better at 1 wt%. This result suggests that PVB-1 wt% nano Fe_2O_3 is more stable against corrosion because of enhanced barrier properties. Higher loading of nano Fe_2O_3 results in agglomeration and hence the impedance at low frequency is less. Commercial Fe_2O_3-PVB composites exhibit least resistance for saline attack and hence the synthesized nano Fe_2O_3 added PVB is better.

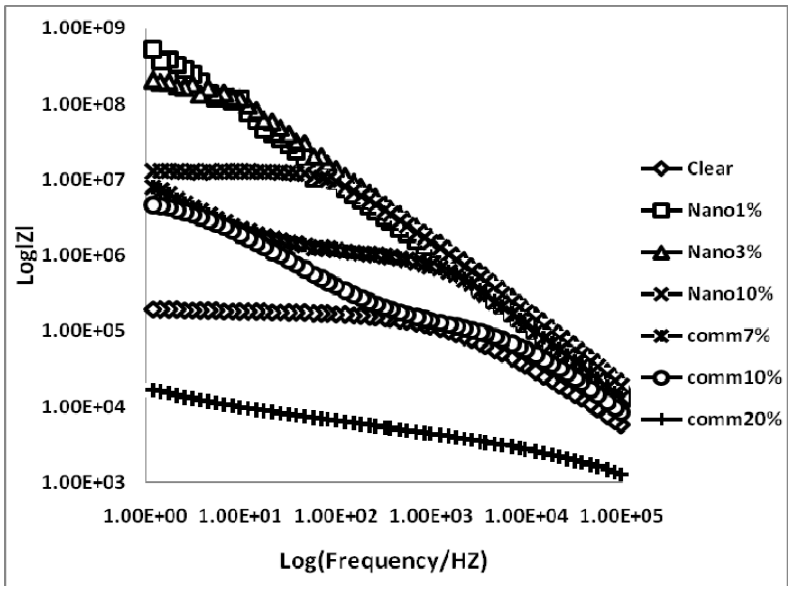

Figure 4.20 : Frequency dependance of impedance log /Z/ for different composition nano and commercial PVB - Fe_2O_3 coatings after 174 hrs

Time dependence of low frequency impedance value is shown in Figure 4.21. This also supports the fact that nano-Fe_2O_3 filled PVB is superior as it has high impedance and the reduction in impedance at high exposure time is less than that of commercial Fe_2O_3 filled PVB. It should be noted that 1 wt% nano Fe_2O_3 filled PVB exhibits much less decrease of impedance with respect to time than other coatings due to better dispersion and absence of defects as explained earlier. Similarly the phase variation with respect to time at 45^o C proves that nano Fe_2O_3 filled PVB is better as the increase in phase is lesser compared to other compositions and commercial Fe_2O_3

filled PVB as shown in Figure 4.21. This is due to the fact that nano Fe_2O_3 filled PVB is effective against corrosion.

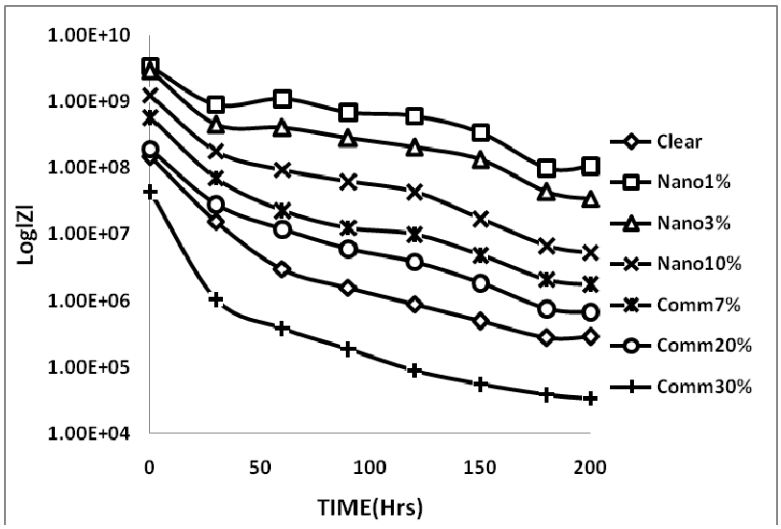

Figure 4.21 : Time dependance of impedance of PVB-Fe_2O_3 coating at 45^0 C immersed in 3.5% NaCl solution

After prolonged exposure of of PVB-Fe_2O_3 coating to 3.5% saline solution, the coatings deteriorate due to various reasons. The Bode plot is generally used to investigate the mechanism for aging of coating. The increase of phase angle at high frequency region is indicative of defect formation in the coating. Figure 4.22 shows the variation of phase angle at high frequency with respect to time of exposure to corrosive conditions . This is very evident in the coatings containing macro-particle Fe_2O_3 where the phase angle(-77.9, -74.5, -60.1 for loading 7%, 20%, 30%) rapidly shifts to upper side giving a broad band peak while there is no such change in the nano-particle containing coatings which remain intact(-93.4, -87.9, -82.5 for loading 1%, 3%, 10%). The ease of defect formation in the macro-particle filled coatings is due to large amount of fillers as well as aggregate formation leading voids and micro-cracks which expand during aging / corrosion testing. The nanocomposite coating with Fe_2O_3 nanoparticles shows good barrier properties because it form good compact structure due to high surface area and aspect ratio. Due to compact structure corrosive species restrict to penetrate that gives better corrosion resistance.

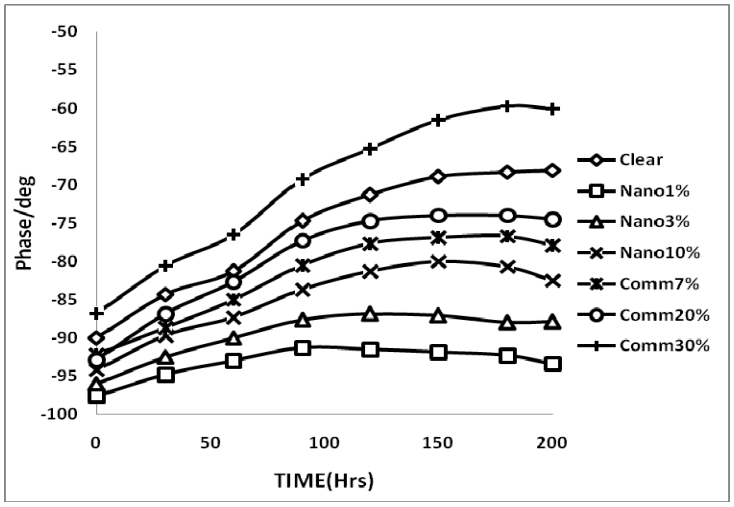

Figure 4.22 : Time dependance of phase of PVB-Fe_2O_3 coating at 45^0 C immersed in 3.5% NaCl solution

4.8 Corrosion inhibition study of PVAc-Nano Fe_2O_3 hybrid composites :

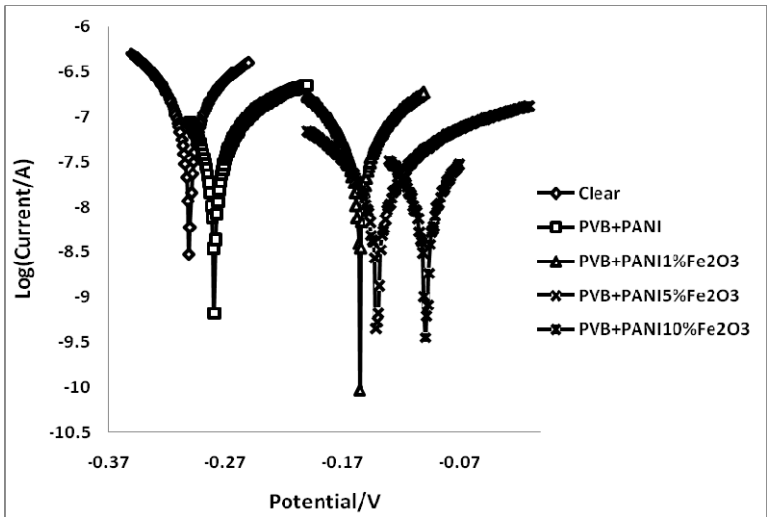

Figure 4.23 : Potentiodynamic polarization plots for composition of PVB- PANI-nano Fe_2O_3 hybrid coating after 150 hrs immersion at 45^0 C exposed to 3.5% NaCl solution

The OCP vs Time Graph shows that gradual decrease in potential due to the initial degradation of coating but the self healing and formation of passivation layer by PANI leads to increase in the potential with respect to the time. In the above graphs, it is observed that PVB+ PANI coating shows little higher OCP values than

pure PVB and little self healing. However, in case of PANI with 1%,5%, 10% Fe_2O_3 the OCP moves to more anodic side. There is tremendous self healing affect observed in these hybrid coatings as compared to single filler system. Thus, the PANI+ nanoFe_2O_3 containing coatings have much better performance in corrosive environment beyond the normal expected life of the common coating. These results together with epoxy hybrid coatings have been published and discussed in detail elsewhere [24].

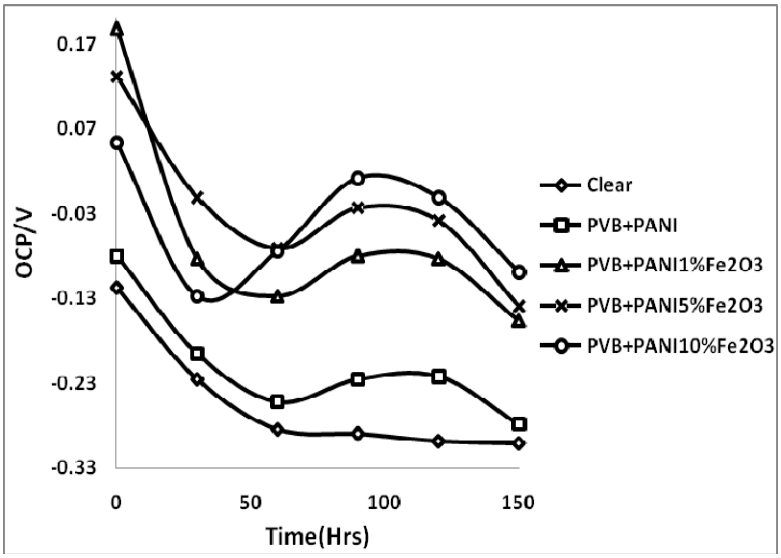

Figure 4.24 : Time dependance of open circuit potential of PVB-PANI-nano Fe_2O_3 coating at 45^0 C for 3.5% NaCl solution

4.9 Conclusions :

Fe_2O_3 nanoparticles have been synthesized using polymer mediated growth technique and further characterized for their structure, particle size and optical properties. The effect of polymer molecular weight with the initial reactant, blending on the Fe_2O_3 produced has been studied. There is a clear shift in the particle size to nano region with increasing molecular weight of PEG used and blending this with PVAc further reduces the Fe_2O_3 size formed in the matrix. The coatings incorporated nanoparticulate Fe_2O_3 exhibit much superior optical properties such as gloss. These coating also have much higher corrosion resistance as compared with coatings

containing commercial Fe_2O_3. There some self healing effect in PVAc-nano Fe_2O_3 coatings for corrosion resistance. This effects very much enhanced in the hybrid coatings containing polyaniline with nano Fe_2O_3. Thus, the nano Fe_2O_3 give much better coatings withstanding highly corrosive environment.

4.10 References:

[1] Subramaniam R., Vattoliparambil V. R.: *US20060138713A1*, **2006**.

[2] Tetsuya Osaka, Tadashi Matsunaga, Takuya Nakanishi, Atsushi Arakaki, Daisuke Niwa and Hironori Iida., *Anal. Bioanal Chem* **2009**, Volume 384, Number 3, 593-600.

[3] Yanyan Xu, Shuang Yang, Guoying Zhang, Yaqiu Sun, Dongzhao Gao and Yuxiu Sun, *Materials Letters,* **2011** Volume 65, Issue 12, 30, Pages 1911-1914.

[4] Mitra Subarna, Das Soumen, Mandal Kalyan and Chaudhuri Subhadra *Nanotechnology,* **2007** Volume 18 Number 27.

[5] Fuchun Liu, Lihong Yang, Enhou Han J. Coat. Technol. Res. **2007**, 23 (4): 551-558.

[6] Saujanya, C., Ashamol, S., Padalkar, S., Radhakrishnan, S. *Polymer*, **2001**, 42 2255.

[7] Saujanya, C., Radhakrishnan, *S. Polymer* **2001** 42 6723.

[8] Saujanya, C., Radhakrishnan, *S. J. Mat. Sci*., **1998** ,33 1063.

[9] Saujanya, C., Radhakrishnan, *S. J. Mat. Sci*., **1998**, 33 1069.

[10]Xianming Shi , Tuan Anh Nguyen , Zhiyong Suo , Yajun Liu , Recep Avci *Surface & Coatings Technology,* **2009**, 204 237–245

[11]Shailesh K. Dhoke, A.S. Khanna *Materials Chemistry and Physics,* **2009**, 117 550–556.

[12Ji-Ming Hu , Jin-Tao Zhang, Jian-Qing Zhang, Chu-Nan Cao, *Corrosion Science* **2005**,47, 2607–2618

[13 K. Lam, K.T. Lau, *Compo. Struc*. **2006,** 75 553.

[14] G. Shi, M.Q. Zhang, M.Z. Rong, B. Wetzel, K. Friedrich, *Wear* , **2003**, 254 784.

[15] Hartwig, M. Sebald, D. Putz, L. Aberle, *Macromol. Symp*. **2005**, 221 127.

[16] L.H. Yang, F.C. Liu, E.H. Han, , *Prog. Org. Coat*. **2005**, 53 91.

[17]Mahdavian Ahadi M., Mohammadzadeh Attar M., *Sci. Iran*. **2007,** 14 (4) 369.

[18] B.S. Skerry, D.A. Eden, *Prog. Org. Coat*. **1987**, 15 269.

[19] J.R. Scully, , *J. Electrochem.Soc.* **1989**, 136 (4) 979.

[20] H. Shi, F. Liu, E. Han, Y.Wei, *J. Mater. Sci. Technol*., **2007** 23 (4) 55.

[21] T.C. Patton (Ed.), *Pigment Handbook Volume III, Characterisation and Physical Relations,* Wiley–Interscience Publications, New York, **1973**, p. 203.

[22] P.A. Lewis (Ed.), *Pigment Handbook Volume I, Properties and Economics*, Wiley–Interscience Publications, New York, **1988**.

[23] A. Kalendova, , *Prog. Org. Coat*., **2003**, 46 324.

[24] J.-M. Yeh, C.-F. Hsieh, C.-W. Yeh, M.-J. Wu, H.-C. Yang, *Polym. Int*., **2007**, 56 343–349.

[25] S.V. Lamaka, D.G. Shchukin, Andreeva S D.V., Zheludkevich SM.L., H. Möhwald,M.G.S. Ferreira, *Adv.Funct. Mater*, **2008**, 18 3137–3147.

[26] M.A. Domínguez-Crespo, A. García-Murillo, A.M. Torres-Huerta, F.J. Carrillo-Romo, E. Onofre-Bustamante, C. Yá˜nez-Zamora, *Electrochim. Acta,* **2009**, 54 (10) 2932–2940.

[27] J.-M. Yeh, C.-J. Weng, W.-J. Liao, Y.-W. Mau, *Surf. Coat. Technol*., **2006**, 201 1788–1795.

[28] S. Radhakrishnan, C.R. Siju, Debajyoti Mahanta, Satish Patil , Giridhar Madrasc *Electrochimica Acta,* **2009** ,54 1249–1254

CHAPTER – V

Effect of $BaSO_4$ nanoparticle Addition on Optical and Corrosion Properties of PVB and Epoxy nanocomposite Coatings.

CHAPTER 5

5.1 Introduction :

Barium sulphate commonly referred to as barite, is one of most important fillers used in the plastics, rubber and paint industries and also used in pharmaceutical formulation. The synthesis of inorganic nanoparticles with controlled morphology has attracted great interest due to its important application in various fields. $BaSO_4$ nanoparticles were widely used as additive in painting to improve the polish. In papermaking, the addition of $BaSO_4$ nanoparticles would make it smooth and the paper obtained would have some novel properties for instance, radiation protection [1]. In other field, such as cosmetics, ceramics, pigments, and off shore oil, the performance of the products would be promoted by addition by $BaSO_4$ nanoparticles. Often the products were endowed with some novel properties. Recently, a great deal of attention has been placed on the mass production of $BaSO_4$ nanoparticles.

Barium sulfate ($BaSO_4$) is one of the versatile mineral fillers used in polymeric compounds to gives improved optical and chemical properties etc.. It has good optical brightness (i.e. whiteness). Due to high brightness, barium sulphate is used as an extender to provide the weight that customers equate with quality and because of its low binder demand for high loadings. Blanc fixe (precipitated barium sulfate) is used where a finer particle size is needed for denser packing of the paint film, as in premium metal primers and to provide resistance to corrosion by acids and alkalis. Contrast to other heavy metal barium sulphate is nontoxic and is reasonably priced, qualities that may ensure good commercial potential for these white fillers. The barium sulfate filled polymer systems have been studied by many researchers [2–3]. From all theses study we analyzed that the effects of addition filler on the mechanical and other properties of the composites depend not only on filler type, but also strongly on the filler's particle shape and size. Not as much of research about the application of nano-$BaSO_4$ into polymeric matrix has been reported. These systems appear as a new class of materials in which inorganic particles with nanoscale dimension are dispersed in the organic polymer matrix.

Barium has been incorporated into polymers to electrically insulating barium sulphate-epoxy composite with x-ray attenuation properties. It is also applied in the studies of biominerilisation and molecular recognition [4-6]. It is very good thermo luminescence material, which is used in the radiation dosimeter field. So far many methods have been proposed to produced the barium sulphate nanoparticles such as precipitation [7], micro emulsion [8], filtration dispersion method [9], modifying different organic acids [10], membrane dispersion [9], presence of polymeric additives [10] and so on. Now a day it is an important challenge to obtain the nanoparticles by simple and versatile method.

One of the important issue in the synthesis of nanoparticles is to curb the particle size and its distribution [1]. Nanoparticles are prone to aggregate because of the high surface area to volume ratio, which affect their application. Among the various methods, precipitation is the most attractive due to its simple operation, easy of mass production and demand for less apparatus compared to other processes. On the other hand precipitation leads to agglomeration and uneven particle size. It is necessary to explore for an efficacious method to resolve this contradiction to extend the application of precipitation. To exert of a mixed solvent is doubtless a new approach path in material synthesis and processing [11]. However, there are only few studies are carried out on the formations of nanoscale materials in the mixed solvent method.

The studies on effect of nanoparticle size of barium sulphate on optical, mechanical and barrier properties of polymer nanocomposites are described in this chapter. These properties are affected due to volume fraction, orientation, aspect ratio, dispersion, interfacial adhesion and filler hydrophilicity of nanoparticles. This performance is compared with those of conventional composites because their unique phase morphology maximizes interfacial contact between inorganic and organic phases and enhanced interfacial properties [14-16]. Ethylene-propylene-diene (EPDM) elastomers have proven to be a useful barrier material in the automotive and electrical construction industries, due to their unique mechanical and chemical properties [17].

5.2 Synthesis of Nanoparticles of Barium Sulphate using PEG with different Molecular Weights :

An extensive discussion of PMG method and nanoparticles synthesis is given in chapter-2 [18-22] together with general features pertaining to the design of polymer-nanoparticles assemblies. There is different ways to control structural parameter in polymer-mediated nanoparticles assemblies.

In this method PEG was used with different molecular weights (20000, 35000) and also blended with PVAc. Molecular weight of PEG plays a vital role in maintaining interparticle distance between first reactant as well as diffusivity of second component which controls the particle size of final product. While controlling nanoparticles formation, the interparticle distance is very important which can be achieve through manipulation of the separating functional group of polymer which is generate space between two particles and regulate the interparticle distance is advantageous as it is modular and can be done with simpler building blocks (23-24) and the diffusion behavior for a given polymer-penetrant system varies with change in molecular weights of polymers. This behaviour depends on the free volume within the polymer, end groups of the chains and on the segmental mobility of the polymer chains.

From Table 5.1 we can see the particle size of $BaSO_4$ is decreases with increasing in molecular weight of PEG. As molecular weight increases the diffusivity is also found to with decrease. If the molecular weight of polymer is less, the length of polymer chains is small and tends to stay away from each other. The path for freely moving sulphate ions in the solution gets easier. Thus, the resistance to the movement of sulphate ions is less. As a result, sulphate ions diffuse more freely and hence diffusivity is more. Based on these findings, it can be said that the rate of diffusion also increases with decrease in molecular weight. If the molecular weight is higher, the length of polymer chains is larger, the molecules entangle with each other so inter particle distance is also more. As a solution becomes highly viscous and polymer chains will very close having close packing as compare to lower molecular weight.

Due to close packing of polymer, the movement of carbonate ions is hindered by polymer.

Table 5.1: Change in crystallite size of synthesized $BaSO_4$ with different molecular weight of PEG and blended with PVAc

Sample	PEG molecular weight	Crystallite size (nm)
A	20000	13.5
B	35000	12.5
C	35000 + 20% PVAc	10.44
D	Commercial* $BaSO_4$	87.3

*The commercial grade mentioned in the table is the precipitated grade used for coatings.

5.3 XRD Characterisation of $BaSO_4$ nanoparticles :

The nanoparticles of $BaSO_4$ formed from solutions of different molecular weights are compiled in Table 5.1. Nanoparticles prepared were subjected to XRD analysis to find out the particle size, which was calculated by using Scherer's formula (Where D, λ, β and θ are the average D = diameter, the X-ray wavelength, half width of the peak (full width at half maximum) and the Bragg's diffraction angle respectively. The crystalline sizes of the $BaSO_4$ are estimated for high intensity peaks. According to Scherrer equation, the average particle size of $BaSO_4$ is range between 10.44 to 13.5 nm) as mentioned earlier [18-22]. Figure 5.1 shows the XRD scans of barium sulphate nanoparticles synthesized using PEG as a polymer medium with different molecular weight. It is observed that, in XRD relevant peaks were becoming broader with increase in molecular weight of PEG. Which indicates that with increase in MW of PEG particle size is decrease the particle size has been reduced from 13.5 nm to 10.44 nm by increasing molecular weight of PEG from 20000 to 35000 and blend of PVAc?

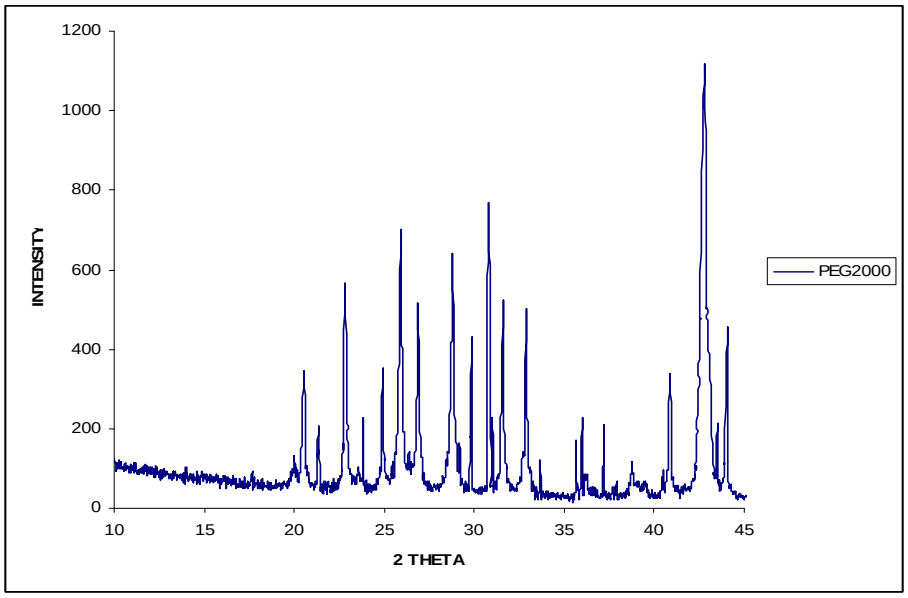

Figure 5.1 : X-ray diffraction scan of synthesized $BaSO_4$ with PEG mol. wt. of 20000

The XRD patterns of the nano $BaSO_4$ particulate with 20000 molecular weight of PEG are shown in Figure 5.1. The samples display the typical orthorhombic structure of $BaSO_4$. The *d*-values of $BaSO_4$ nanomaterial is 4.34, 2.125 and 3.904 (JCPDS No. 83-1718), 3.44, 3.10, and 2.127 (JCPDS No. 83-2053) with *hkl* values of (101), (311), (111) and (210), (211), (401) respectively. The XRD pattern was indexed with reference to the unit cell of the barite structure (a~8.87, b~5.45, c~7.15 Aº; space group. The intensity of the peaks and broadening of the XRD peaks showing crystallite size of nano $BaSO_4$. As the molecular weight of PEG increased, the crystallite size of $BaSO_4$ is decreased which can be seen by comparison with Figure 5.2 where XRD of nanoparticles prepared with PEG 35000 is displayed. Another important feature is seen if these two XRD patterns are compared: the intensities of some of the peaks is seen to decrease for $BaSO_4$ synthesized in higher molecular weight PEG. This is due to restrict growth of the crystallite in certain direction giving rise to less number of available reflections.

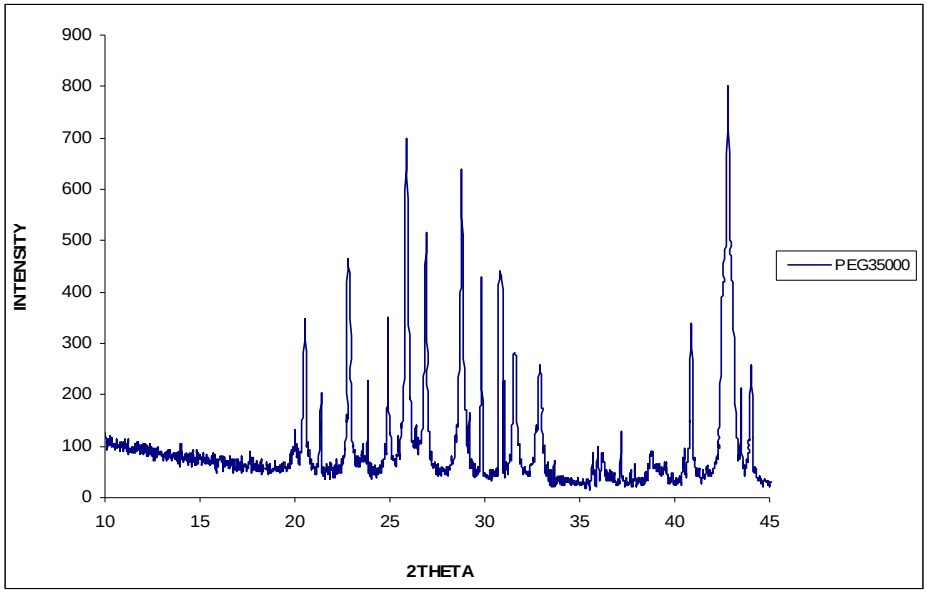

Figure 5.2 : X-ray diffraction scan of synthesized $BaSO_4$ with PEG mol. wt. of 35000

TEM image shown in Figure 5.3 indicates that there are nanosize particles embedded in polymer matrix. In this image the aggregation is obvious due to the polymer binding the particles. However, the smaller dark particles can be distinctly seen which have spherical shape. From the TEM taken at higher magnification (not shown here due to lack of sharp contrast) the particles obtained with PEG 35000 had the diameter in the range of 10-15 nm. The average diameter was about 12.50 nm as shown in Table 5.1.

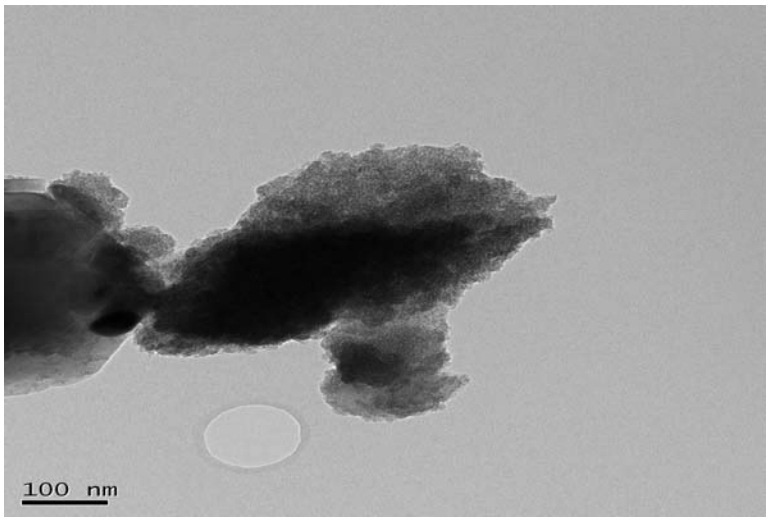

Figure.5.3 TEM image of nano $BaSO_4$ synthesized by PEG 35000

5.4 Synthesis of nanoparticles of Barium Sulphate using PEG-PVAc blend :

As per discussion in section 5.2, the complex forms between PEG-$BaCl_2$ which is more stable in high molecular weight PEG. In blend of PEG-PVAc system, synthesis of nanoparticles of barium sulphate, the particles of $BaCl_2$ form a complex with PEG when the PVAc form more complex structure around PEG-$BaCl_2$ through additional hydrogen bonding which is restrict the movement of $BaCl_2$ particles and form more stable complex network due to that the diffusivity of second reactant take place very slowly.

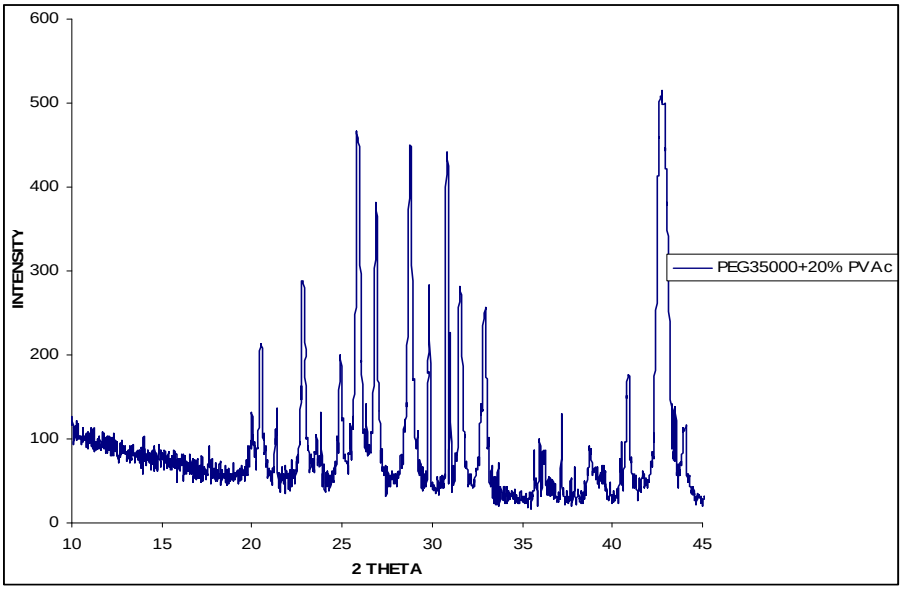

Figure 5.4 : XRD scan of synthesized $BaSO_4$ by blending PEG 35000 and 20% PVAc

The Figure 5.4 shows the typical XRD pattern of $BaSO_4$ particles prepared with PMG having blend of two polymers. The diffraction peaks of (h k l) values (101), (111), (021), (121), (002) and (212) were the characteristics of orthorhombic $BaSO_4$ crystals, only $BaSO_4$ peaks were observed in the XRD spectra which indicates very little presence of polymer. There is broadening of x-ray peaks, which is showing that the crystallite size of the particle is considerably reduced in blend system. The nanoparticles are stabilized due to polymer blend through additional hydrogen bonding and lack of agglomeration due to the particles getting coated with PEG-PVAc. The crystallite size was calculated using the Scherrer's equation, which is shown in Table 5.1.

From XRD (Figure 5.4) and TEM (Figure. 5.5) it appears that blend of PEG and PVAc resulted in smaller size (10.5 nm) and with better dispersion. The average diameter of the particles decreased greatly due to PEG 35000 blend with PVAc.

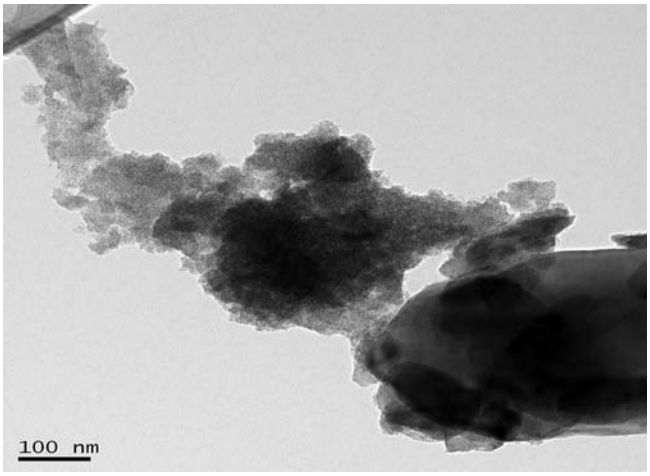

Figure 5.5 : TEM image of nano $BaSO_4$ synthesized by PEG 35000:PVAc 20% blend

5.5 Fourier Trannsform Infrared Spectroscopy(FTIR) study of commercial and nanoparticles of $BaSO_4$:

The surface characteristics of commercial and nanoparticulate of BaSO4 powder materials were examined by the infrared (FTIR) spectra. According to Alder and Kerr, (1965) [25], the sulfur-oxygen (S-O) stretching of inorganic sulfates are found in the region 1179 – 1083 cm^{-1}. The bands centered at 1187 to 1079cm^{-1} and the shoulder at 982cm^{-1} is the symmetrical vibration of SO_4^{2-}. From this observation the slight shift in the peak position may be attributed to the smaller particle size. Hence, the FTIR spectra were recorded in the present case, which are shown in Figure 5.6. There are four major bands and a few minor peaks observed in both the cases. However, the peaks at 1170, 1080, 980 and 637 cm^{-1} are substantially shifting in smaller particle size of $BaSO_4$.

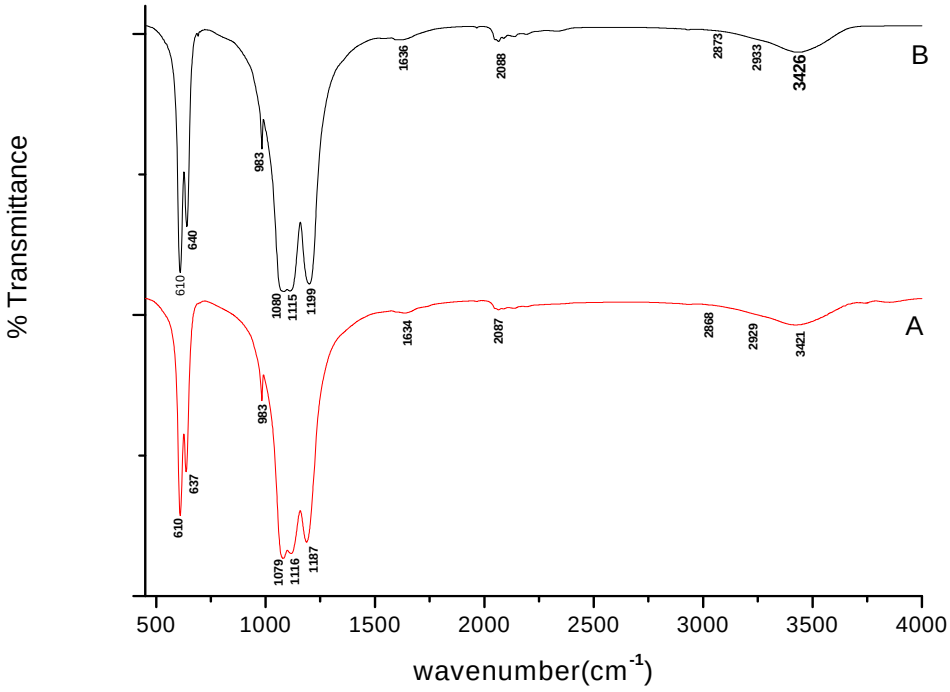

Figure 5.6 : FTIR Spectra of $BaSO_4$ A) without PEG B) PEG 35000

According to Shen et al. (2007) [26], the peaks at 608 and 637 cm^{-1} are due to the out-of- plane bending vibration of the SO_4^{2-}. Generally, bending bands are shaper than the stretching bands, which is observed in the above spectrum. In order to correlate the particle size and the peak position of the 1170 to 1080 cm-1 band, this region was studied in detail Figure 5.7A shows the FTIR in this region for all the $BaSO_4$ particles synthesized by PMG route along with the commercial grade. It is evident that the particle size has considerable effect on the peak position. This is more clear from Figure 5.7B which gives the plot of peak position with (1/particle size). The weak absorption peaks also appeared at about 3421 and 1634cm-1 which are due to the stretching and deformation of adsorbed molecule. The bands at 2855 and 2925cm^{-1} could be assigned to the symmetric and asymmetric vibrations of $-CH_2$ and $-CH_3$ groups. The polyethylene glycol absorption band occurred around 2925 cm^{-1} ($\nu(CH_2)$), 1437 cm^{-1} ($\delta(CH_2)$) which are consistent with the appearance of the alkyl groups from the polyethylene glycol. According to Manam and Das, (2009) [27], the peaks near 2000cm^{-1} are overtones and combination bands

of the lower wave number of sulfur-oxygen stretching and bending vibrations and these peaks do not affect the identification of the substance involved in the experiment. It may be pointed out that smaller the particle size, greater is the surface area and surface defects. Thus, the smaller particles are expected to retain the adsorbed low molecular weight fraction of the PEG used during synthesis. This is confirmed by the FTIR spectra which clearly show increase in the intensity of the bands in the region of 2925 and 2855 cm^{-1}.

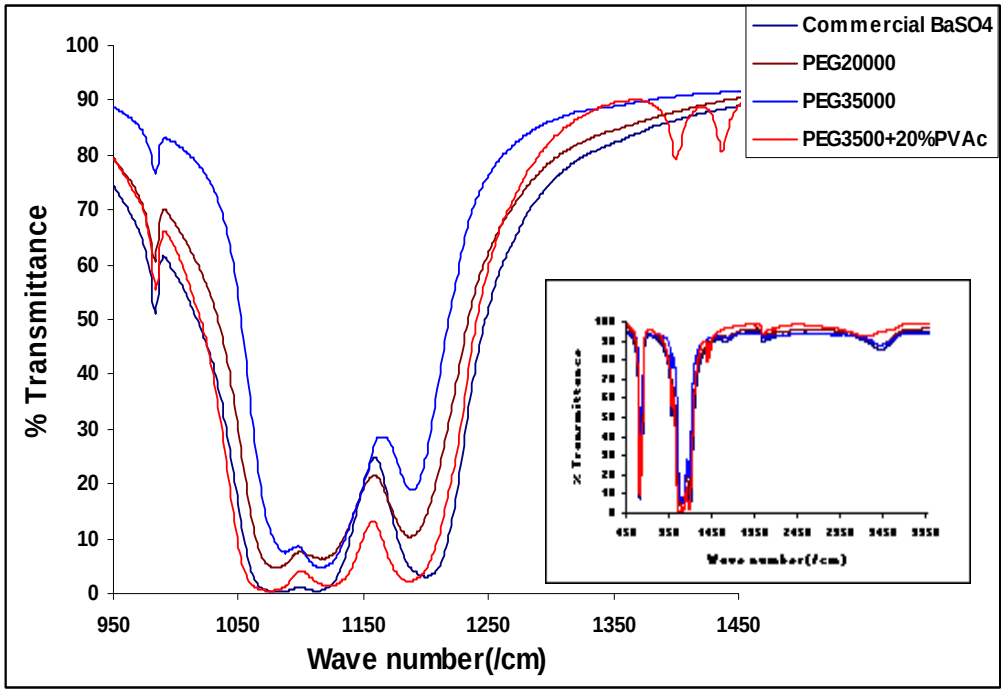

Figure 5.7A : FTIR Spectra of nano $BaSO_4$ having different particle size together with commercial grade included for comparison. Inset shows full region spectra

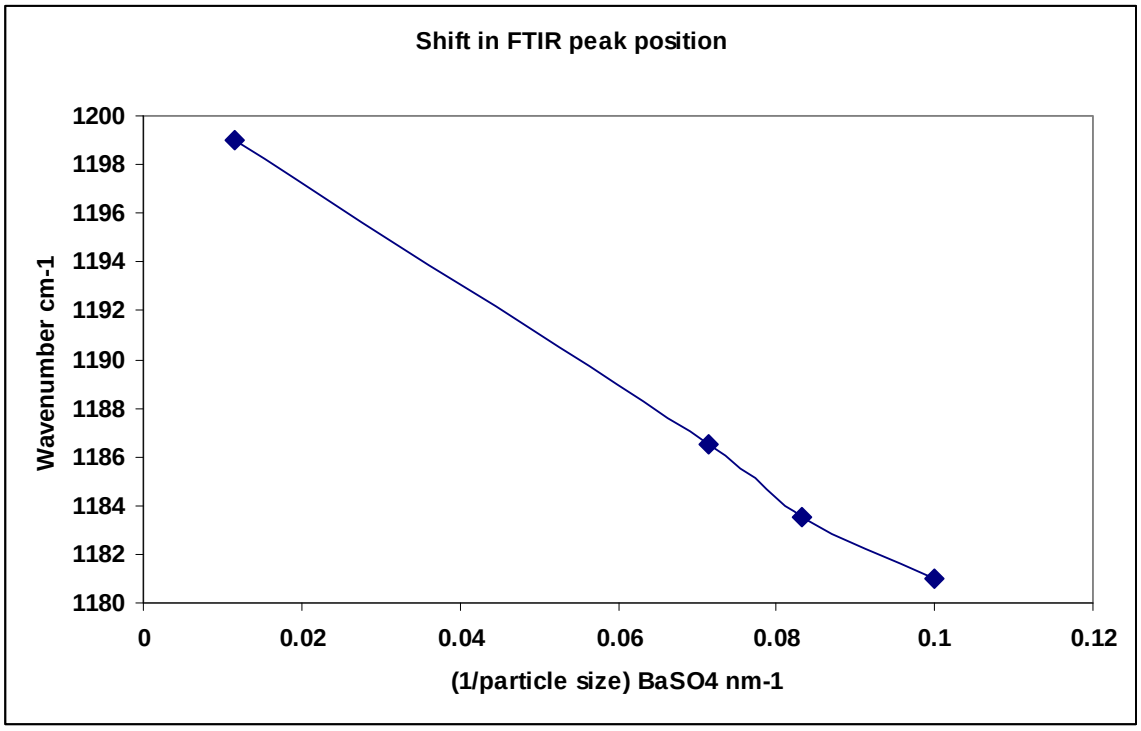

Figure 5. 7 B : Shift of the FTIR absorption band with inverse of particle size for $BaSO_4$

The earlier reports had only mentioned that FTIR bands are sensitive to particle size but now the present studies gives detailed analysis of the exact co-relationship between peak shift and the particle size.

5.6 Preparation of PVB-$BaSO_4$ based nanocomposites coating for optical and corrosion studies :

PVB is widely used in paints and coatings due to its high transparency and good adhesion to various types of surface. It also enhances mechanical properties of coating. It's one of the major application in paints is as "wash primer". These wash primers prevents corrosion in single treatment by several means. These anti corrosive primers adhere better and dry faster than conventional materials. It is widely used on a variety of metal surfaces, such as storage tank, ship, airplane, bridge, dam lock, electronic appliances etc. Incorporation of nanoparticles of $BaSO_4$ in "wash primer" improves the anti corrosive properties further since it is expected to enhance the barrier properties of "wash primer". Nanocomposite "Wash primer" is more effective

than other corrosion inhibiting materials [28-30]. Hence, PVB-nano $BaSO_4$ coating were prepared by the procedure given in chapter 2 and studied for different properties.

5.6.1 Optical properties :

Optical properties of polymer composite coatings are dependent on particle size, shape and loading of the filler. These are also important for the final appearance of the coatings. The properties such as gloss, transparency and blistering are considered here.

5.6.2.1 Gloss :

Gloss being one of the important characteristics of optical properties was studied and compared for commercial and lab synthesized nanoparticulate $BaSO_4$, with different loading percentage, which affects surface smoothness, and leveling of the film [31]. Figure 5.8 indicates the gloss observed at 60^o for the nano and commercial grade $BaSO_4$ at different loading levels. Higher concentration of nanoparticle fillers (>15%) could not be used due to high viscosity of the slurry. It is evident that the nano particle containing coatings have much higher gloss than the commercial grade. Further there is rapid decrease in gloss in coatings with commercial grade $BaSO_4$ that is due to surface roughness. It was observed that with >7% loading of $BaSO_4$ nanoparticles, gloss level dropped down significantly which is attributed to the formation of agglomeration of nanoparticles due to increase in higher loading level above the critical pigment volume concentration (cpvc) for the system. In case of commercial filler there is also surface roughness and uneven surface. This can be attributed to heavy particles in commercial grade which do not disperse well in the matrix and settle during drying /curing of the coatings.

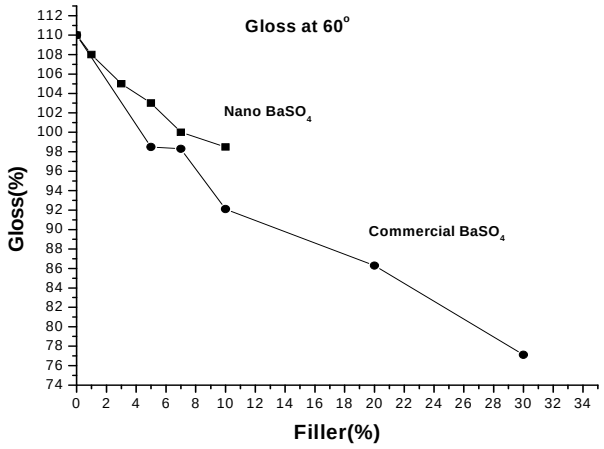

Figure 5.8 : Comparison of gloss between commercial and nanoparticles of $BaSO_4$ in PVB coating at 60^o angle

5.6.2.2 Transparency :

From Figure 5.9 depicts the transparency of the coatings recorded at 550 nm for the case of nano $BaSO_4$ and commercial grade $BaSO_4$. It is quite clear that the transparency of nanoparticulate coatings is very much higher than the coatings with commercial grade filler. Poor transparency in commercial grade $BaSO_4$ containing coatings is due heavy light scattering from the large particles rendering the coating to be opaque.

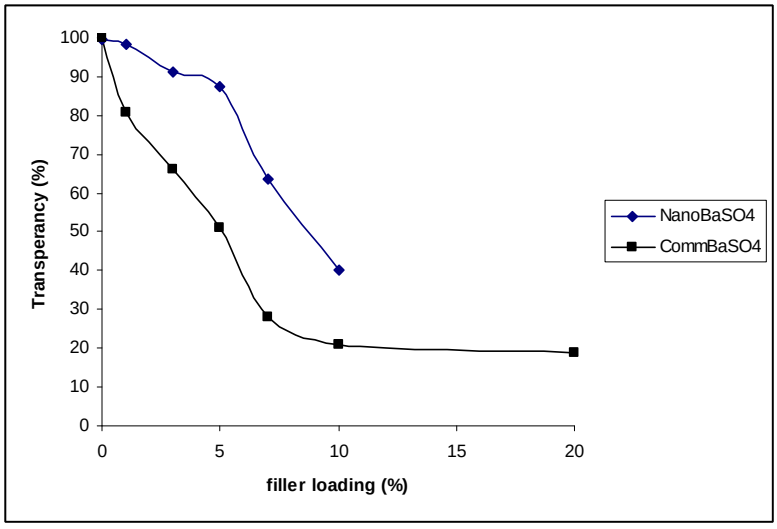

Figure 5.9: Transparency variation with filler concentration of synthesized $BaSO_4$ in PVB - $BaSO_4$ nanocomposite coating

5.6.2 Corrosion resistance study :

The $BaSO_4$ coatings are usually applied on metal surfaces for radiation protection in radiological departments such as hospitals. It is exposed to humid conditions and it has to withstand all the rough handling. To protect a substrate against moisture, the organic coatings must possess well-defined "hygro" properties. In other words, this means that the organic coatings must be formulated with specific moisture characteristics, such as coefficients of permeability, diffusion and solubility, for each type of substrate. To conceive such type of organic coatings, it is necessary to know how the pigmentation affects the water transport. In order to study the effect of pigment filler loading on the coating performance, these were studied by electrochemical techniques after continuous prolonged exposure to saline corrosive environment.

5.6.2.1 Polarisation Measurement (Tafel Plot) :

The Tafel plots of PVB-$BaSO_4$ coatings having nanoparticles (synthesized using PEG35000 12.5 nm) and commercial grade material are shown in Figure 5.10. These are typical plots obtained after exposure to saline environment at 45^0 C for 300 hours, similar curves were also obtained for other times of exposure. From these figures, the open circuit potential (OCP) in each case was derived and its dependence on exposure time plotted as indicated in Figure 5.11. The OCP shifts considerably to cathodic side after exposure of 40 hours in the case of commercial $BaSO_4$ coatings while it remains on the high anodic regions with respect to bare steel for nano $BaSO_4$ composite coatings. In the nanoparticle cases, there is only a small change of OCP even after 300 hours exposure at 45^0 C to corrosive conditions.

The tafel plots shown in Figure 5.10, reveals that the nanocomposite coating have E_{corr} potential at anodic side (0.051, -0.106 and -0.136 V) which indicate the good corrosion protecting properties even after 300 hrs. In case of pure PVB coating the curve is considerably on the negative potential side as compared to nanocomposite coating (-0.269). Coatings with commercial $BaSO_4$ also exhibit Tafel curve on the negative (cathodic side -0.324,-0.354, -0.340 V) after 300 hours which is close to bare steel (-0.46 V) which indicates that the coating for these commercial BaSO4 are almost destroyed under such corrosive conditions.

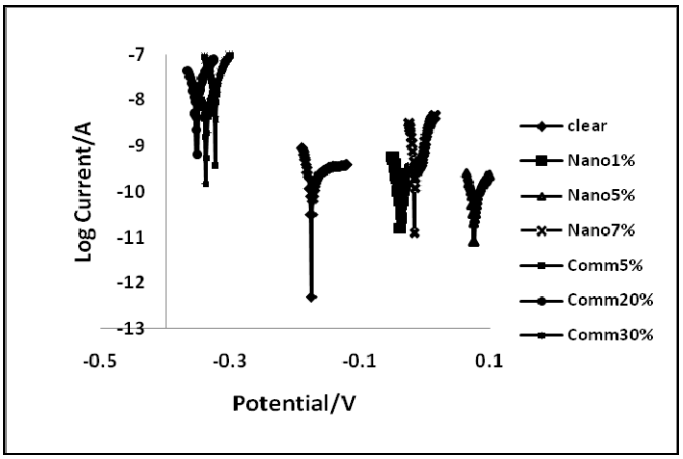

Figure 5.10 : Potentiodynamic polarization plots(Tafel) for composition of PVB–$BaSO_4$ coating after 300 hrs immersion at 45^0 C exposed to 3.5% NaCl solution

Figure 5.11 shows OCP with exposure time for all the samples. In coatings with commercial $BaSO_4$, the OCP drastically come down after 40 hrs and continuously drops till the end of the experiment. Similar trend is seen for polymer coating without additives. In nanocomposite coatings, the OCP decreased slightly initially at nominal level and then remained almost steady after 300 hours. It was high on anodic regions even after 300 hours for 5% nanoparticle coatings, which implies high corrosion resistance for these compositions. This clearly suggests nanocomposite have good compact structures which restrict the transport the corrosive ion though the coatings and this trend is observed in case 1 to 5% of nanosize additive.

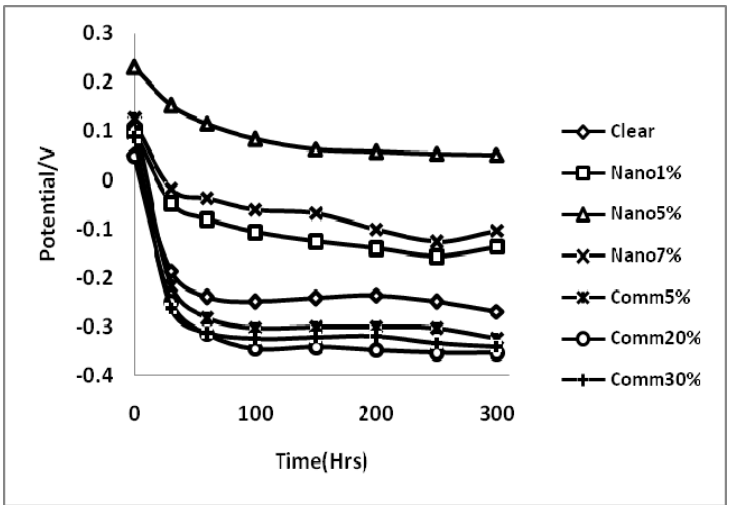

Figure 5.11: Time dependance of corrosion potential of PVB- $BaSO_4$ coating at 45^0C exposed in 3.5% NaCl solution

Figure 5.12 shows I_{corr} with respect to exposure time in polymer with and without additives for nano and commercial grade $BaSO_4$. In nanocomposite coatings, I_{corr} values are much lower than 10^{-11} A while the commercial grade $BaSO_4$ containing coatings exhibit rapid increase of I_{corr} even beyond 10^{-8} A. The rapid rise of I_{corr} in macro particle cases is indicative of degradation of the coating surface. Thus the nanocomposite coatings are clearly remaining intact even after 300 hrs of exposure. This is especially true for 5% nano $BaSO_4$ coating

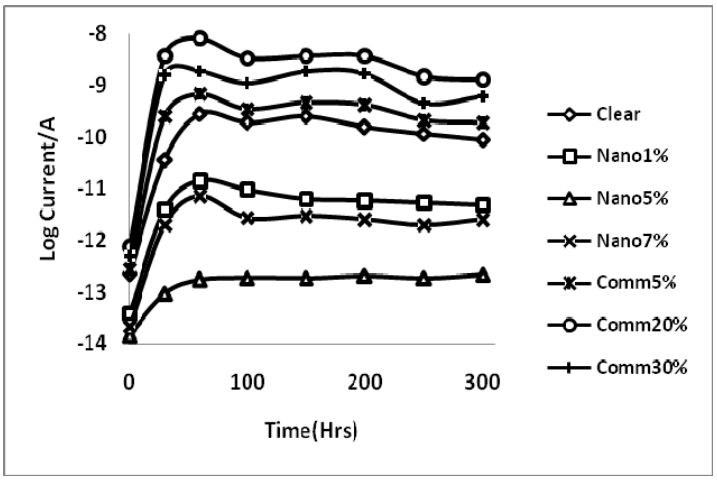

Figure 5.12 : Time dependence of corrosion current of PVB - $BaSO_4$ coating at 45^0C for 3.5% NaCl saline solution

5.6.2.2 Electrochemical Impedance spectroscopy (EIS):

EIS study characterised the stability and corrosion resistance properties of PVB-$BaSO_4$ coatings. This test is carried out over a 300 hours in 3.5% Saline solution at 45^0 C. The time dependent Bode plots were recorded from which the high frequency phase angle was estimated. Figure 5.13 shows the variation of phase angle with time for coatings containing different amount of nano and macro $BaSO_4$. It can be seen that even after 300 hours, the nanocomposite coating remain more intact since there was no rapid increase of phase angle. The phase value with different percentage of loading of nanofiller 1, 5 and 7% was -79.6, -85.9, and -82.9 degrees respectively. The coatings of pure polymer or with commercial grade $BaSO_4$ gets damaged as indicated by rapid rise in phase angle at higher frequency with time of exposure to corrosive solution.

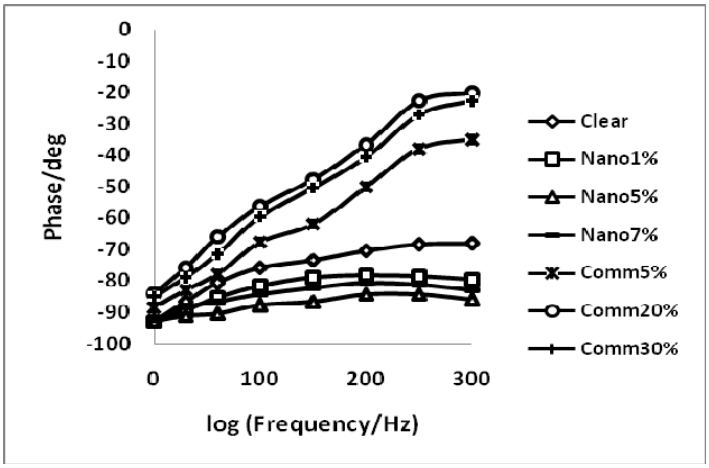

Figure 5.13 : Time dependance of phase of PVB - $BaSO_4$ coating at 45^0 C immersed in 3.5% NaCl solution

In pure PVB coating, initially the phase angle value is -90 indicating that resistance is more. But after 40 hours it starts to detoriate because ionic conduction of electrolyte through film breaks down such as pores or crevasse. Due to the pores the electrolyte contact with metal and corrosion process taken place at delamination area of coating. In commercial coating the phase angle values are -35, -20 and -22.8 it self shows that commercial coating deteriorates more because of the micro sized filler portrate have more porosity so ion transport becomes fast.

The low frequency impedance was used to characterize corrosion properties of the PVB coating with respect to time of exposure to corrosive environment. The test was carried out for over 300 hrs without the coating dissolution. The selected impedance plots are shown in Figure 5.14, which indicate how stable the coating was over that time period.

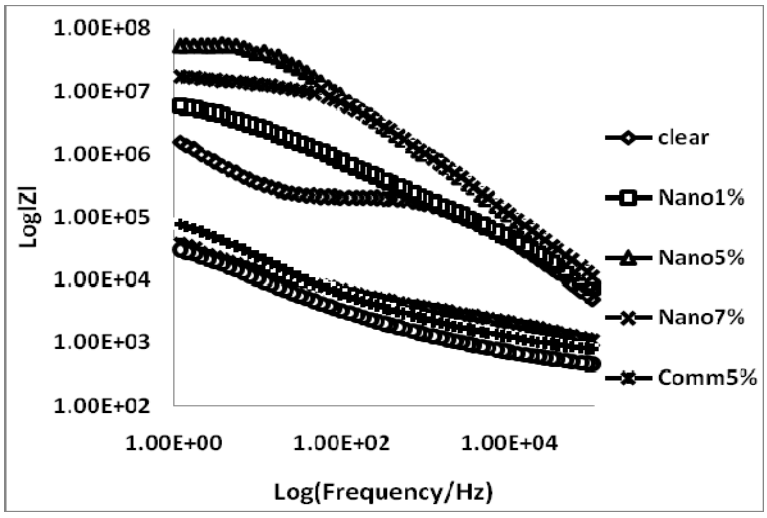

Figure 5.14 : Frequency dependance of impedance log /Z/ for different composition nano and commercial PVB - $BaSO_4$ coatings after 300 hrs

The coating impedance (Figure 5.14) and low frequency impedance with time (Figure 5.15) were somewhat stable over this time period in clear and commercial coating. There was a decrease after 40 hours for the coating resistance, which is consistent with the time till after 300 hours. The drop is believed to be due to micron size of commercial filler, which allow the corrosive ion to penetrate due to high porosity. About nanocomposite coating all plot exhibited high impedance vale high coating resistance at all frequencies. Since these low values of resistance at low frequencies correlate to the ionic conductivity, it is likely to originate from the ionic diffusion through defects.

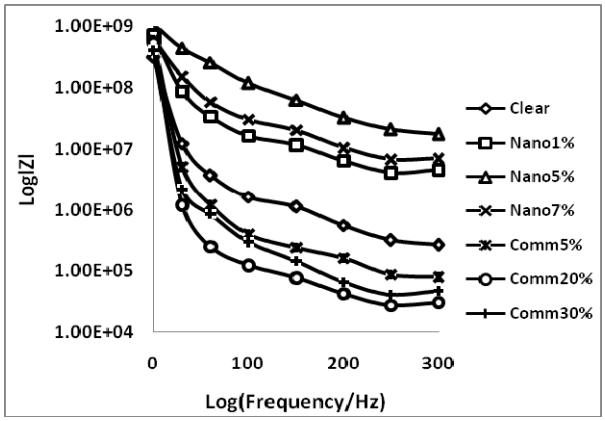

Figure 5.15 : Time dependance of impedance of PVB - $BaSO_4$ coating at 45^0C immersed in 3.5% NaCl solution

The optical polarized micrographs in reflection mode for the coatings after treatment to corrosive conditions are indicated in Figure 5.16 for nano and commercial grade $BaSO_4$. It is quite evident that there are large voids and defects created in coatings with commercial grade $BaSO_4$ while the are only few microvoids in the nanocomposite coatings. Thus the latter type are much more stable under corrosive environment.

a) PVB-5%nano$BaSO_4$ coating b) PVB-5%comm.$BaSO_4$

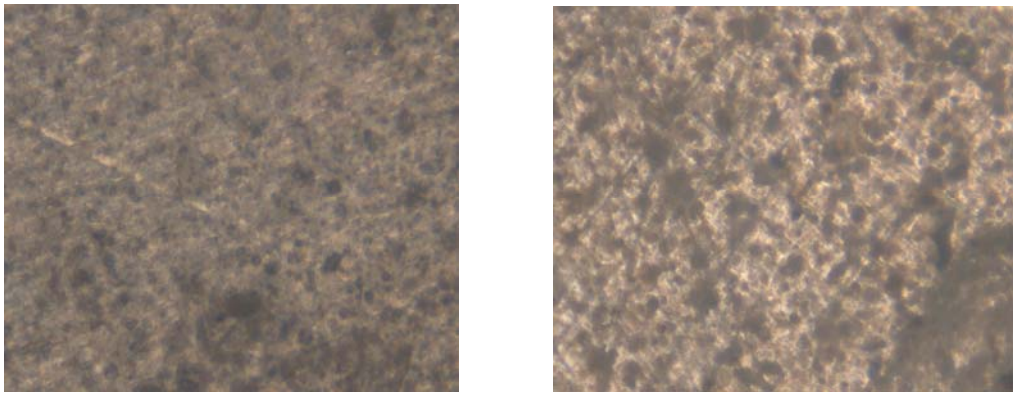

Figure 5.16 : Optical Microscopy image in reflection mode for PVB-$BaSO_4$ coating exposed for 300hrs in 3.5% NaCl solution

5.7 Preparation of epoxy–$BaSO_4$ Coating for optical and corrosion studies :

Application of epoxy resin has been widely used as a coating material to shield the steel reinforcement in concrete structures, pipe coating, rebar coating [34–35], because of its outstanding processability, excellent chemical resistance, good electrical insulating properties, and strong adhesion/affinity to heterogeneous materials. Epoxy coatings are good for decrease in the corrosion of a metallic substrate subject to corrosive species in two different mechanisms. Firstly, it acts as a physical barrier layer to control the way in of deleterious species due to high cross linked structure. Secondly, it acts as a reservoir for corrosion inhibitors to aid the steel

surface in resisting attack by aggressive species such as chloride anions. About second mechanism there is possibility of introduce localized defects in the coating and damage their appearance and mechanical strength. This defect can introduce the pathways to the ingress of water, oxygen and aggressive species onto the metallic substrate, which is responsible for localized corrosion. Furthermore, due to hydrophilic in nature, epoxy coatings can absorb water from surrounding at the time of curing process, which is responsible for large volume shrinkage [36-37]. This forms the pores in the cured epoxy coating and can assist in the movement of absorbed water and other corrosive species to the epoxy–metal interface, which could start of corrosion of the metallic substrate and delamination of the coating.

The barrier performance and optical properties of epoxy coatings can be enhanced by the introducing nanoparticulate in the coating. This is responsible for decreasing the porosity and forms compact structure of coating due to which the diffusion of corrosive species controlled. Inorganic filler particles at nanometer scale can be dispersed within the epoxy resin matrix to form an epoxy nanocomposite. The incorporation of nanoparticles into epoxy powder coating paints can enhance the integrity and durability of coatings, since the fine particles dispersed in coatings can fill the cavities [38–40]. Nanoparticles tend to occupy small hole defects formed from local shrinkage during curing of the epoxy resin and act as a bridge interconnecting more molecules. This results in a reduced total free volume as well as an increase in the cross-linking density [41-42]. In addition, epoxy coatings containing nanoparticles offer significant barrier properties for corrosion protection [43-44] and reduce the trend for the coating to blister or delaminate.

Optical properties are a function of the properties at the interfaces. Gloss is the ratio of specularly reflected light to incident light. For optically smooth surfaces, gloss varies with refractive index and angle of incidence.

Barium sulphate in one of the important filler in epoxy powder coating. This topic is concern with impact of nanoparticles of barium sulphate on epoxy powder coating on its optical, mechanical and chemical properties and particularly influence of nanoparticles of $BaSO_4$ on the anticorrosion behavior and optical properties of epoxy coatings.

5.7.1 Optical properties :

In the case of the epoxy–$BaSO_4$ coating containing nanoparticle and commercial filler the gloss was determined as described previously. We can see in Figure 5.17 that loading of nanoparticle with 1%, 3% and 5% (99, 98 & 97.3%) the gloss level reduces very less but in case of 7 and 10% (93 and 87.3%) loading of nanoparticles, the reduction is significant.

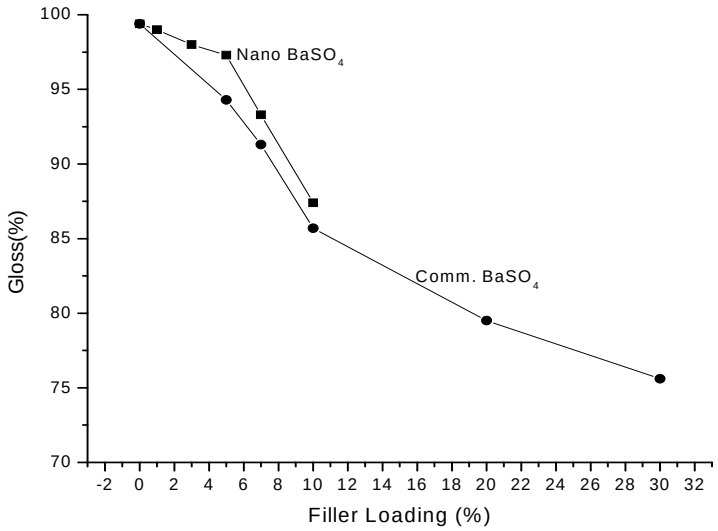

Figure 5.17 : Comparison of gloss between commercial and nanoparticles of $BaSO_4$ in epoxy coating at 60^o angle

This is due to higher loading of nanoparticles which impact on surface smoothness along with aggravated micro cracks. Epoxy coating with commercial $BaSO_4$ particles shows drastic decrease in the gloss value with increase in filler loading from 5 to 30% and gloss dropped down from 94.3 to 75.6%. It may be noted that although the above behaviour is quite similar to vinyl coatings studied and reported in the earlier chapters of this thesis, there difference in the gloss value between the nano and macro $BaSO_4$ is not that high for epoxy coatings at low filler loading. This can be due to the crosslinking of epoxy which is main factor deciding the surface gloss rather than particle dispersion and size.

5.7.2 Thermal analysis of Epoxy- $BaSO_4$ coating :

The effect filler is confirmed by the high values of the glass-transition temperature obtained, evaluated by DSC analysis: an increase in the T_g values was observed with increase in $BaSO_4$ content in the nanocomposite formulations. In general, the increase in the T_g values is attributed to good adhesion between the polymer and the filler, such that the nanometer-sized particles can restrict the segmental motion. In the present case, this good adhesion is possible due to the functional groups present on the nanofiller surface, which takes part in the polymerization process. Furthermore, the inorganic component with a small particle size can easily infiltrate the free-volumes of the organic phase; thus, the decrease of the free-volume leads to a further increase in the T_g values.

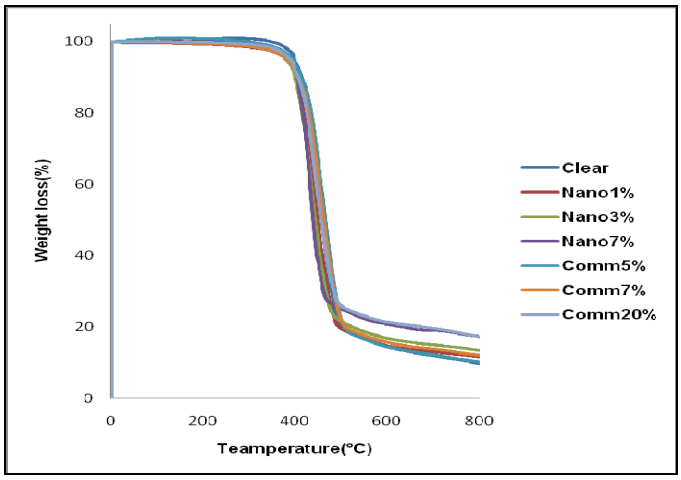

Figure 5.18 : TGA polt of Commercial and Nano Epoxy Coating

5.7.3 Corrosion Resistance Study :

5.7.3.1 Polarisation measurement (Tafel Plot) :

Electrochemical polarization was run to measure the resistance of the coating. It was believed that electrode polarization could cause due to degradation of the film. The film degradation depends on cross linking and porosity of the coating. Figure 5.19 shows Tafel plot of epoxy coating containing nano and commercial $BaSO_4$

having different concentration. The open circuit potential (OCP) determined from these plot recorded after different time of exposure to hot 3.5% NaCl solution are indicated in Figure 5.20. The initial OCP of pure epoxy and commercial $BaSO_4$ coating on to be cathodic side (0.006V SCE) and (0.109V SCE) respectively, than that of bare steel (-0.6V SCE) but after prolong exposure to corrosive environment, the OCP shifted to more cathodic region (-0.386V SCE). On the other hand the coating containing nanoparticles of $BaSO_4$ exhibit a good barrier effect that is showing the OCP, which is shifted to more anodic side than other cases.

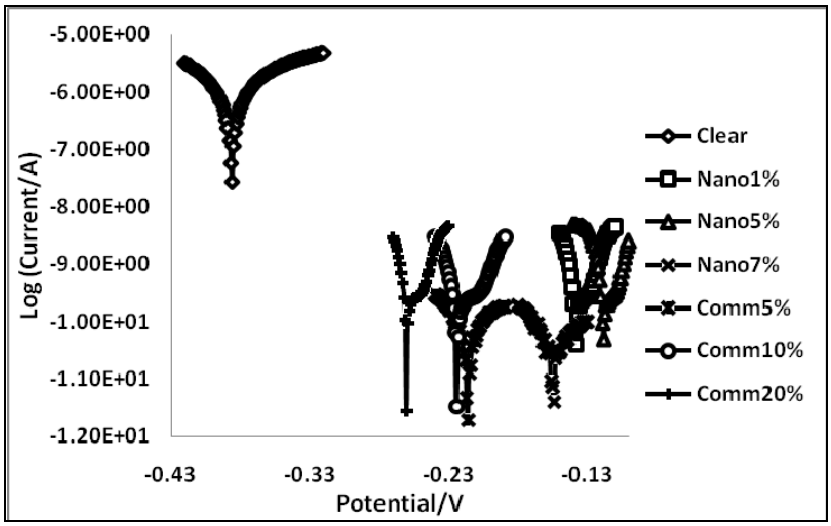

Figure 5.19: Potentiodynamic polarization plots(Tafel) for composition of epoxy – $BaSO_4$ coating after 500 hrs immersion at 45^0 C exposed to 3.5% NaCl solution

Although, there is tendency of shifting the OCP to the potential more noble side with the incorporation of nanoparticle $BaSO_4$ in epoxy coating, it is also seen that the difference in macro and nano $BaSO_4$ is not as high as in the case of vinyl coatings. This can again be attributed to the crosslinked matrix and good interaction between the particle and the matrix, which make is more intact even after exposure to corrosive environments.

Figure 5.20 shows variation of OCP with exposure time for epoxy coatings incorporated with different concentration of nano (12-13 nm) and macro-$BaSO_4$ particles Here again one sees the drop in OCP in the initial period but then tending to

a constant value which is much above than that of bare steel and coating without fillers. Addition of nano $BaSO_4$ particle clearly enhances barrier performance of coating. From Tafel plot it was observed that nanocomposite coating served as anodic-type corrosion inhibitor. The corrosion protection increases with increase in nanoparticles by loading from 3% to 5% with value -0.144V and -0.118V respectively.

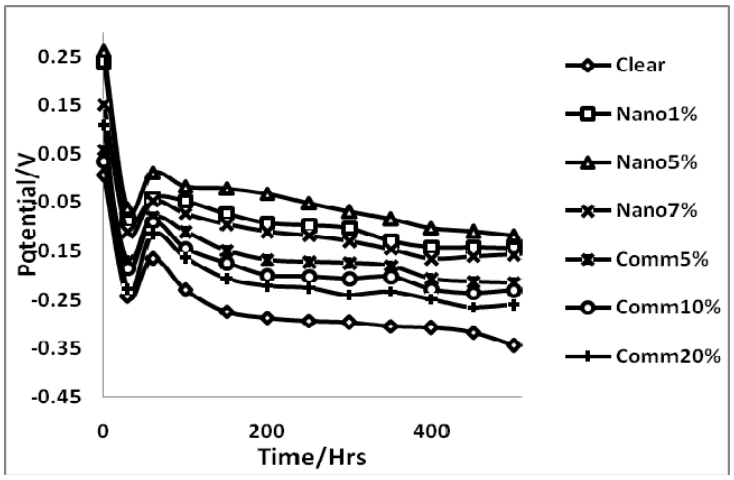

Figure 5.20: Time dependence of corrosion potential of epoxy - $BaSO_4$ coating at 45^0 C exposed in 3.5% NaCl solution

From Figure 5.21corrosion current (I_{corr}) variation with exposure time is seen. The initail low value of I_{corr} for all coating which is about 10^{-12}A to 10^{-13}A showing protective behaviour, increases but after 30 hours the nanoparticle coatings have much lower I_{corr} value than the macro-particle coatings as well as the pure epoxy. Thus, there is no continued degradation of nanoparticle coatings while the other coatings degrade over the whole period of exposure. This behaviour is also similar to that observed for vinyl coatings. However, in the case of epoxy coatings, the I_{corr} values are much lower than those for vinyl coatings. This indicates that only small level of defects are created in the case of epoxy coatings and its base resistance is quite high.

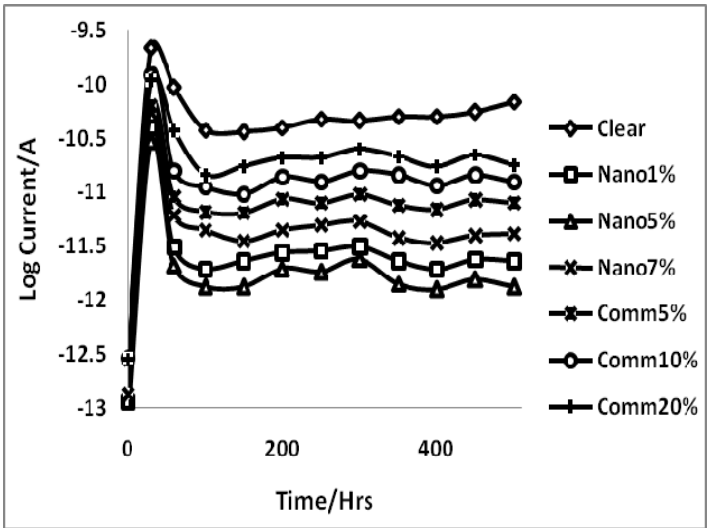

Figure 5.21 : Time dependance of corrosion current of epoxy - $BaSO_4$ coating at 45^0C exposed in 3.5% NaCl saline solution

5.7.3.2 Electrochemical impedance study :

For steel protected by the nanocomposite epoxy coatings, incorporation of nanoparticles into the epoxy coating significantly enhanced the coating resistance. The Bode plots for epoxy-coated steel in 3.5% electrolytes solution after 500hr exposure is shown in Figure 5.22. The high frequency ragion mainly provide information about coating defects and delamination of coating at metal surface. As we know for any coating, the a.c. impedance response of the steel specimens with composite coatings is dependent on immersion time in the sodium chloride environment for anticorrosion coating. The phase angle in the high frequency region hardly changes for all the coatings. On the other hand there is a broad peak appearing in the low frequency region in coating with no fillers or commercial $BaSO_4$ containing coatings. This can be due to ionic diffusion and resulting conductivity. Figure 5.23 shows the variation of high frequency phase angle with exposure time for all these cases. The increase of phase angle is more pronounced in the case of unfilled and macro–$BaSO_4$ filled coatings than that for nanoparticle containing coatings. These finding support the above conclusions regarding the intactness of nanocomposite coatings.

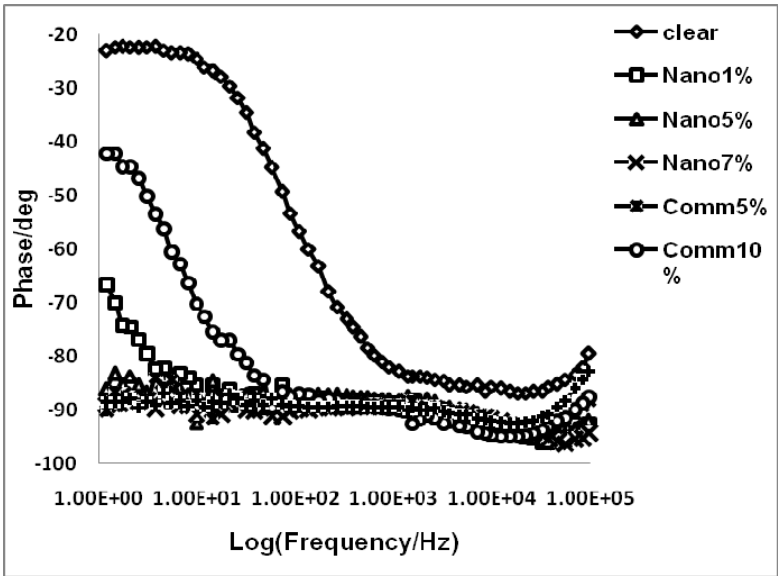

Figure 5.22: Bode plot of epoxy- $BaSO_4$ coating after 500 hrs immersion at 45^0 C exposed in 3.5% NaCl solution

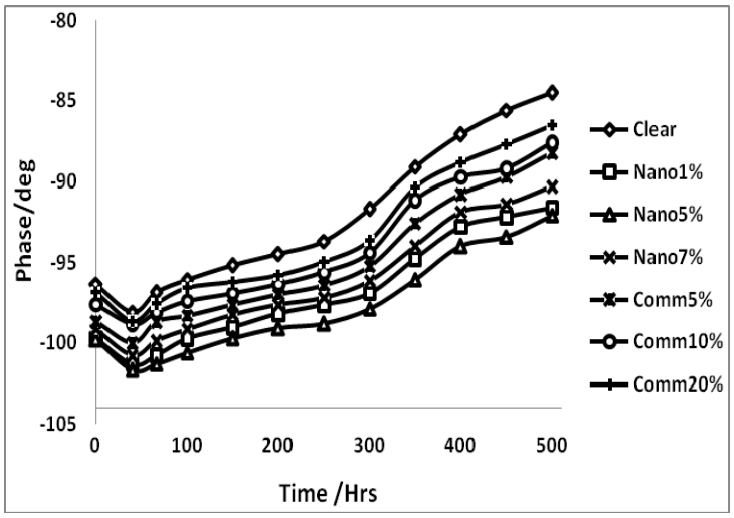

Figure 5.23: Time dependance of phase of epoxy - $BaSO_4$ coating at 45^0C exposed in 3.5% NaCl solution

Epoxy-nano $BaSO_4$ coating has higher resistance than the coatings with pure PVB especially at low frequency, which is associated with ionic transport through the film. All coatings have higher impedance on initial immersion in the electrolyte close to 10^9 Ω as shown in Figure 5.24.

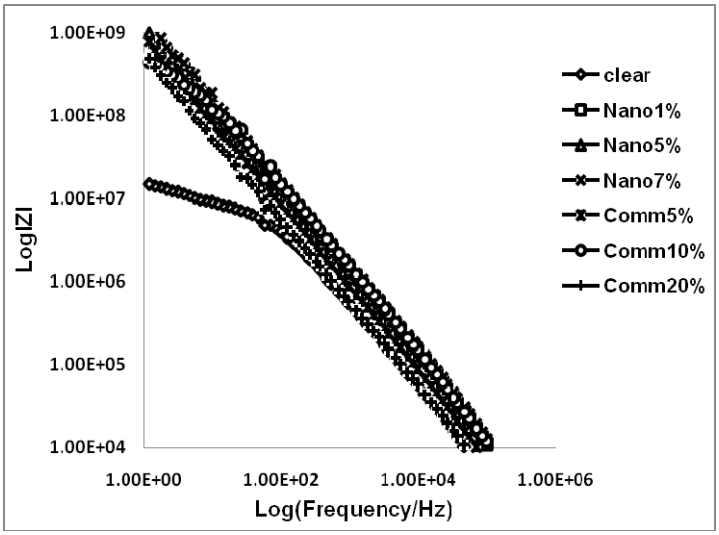

Figure 5.24 : Frequency dependence of impedance log /Z/for different composition of nano and commercial epoxy-$BaSO_4$coating after 500 hrs.

However as immersion time increases the pure PVAc and commercial $BaSO_4$ degrades more quickly than that of the nano $BaSO_4$ coating and after around 500 hours the pure PVB and commercial coated substrates show similar resistance, around $10^8\,\Omega$. One possible reason for this continued corrosion protection via the nano $BaSO_4$ coating due to the coating having compact nanostructure sealing and penetration of corrosive species is very difficult so that after 200 hours the coating resistance is $10^9\,\Omega$. It should be noted that the measured resistance consists of a component characteristic of the coating-electrolyte interface inside the coating (indicating coating porosity/compactness) and another component characteristic of the steel-electrolyte interface (indicating charge transfer resistance). Also, 3.5% NaCl solution can be used to estimate the relative void fractions within the coating matrix, assuming an inverse proportional relationship between the coating compactness and the measured resistance value. Thus, nanoparticle $BaSO_4$ containing epoxy coatings have very good compactness than other coatings studied.

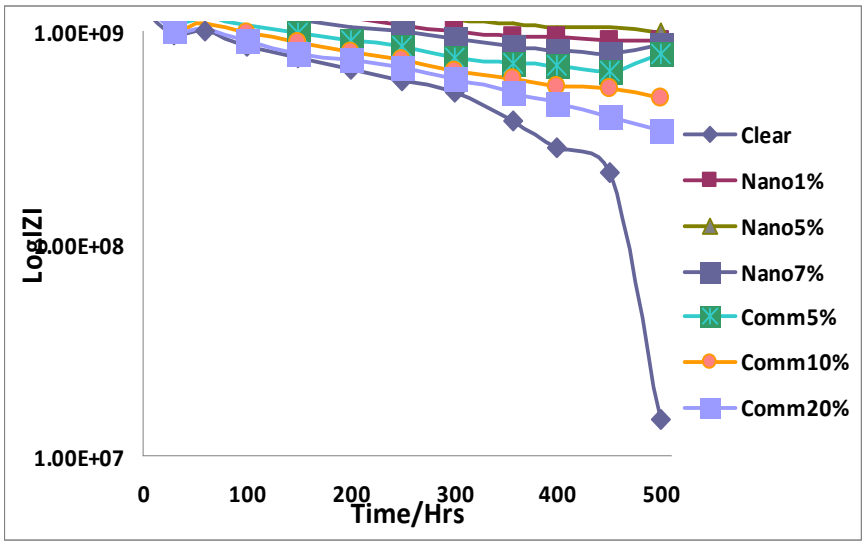

Figure 5.25: Time dependence of Impedance of epoxy - $BaSO_4$ coating at 45^0 C for 3.5% NaCl saline solution

The coating resistance of epoxy-$BaSO_4$ has higher side than the coatings with pure epoxy especially at low frequency, which is associated with ionic transport through the film. So it seen in Figure 5.25 with time, all coatings have higher impedance on initial immersion in the electrolyte close to 10^9 Ω. However as exposure time increases the pure epoxy and commercial $BaSO_4$ degrades more quickly than that of the nano $BaSO_4$ coating and after around 90 hrs the pure coated substrates show similar resistance, around 10^7 Ω. One possible reason for this continued corrosion protection via the nano $BaSO_4$ coating may be due to the fact that coating having compact nanostructured sealing and penetration of corrosive species is very difficult so that after 90 hours the coating resistance is 10^8 Ω.

5.8 Conclusion :

$BaSO_4$ has been synthesized in nanoparticle size using PMG route using different molecular weight PEG as the growth matrix. These nano-$BaSO_4$ were well characterized by XRD, TEM as well as FTIR. The structure was confirmed as

orthorhombic baryte type by comparing the d-values with standard. The particle size ranged from 10 to 13 nm as confirmed by TEM. The most interesting part of present observations was in FTIR spectra which showed clear shift of the absorption band with particle size. Also, it indicated the presence of adsorbed PEG which increased with lowering of particle size. The coatings were made using nano-$BaSO_4$ and commercial grade $BaSO_4$ which were studied for optical and corrosion resistance properties. PVB as well Epoxy were used as matrix for coatings on steel substrates with latter being made by powder coating technique. The comparison of the data shows that nano-particle $BaSO_4$ coatings are very much superior to the macro commercial grade $BaSO_4$, especially for PVB (or vinyl) coatings. The epoxy coatings show some improvements with incorporation of nano-particle $BaSO_4$ but the crosslinking effects are more dominant in controlling the final properties of the coatings. Hence, nanoparticles are more effective in vinyl polymer based coatings.

5.9 References :

[1] Ujhelyiova, A., Marcincin, A., Kiss, M. and Marcincinova, T.. *Journal of Thermal Analysis,* **1996**, 46: 619–623.

[2] Qu, M.H., Wang, Y.Z., Liu, Y., Ge, X.G., Wang, D.Y. and Wang, C. *Journal of Applied Polymer Science*, **2006**, 102: 564–568.

[3] Siegel R. W., *Sci. Am*., **1996**, 275, 74-79.

[4] Unsworth J., Lunn B. A., Innis P. C., *J. mater. Sci. lett*., **1993**,12, 132-134.

[5] Mann S., *Nature*, **1993**, 365, 499-505.

[6] Heywood B. R., Mann S., *Adv. Mater*., **1994**, 6, 9-20.

[7] Yoshikawa Y., Nanncollas G. H., *J.Cryst. Growth*, **1984**, 69, 357-361.

[8] Qi L., Ma J., Cheng H., Zhao Z., *Colloids Surfaces A: Physicochem. Eng. Aspect,* **1996**,108, 117-126.

[9] Chen G., Luo G., Xu J., Wang J., *Powder Technol*., **2005**,153,90-94.

[10] Shen Y., Li C., Zhu X., Xie A., Qiu L., Zhu J., *J. Chem Sci*., **2007**, 119, 319-324.

[11] Li S. W., Xu J. H., Wang Y. J., Luo G. S., *Powder Technol*.,**2009**, 195, 213-220.

[12] Colfen H., Qi L., Mastai Y., Borger L., *Cryst. Growth Des*., **2002**, 2 , 191-196.

[13] Lv. Y., Wu X., Wu D., Huo D., Zhao S., *Powder Technol*., **2007**, 173, 174-178

[14] Okada A, Usuki A.. *Mater Sci Eng*; **1995**, 3(2):109–15. (1995)

[15] Ogawa M, Kuroda K.. Bull *Chem Soc Jpn* **1997**, 8:70:2593–61

[16] Kojima Y, Usuki A, Kawasumi M, Okada A, Fujushima A, Kurauchi T, *J Mater Res*; **(1993)**, **8**:1185–99

[17] Wang, K., Wu, J.S., Ye, L. and Zeng, H.M., *Part A Applied Science and Manufacturing,* **(2003)**, 34: 1199–1203.

[18] Saujanya, C., Ashamol, S., Padalkar, S., Radhakrishnan, S. *Polymer* **2001 42,**2255.

[19] Saujanya, C., Radhakrishnan, S. *Polymer* **2001, 42,** 6723.

[20] Saujanya, C., Radhakrishnan, S. *J. Mat. Sci*. **1998**, **33** 1063.

[21] Saujanya, C., Radhakrishnan, S. *J. Mat. Sci.* **1998**, **33** 1069.

[22] T. B. Noorsten, B. L. Frankamp, V. M. Rotello, *Nano Letter.* **2002**, 2’ 1345

[23] S.J. Park, A. A. Lazarides, J. J. storhoff, l. Pesce, C. A. Mirkin, *J. Phys. Chem. B* **2004**, 108, 12375.

[24] H. H. Adler, P. F. Kerr, *Am. Mineral*., **1965**, 50, 132-147.

[25] Y. Shen, C. Li, X. Zhu, A. Xie, L. Qiu, *J. Zhu, J. Chem. Sci*., **2007**, 119, 319-

324.

[26] J. Manam, S. Das, *Indian J. Pure Ap. Phy*., **2009**, 47, 435-438.

[27] S. Sathiyanarayanan, S. Syed Azim and G. Venkatachari *Progress in Organic Coatings* ,April **2009**, Volume 65, Issue 1, , Pages 152-157

[28] O. A. Tarakanovskaya, N. P. Zhil'tsov, L. A. Vericheva and I. N. Nikolaeva *Chemical and Petroleum Engineering*,August, **1986** Volume 22, Number 8, 392-393,

[29] S. Radhakrishnan, C.R. Siju, Debajyoti Mahanta, Satish Patil , Giridhar Madrasc *Electrochimica Acta*, **2009** 54 1249–1254

[30] Chen, S, You, B, Zhou, S, Wu, L, *J. Appl. Polym.Sci.*, **2009**, 112 3634–3639

[31] D.Y. Perera, *Prog. Org. Coat*., **1980**, 8 (2) 183.

[32] J. Crank, G.S. Park (Eds.), *Diffusion in Polymers, Academic Press*, New York, **1968.**

[33] F. Galliano, D. Landolt, *Prog. Org. Coat*. **2002**, 44, 217.

[34] A. Talo, O. Forsén, S. Yläsaari, *Syn. Met*. **1999,** 102, 1394.

[35] D. Perreux, C. Suri, *Compo. Sci. Technol*. **1997,** 57, 1403.

[36] C. Loos, G.S. Springer, *J. Comp. Mater*. **1979,** 13, 131.

[37] K. Lam, K.T. Lau, *Compo. Struc*. **2006,** 75, 553.

[38] G. Shi, M.Q. Zhang, M.Z. Rong, B. Wetzel, K. Friedrich, *Wear*, **2003**, 254, 784.

[39] Hartwig, M. Sebald, D. Putz, L. Aberle, *Macromol. Symp.,* **2005**, 221, 127.

[40] N.Huong,*Improvement of bearing strength of laminated composites by nanoclay and Z-pin reinforcement, PhD. Dissertation*, University of New South Wales, Australia **(2006).**

[41] O. Becker, R. Varley, G. Simon, *Polymer* **2002**, 43 (16) 4365.

[42] L.H. Yang, F.C. Liu, E.H. Han, *Prog. Org. Coat*. **2005**, 53 91.

[43] S.V. Lamaka, M.L. Zheludkevich, K.A. Yasakau, R. Serra, S.K. Poznyak, M.G.S. Ferreira, *Prog. Org. Coat*,.**2007**, 58 127

CHAPTER – VI

Summary and Conclusions

CHAPTER - 6

Nanomaterials in general and nano-particulate additives in particular have attracted tremendous attention in recent years for their variety of applications in diverse areas. Amongst these, nanoclays have been used in commodity polymers and in recent times also for paints and coatings. However, common fillers and additives used in the coating industry have not been studied extensively in nano-particle sizes. The additives such as $CaCO_3$, Fe_2O_3 and $BaSO_4$ are the most attractive for different organic coatings and hence these were chosen for the present studies. Synthesis characterisation and application of these compounds in polymer nanocomposite coatings has been carried out and the present thesis describes the novel results obtained for the various systems.

Polymer mediated growth technique was employed for the synthesis of the nano-particulate additives. In this technique a polymer such as PEG, PVAc, etc was used for modification and control the morphology, crystalline phase, and orientation and growth habit of the final product. It was shown that the PMG can be effectively used for the synthesis of nano-particulate additives on large scale. These were then incorporated in polymer matrix mainly vinyl coatings and studied for their corrosion resistance properties.

The synthesis of nano particulate $CaCO_3$, Fe_2O_3 and $BaSO_4$ was carried out using the PMG route by first complexing the reacting salts with PEG and PEG/PVAc blend in aqueous or mixed solvent media and then allowing the diffusion of ions which reacted to give in situ precipitation of the final product. Typically, $CaCl_2$ was complexed with PEG first and then K_2CO_3 was allowed to diffuse through the polymer to form $CaCO_3$. Similarly $FeCl_3$ bound by PEG and $BaCl_2$ with PEG was reacted with NaOH and Na_2SO_4 respectively to give the corresponding compounds in nanoparticle form. The resulting products were characterized by XRD, SEM, FTIR etc.

The nanosize calcium carbonates were synthesized by using the PMG technique using PEG of different molecular weight, concentrations and blending with PVAc. The in-situ generated particles using PMG technique had crystallite sizes ranging from 50 nm to 15 nm. The effect of polymer concentration and molecular weight of polymer medium on the particle size indicated that viscosity of the growth medium plays the most important role since it controls the diffusion of reacting ions. The crystallite size was found to decrease with increasing molecular weight of polymer and medium viscosity. The molar ratio of the reactant to the monomer unit of the polymer also is important for good stability of the complex initially formed.

The coatings prepared from PVAc and PVB containing commercial as well as nanoparticles of $CaCO_3$ were prepared by using dip coating technique in aqueous slurry. The optical properties such as gloss, reflectance, transparency, etc. of PVAc and PVB containing commercial as well as nanoparticles of $CaCO_3$ gave an ample proof of uniform dispersion of the $CaCO_3$ nanoparticle addition in polymer matrix. The gloss at 60^o angle was observed to increase upto 95 by the addition of only 1% of nano $CaCO_3$ fillers. For concentration of 10% or greater of nano-$CaCO_3$ fillers the gloss decreased to 86 which could be due to agglomeration of particles. On the other hand, the gloss was observed to decrease from 84 to 69 after the addition of commercial grade $CaCO_3$ in polymer matrix. The opacity was observed to decrease from 60 to 26 by an addition of commercially available $CaCO_3$ in the polymer matrix while in case the of nano $CaCO_3$. The opacity was observed to decrease from 95 at 1% nano-$CaCO_3$ to 63 at 10% nano-$CaCO_3$ addition. Thus, nano-$CaCO_3$ have much better optical properties than commercial grade filler.

The corrosion protection ability for PVAc and PVB with nano $CaCO_3$ was studied using electrochemical impedance spectroscopy at periodic intervals during exposure to hot saline (45^0 C and 55^0 C) conditions for prolonged durations over a period of 122 hrs and 150 hrs for PVAc and PVB coating respectively. The open circuit potential (OCP) was found to shift with time from −0.435 V SCE to more anodic side (−0.022 V SCE) much above that of bare steel (−0.5 V SCE). The

presence of nano-$CaCO_3$ was found to be vital in the prevention of corrosion and the shift of OCP to anodic side. The exceptional improvement of performance of these coatings has been associated with the increase in barrier to diffusion of ions and prevention of charge transport by the nano-size $CaCO_3$. The Bode plot data was used to calculate the impedance and coating resistance of nanoparticulate and commercial filler incorporated coatings with PVB and PVAc polymer matrix. This indicated that the incorporation of Nano-$CaCO_3$ into polymer matrix exhibited quite high Coating resistance of the order of $10^9\,\Omega$ to $10^7\,\Omega$ at different operational temperatures (45^0 C, and 55^0 C) while commercial $CaCO_3$ coating shows much coating resistance of the order$10^6\,\Omega$ to$10^5\,\Omega$ under same conditions.

The nanosize iron oxide particles were synthesized using PMG technique as explained above. The insitu generated iron oxide particles using this technique had crystallite sizes ranging from 25 nm to 7 nm. The crystallite size was found to decrease with increase in molecular weight of polymer medium. The crystal structure and particle size were investigated by using X-ray diffraction (XRD) and TEM. Reflectance spectra of Fe_2O_3 nanoparticles show shifting the wavelength from 636.5 to 544 with respective decrease in crystallite size (7 to 25 nm). A brief introduction to polymer nanocomposites containing Fe_2O_3 nanoparticulate used in coating applications and Fe_2O_3 nanoparticulate used in coating because it enhances the optical and corrosion resistance through high barrier resistance and self healing was associated with the scavenging of ions which prevented corrosion of the underlying substrate.

The optical properties of coating containing nanoparticulate such as gloss showed higher value 95 to 85% as compared to commercial Fe_2O_3 (87 to 56%). The electrochemical impedance spectroscopy was studied at periodic intervals during exposure to hot saline conditions (3.5% NaCl solution) for prolonged durations over a period of 145 hrs for PVAc coating. The OCP value of PVAc coating containing Fe_2O_3 nanoaparticles was found to shift with exposure time from −0.446 V SCE to more anodic side (−0.168 V SCE) much above that of bare steel (−0.5 V SCE). The

exceptional improvement of performance of these coatings has been associated with the increase in barrier to diffusion, prevention of charge transport by the nano-size Fe_2O_3. By adding of nano-Fe_2O_3 into polymer matrix exhibited a high barrier resistance (determined from Bode plot) of the order of 10^7 Ω to 10^6 Ω while commercial Fe_2O_3 coating shows barrier resistance of the order 10^6 Ω to10^4 Ω after testing at different operational temperatures in aggressive saline condition .

The corrosion protection properties of PVB hybrid composite coatings filled with Fe_2O_3 nanoparticles and polyaniline composite were studied. Electrochemical impedance spectroscopy has been used for monitoring the barrier characteristics of the bulk phase of the coating. The open circuit potential (OCP) was found −0.432 V SCE for commercial Fe_2O_3 while for nano-Fe_2O_3 very much on the anodic side 0.234 V SCE much above that of bare steel (−0.5 V SCE).

The nanosize barium sulphate particles were synthesized using PMG technique as explained above. The insitu generated barium sulphate particles using this technique had crystallite size of 35 nm. The crystal structure and particle size were investigated by using X-ray diffraction (XRD) and TEM.

The electrochemical impedance spectroscopy was studied for prolonged durations over a period of 150hrs and 460hrs for PVB and Epoxy coating respectively. The open circuit potential (OCP) was found to shift with time from −0.325 V SCE to more anodic side (0.033 V SCE) much above that of bare steel (−0.5 V SCE). The presence of nano-$BaSO_4$ was found to be vital in the prevention of corrosion and the shift of OCP to anodic side. The exceptional improvement of performance of these coatings has been associated with the increase in barrier to diffusion, prevention of charge transport by the nano-size $BaSO_4$. The Bode plot data was used to calculate the capacitance evolution of Nanocomposite and commercial coating PVB and Epoxy polymer matrix. This indicated that the incorporation of nano-$BaSO_4$ loading into polymer matrix exhibited a high barrier resistance of the order of 10^9 Ω to 10^8 Ω

different operational temperatures (45^0 C and 55^0 C) while Commercial $BaSO_4$ coating shows barrier resistance of the order$10^7\ \Omega$ to$10^6\ \Omega$ under same conditions.

Table 6.1: Comparison of additive performance in nano-composite coating protection

Sample	Normalized Log (Coating Resistance)decay rate /day					
	$CaCO_3$ PVAc	$CaCO_3$ PVB	Fe_2O_3 PVAc	Fe_2O_3 PVB	$BaSO_4$ PVB	$BaSO_4$ Epoxy
No additive	1	1	1	1	1	0.1
3-5% Nano	0.11	0.13	0.28	0.35	0.27	0.06
10 % Macro	0.77	1	0.8	0.71	0.95	0.09

From these different studies, a few salient features emerge as regards the effective performance of the nano-size additives in coatings for metal protection. A comparison has been made in Table-1 of this chapter for the decay of coating resistance with time using the data reported earlier chapters 3, 4 and 5. The decay rate was estimated from the log Z with respect to time of exposure to saline condition at 45^0 C. This data is compiled in Table-1 for different filler/ polymer systems used in the present studies for comparison. It is interesting to note that the nano-particulate filler is very effective in reducing the decay of coating resistance in all cases especially in vinyl coatings. Amongst the various materials studied, nano $CaCO_3$ appears to be the most effective in enhancing the coating stability in saline conditions for the vinyl coatings. The macro-size particulate fillers give some enhancement 20 to 30% in terms of reduction of decay rate. The effect is least for macro size $BaSO_4$ while better results are obtained for vinyl coatings with $CaCO_3$ and Fe_2O_3. The nano fillers are much more effective by reducing the decay to 0.11 or 0.2 of original, thus giving 80 to 90% improvement in the stability under similar conditions. Another reason for nano $CaCO_3$ having better properties in coatings can be the density of the substance. The material density is lowest for $CaCO_3$ and highest for $BaSO_4$ with Fe_2O_3 lying in between. During mixing of the coating formulations the heavier particles will not disperse properly and would have tendency to settle down and this will be also taking place during the drying and curing of the final coating. Thus the nano $CaCO_3$ particles will be uniformly dispersed throughout the matrix while $BaSO_4$

possibly not. Further, the nano- particle matrix interaction is better for $CaCO_3$ / vinyl system which is further enhanced due to adsorbed PEG. Hence, the performance of these nano-particle additives is seen to follow the order nano-$CaCO_3$ > nano-$Fe2O_3$> nano-$BaSO_4$. Epoxy coatings on the other hand have as such excellent life and very little change is seen in their properties over long durations of exposure. This is because the epoxy coatings are highly cross linked and there is very little diffusion of ions/ water through these at ordinary temperatures. The nano additives give some more improvements of already stable epoxy coatings.

Thus, it is seen from these studies, that the common additives if made in nanoparticulate form, impart very much higher properties in vinyl coatings and that too at quite low additive concentrations. It may be mentioned here that the cost has been a barrier in the past for extensive use of nano particulate materials. However, the present studies clearly open up a new route to synthesize common materials in nano form on large scale and which is easy for industrial implementation. This has been demonstrated by making sufficient quantity of the nano additives, formulating coating compositions in the industrial environment and applying these on coupons in the usual manner which is practiced for industry. One can now certainly state that these nano-particulate additives are not just laboratory curiosity but industrially useful novel new materials.

LIST OF PUBLICATIONS

1. S. Radhakrishnan and **Narendra Sonawane,** C. R. Siju "Epoxy powder coating containing polyaniline for enhanced corrosion protection"**.** ***Progress in Organic Coatings 64 (2008) 383–386***

2. **Narendra Sonawane** and S. Radhakrishnan. "Effect of nano-Fe_2O_3 on Corrosion resistance properties on polyvinyl Nanocomposite Coatings". (Manuscript under preparation).

3. **Narendra Sonawane** and S. Radhakrishnan "Conducting polyaniline-Nano-Fe_2o_3 composites for smart corrosion resistant coating" (Manuscript under preparation).

SYMPOSIA / CONFERENCES

- Research paper presented at **International Conference**, ICAM 2008 on advanced materials, at Mahatma Gandhi University, Kerala, India.

- Research paper accepted for presentation in **International Conference**, BOYA PAINT 2008, India.

- Participated a workshop on "Biodiversity conservation and management" Organized by Maharashtra Academy of Science at NCL, Pune, India 2008.

- Participated a symposium on "Materials for Automotive Industries" organized by Material Research Society of India (MRSI), Pune, India in 2005.